

## 5. SITE 718: BENGAL FAN<sup>1</sup>

### Shipboard Scientific Party<sup>2</sup>

#### HOLE 718A

**Date occupied:** 20 July 1987  
**Date departed:** 20 July 1987  
**Time on hole:** 1 hr  
**Position:** 01°01.252'S, 81°24.065'E  
**Water depth (sea level, m, bottom felt):** 4730.2  
**Penetration (m):** 9.5  
**Number of cores:** 1  
**Total length of cored section (m):** 9.5  
**Total core recovered (m):** 9.42  
**Core recovery (%):** 99.1  
**Deepest sedimentary unit cored:**  
Depth sub-bottom (m): 2.0  
Nature: micaceous silts and calcareous clays  
Age: late Quaternary  
Measured vertical sound velocity (km/s): 1.55

#### HOLE 718B

**Date occupied:** 20 July 1987  
**Date departed:** 20 July 1987  
**Time on hole:** 2.5 hr  
**Position:** 01°01.252'S, 81°24.065'E  
**Water depth (sea level, m, bottom felt):** 4730.2  
**Penetration (m):** 18.8  
**Number of cores:** 1  
**Total length of cored section (m):** 9.5  
**Total core recovered (m):** 9.26  
**Core recovery (%):** 97.5  
**Deepest sedimentary unit cored:**  
Depth sub-bottom (m): 2.0  
Nature: micaceous silts and calcareous clays  
Age: late Quaternary  
Measured vertical sound velocity (km/s): 1.55

#### HOLE 718C

**Date occupied:** 20 July 1987  
**Date departed:** 1 August 1987  
**Time on hole:** 11.3 days  
**Position:** 01°01.252'S 81°24.065'E  
**Water depth (sea level, m, bottom felt):** 4730.2  
**Penetration (m):** 935.0

**Number of cores:** 98  
**Total length of cored section (m):** 925.7  
**Total core recovered (m):** 274.05  
**Core recovery (%):** 29.6  
**Deepest sedimentary unit cored:**  
Depth sub-bottom (m): 189.8  
Nature: silt and silt mud turbidites  
Age: early Miocene  
Measured vertical sound velocity (km/s): 1.7 to 2.3

#### HOLE 718D

**Date occupied:** 2 August 1987  
**Date departed:** 3 August 1987  
**Time on hole:** 2.6 days  
**Position:** 01°01.252'S, 81°24.065'E  
**Water depth (sea level, m, bottom felt):** 4730.2  
**Penetration (m):** 90.0  
**Number of cores:** 2  
**Total length of cored section (m):** 19.0  
**Total core recovered (m):** 0.17  
**Core recovery (%):** 0.9  
**Deepest sedimentary unit cored:**  
Depth sub-bottom (m): 2.0  
Nature: silt and silt mud turbidites  
Age: Quaternary  
Measured vertical sound velocity (km/s): unknown

#### HOLE 718E

**Date occupied:** 9 August 87  
**Date departed:** 17 August 1987  
**Time on Hole:** 6.9 days  
**Position:** 01°01.252'S, 81°24.065'E  
**Water depth (sea level, m, bottom felt):** 4730.2  
**Penetration (m):** 961.6  
**Number of cores:** 3  
**Total length of cored section (m):** 28.5  
**Total core recovered (m):** 9.92  
**Core recovery (%):** 34.8  
**Deepest sedimentary unit cored:**  
Depth sub-bottom (m): 933.1  
Nature: silt and mud and massive mud  
Age: early Miocene  
Measured vertical sound velocity (km/s): 2.2

#### SITE SUMMARY

Site 718 is located in the central Indian Ocean approximately 800 km south of Sri Lanka and 200 km northwest of the Afanasy Nikitin seamount group. It lies at the distal end of the Bengal Fan within a large region of intraplate deformation,

<sup>1</sup> Cochran, J. R., Stow, D.A.V., et al., 1988. *Proc. ODP, Init. Repts.*, 116: College Station, TX (Ocean Drilling Program).

<sup>2</sup> Shipboard Scientific Party is as given in the list of Participants preceding the contents.

which affects both the basement and the overlying sediments. Site 718 was drilled on a tilted fault block immediately to the south of the fault block drilled at Site 717 and is situated on a local heat flow high within a region of high and quite variable heat flow. One objective at Site 718 was to investigate the presence and nature of possible hydrothermal circulation inferred from the heat-flow pattern and, in particular, the relationship between the fault zones, bedding planes and the flow of water. A second objective was to investigate the development of the fan and distal fan depositional processes through time.

Hole 718A was dedicated to detailed pore-water geochemical studies. Holes 718B, 718C and 718E together drilled a continuous section from the seafloor to 961.6 mbsf. The low recovery at Hole 718C is a direct reflection of the thick section of relatively unconsolidated silt and silt to mud turbidites making up the distal fan sediments. Hole 718D was washed down to 70 mbsf to obtain additional interstitial water samples and temperature measurements. Two logging runs were made in Hole 718C; we obtained a good set of logs from 140 mbsf to a depth of 559.5 mbsf, where a bridge prevented further penetration. One logging run was made in Hole 718E from 935 mbsf to 173 mbsf. Coring results are summarized in Table 1.

**Principal drilling results:** The stratigraphic section recovered at Site 718 ranges from late Quaternary to early Miocene in age and has been divided into five main lithologic units. The dominant lithologies and ages of the stratigraphic sequence are as follows:

Unit I (0.0–2.0 mbsf): Clay and calcareous clay of Holocene to latest Pleistocene age.

Unit II (2.0–100.0 mbsf): Micaceous silt and silty mud turbidites of late Pleistocene age.

Unit III–IV (100.0–189.8 mbsf): Mud turbidites and silty mud turbidites with thin interbedded pelagic clays of Pleistocene to late Miocene age.

Subunit VA (189.8–605.0 mbsf) Silt and silty mud turbidites with thin, sporadic interbeds of mud turbidites and pelagic clays of late to middle Miocene age.

Subunit VB (605.0–961.6 mbsf) Silt and silty mud turbidites with up to 20-m-thick intervals of interbedded mud turbidites, biogenic turbidites and pelagic clays of middle to early Miocene age.

Sedimentation at Site 718 has been almost exclusively through fan deposition processes. The section consists mainly of a sequence of turbidites. An important discovery is that the Bengal Fan was well established at Site 718, 2500 km from the Ganges delta, by the early Miocene and has been receiving sediment, including wood fragments and sand-sized grains, since that time. Interpretation of seismic reflection data in light of the drilling results implies that fan sedimentation here may have begun suddenly in the earliest Miocene and that nearly the entire sedimentary section in this part of the central Indian Ocean consists of Bengal Fan turbidites. One implication is that major Himalayan uplift may have occurred at approximately 20 Ma.

Geochemical and temperature measurements at Site 718 found evidence for vigorous hydrothermal circulation. Geochemical studies of interstitial water shows throughout the section the effects of mixing between two end members, one of which is sea water and the other a water which has been chemically altered by interaction with basement rocks or by diagenetic processes. Temperatures measured in the silty turbidites of Unit II were actually higher than those measured in the upper part of the underlying clay turbidites of Unit III. Warm water appears to be rising up the fault to the north of Site 718 and spreading laterally through permeable layers in the upper silty turbidites. At the same time, cooler sea water may be flowing downward through silt layers within the predominantly clay turbidites below, which appear on seismic records to crop out several kilometers to the south along the upthrown side of the fault block.

## BACKGROUND AND OBJECTIVES

### Background

Site 718 is the second of three closely-spaced sites drilled near 1°S, 81°24'E in the central Indian Ocean approximately

800 km south of Sri Lanka and 200 km northwest of the Afanasy Nitikin Seamount group (Fig. 1). It lies at the distal end of the Bengal Fan within a large area of intraplate deformation, that affects both the ocean crust and the 1 to 2-km-thick pile of overlying strata.

Both deposition and deformation in this part of the central Indian Ocean have been affected by the collision between continental blocks on the Indian and Asian plates. This plate interaction began in the Eocene at anomaly 22 time (approximately 53 Ma ago) with a "soft collision", possibly between continental India and an island arc lying seaward of Asia (Powell and Conaghan, 1973), based on a halving of the spreading rate to 4 cm/yr at this time (Sclater and Fisher, 1974; Curray et al., 1982). A related regional unconformity observed on the proximal and mid fan areas (Curray and Moore, 1971) appears to coincide with a hiatus between Paleocene and middle Eocene strata based on extrapolation from DSDP Site 217 (Moore et al., 1974). During the Oligocene the spreading direction of the southeast Indian Ridge changed from N-S to NE-SW (Sclater et al., 1976), the spreading rate decreased still further to 2.5 cm/y and sedimentation in the area now covered by the Bengal Fan probably increased (Powell and Conaghan, 1973). The "hard" continent-continent collision may have occurred at this time, though other estimates are as late as late Miocene (Powell and Conaghan, 1973). A second prominent regional unconformity in the area of the Bengal Fan has also been dated as late Miocene by drilling at DSDP Site 218 (Thompson, 1974). The unconformity marking the onset of deformation in the distal fan is inferred by extrapolation to be this same event (Weissel et al., 1980).

Development of an incipient Bengal Fan probably began in the Eocene as a response to the "soft" collision and has continued to the present day, constructing the world's largest submarine fan over 2500 km long and over 12 km thick under the northern Bay of Bengal. In the area of Site 718, the sediment is approximately 1.5–2 km (2 s of two-way traveltime) thick under the very distal part of the fan. This enormous volume of sediments is assumed to have been derived principally from denudation of the uplifting Himalayan Mountains and supplied to the delta front via the Ganges-Brahmaputra river systems. Sediments are funneled efficiently to the fan via a delta-front trough, the "Swatch of No Ground." This trough is presently connected to only one active fan channel, but has been effectively cut off from rapid sediment supply as the most recent rise in sea level, probably about 7,000–10,000 yr ago. The fan channel appears to terminate some 50 to 100 km north of Site 718, and no channel or levee-type features have been observed on seismic reflection records from the Leg 116 study area.

Resistance to subduction of continental crust, combined with continued spreading on the southeast Indian Ridge, has apparently placed the central Indian Ocean under a north-south compressive stress regime (Stein and Okal, 1978). Deformation of the ocean crust is demonstrated by east-west striking long-wavelength (100–300 km) undulations with peak-to-trough amplitudes of 1–3 km extending roughly from the Chagos-Laccadive Ridge to the Ninety East Ridge and from 5°N to 10°S latitude (Weissel et al., 1980; Geller et al., 1983). Superimposed on the long-wavelength undulations are high-angle faults, spaced 5–20 km apart (Weissel et al., 1980; Geller et al., 1983). The top of the ocean crust is offset across these faults by up to 0.5 s (> 500 m) on seismic reflection records (Fig. 2). Up-to-the-north displacement of basement and predeformation strata has produced a series of rotated-fault blocks (Fig. 2). A prominent unconformity separates the predeformation sequence from an upper syn-deformation sequence that thins to the south against tilted (2–5°) block highs.

Heat-flow values from the deformed region are generally higher than expected for the 78-Ma age of the underlying crust,

however considerable scatter is present in the measurements. In particular, abnormally high heat-flow values are distributed widely over the central Indian Ocean (Anderson et al., 1977; Weissel et al., 1980; Geller et al., 1983). A detailed heat-flow study conducted as part of the precruise site survey for Leg 116 shows that there is great variability in the heat flow on a scale of a few kilometers (Fig. 3). The measured temperature-depth profiles associated with some of the highest values are nonlinear, suggesting an upward flow of water through the sediments (Geller et al., 1983).

### Objectives

Site 718 is located in 4730 m water depth on the back (north-ern) side of the fault block immediately south of the fault block on which Sites 717 and 719 were drilled (Fig. 2). The fault at the southern end of the block is exposed at the surface and the tip of the block outcrops, giving a positive seafloor relief of about 30 m. Sediment has been ponded locally to the north of this high and reflectors within the upper seismic unit are seen to lap onto and pinch out against reflector "A", which appears to mark the onset of deformation and may be equivalent to the upper unconformity of Curray and Moore (1971). The topmost, nearly flat-lying sediments are separated from the underlying tilted section by unconformity "B" at about 0.15 s depth.

The syn-deformation sedimentary section at Site 718 appears from the seismic records to be approximately half as thick as that at Site 717. The site is located on a heat-flow high (Fig. 3) to intersect any lateral migration of water that may be taking place.

The principal objectives of Site 718 were:

1. To investigate the possible migration of water along or upward through permeable zones within the sedimentary section and to assess the nature of this flow and its possible relationship to the high heat-flow anomaly;
2. To sample the different packets of strata (seismic sequences) separated by unconformities to investigate the relationship between these stratigraphic sequences and the various controls on sedimentation (i.e., Himalayan uplift, intraplate deformation, sea-level variation, fan channel migration);
3. To compare sedimentation on two adjacent fault blocks that have had different histories of uplift;
4. To drill a stratigraphically lower section than that drilled at Site 717 to study depositional processes on the distal fan prior to the onset of deformation; and
5. To examine and document the early stages of diagenesis that take place in deep-water fan sediments and, by comparison with the reference section drilled at Site 717, to assess the role of higher than normal heat flow on those early diagenetic changes.

### OPERATIONS

*JOIDES Resolution* approached Site 718 from the north, running a short seismic survey over the location of Site 717 and the proposed location of Site 719 as well of Site 718. The beacon was dropped as we passed over Site 718 and the line continued about 8 km farther south before the gear was pulled in and the ship returned to location at 01° 01.252'S, 81° 24.065'E at 0145 hours on 20 July 1987.

The PDR indicated a water depth of 4746.3 m. The first APC core was shot with the bit at 4741.3 m below the rig floor (4730.3 m below sea level) and 9.42 m of sediment was recovered. The entire core was dedicated to geochemical studies (Hole 718A). The bit was then positioned at 4741.5 m and a mud-line core of 9.26 m was recovered (Hole 718B). A second APC core was fired but the outer barrel failed in compression just below the latch assembly, probably as a result of discharg-

ing into a thick sandy silt layer just below the surface. The ship was moved 10 m and Hole 718C was washed down to 9.3 mbsf. The XCB was then deployed and continuous coring was undertaken to a depth of 935 mbsf, thereby setting yet another new record for XCB penetration. The last core of Hole 718C was brought on deck at 0815 hr on 29 July 1987. Average core recovery was 29.6%, being markedly better in the mud than in the silt lithologies.

The hole was prepared for logging and, after both hole and tool problems, two logging runs were made successfully from a bridge in the hole at 565 mbsf to the seafloor. The bottom of the drill pipe was positioned at 129 mbsf.

The pipe was then pulled to the surface and a new bit picked up. After we ran the pipe back to the seafloor, Hole 718D was drilled to 71 mbsf. Three heat-flow measurements were made and two cores attempted between 71 and 90 mbsf. Only 0.17 m of sandy silt was recovered. The TV camera was then lowered to the seafloor to test the equipment and to look for signs of upwelling hot water.

The ship departed Site 718 at 1630 hr on 2 August 1987 for Site 719. Following successful completion of the cruise objectives for Site 719, the ship returned to Site 718 so we could deepen the site as far as time would allow. The original beacon was found and the ship was on location at 1645 hr on 9 August 1987. Hole 718E was first drilled ahead with a rotary coring bit to a depth of 935 mbsf and then continuous rotary coring proceeded. However, hole conditions encountered were so severe that coring had to be terminated at a total depth of 961.6 mbsf, after we obtained only three additional cores (35% recovery). Details of the coring operation are given in Table 1.

The hole was then prepared for logging, but the bit-release mechanism failed to operate. A minicone was prepared and dropped at 1330 hr on 13 August and reentry achieved at 0915 hr on 15 August. The hole was reconditioned for logging. One successful logging run was made from 950 mbsf to the pipe, the bottom of which was set at 173 mbsf. The second tool string failed to get out of the pipe and into the hole because of a severely bent stand. With little time remaining, further attempts at logging were abandoned and Hole 718E was terminated.

The ship got underway for Colombo at 1500 hr on 17 August 1987.

## LITHOSTRATIGRAPHY

### Lithofacies

The stratigraphic sequence recovered at Site 718 ranges in age from Quaternary to early Miocene and consists predominantly of interbedded clay, silty clay and silt, with lesser amounts of sandy silt and calcareous clay. Seven facies are recognized at Site 718 on the basis of texture, sedimentary and biogenic structures, color, organic carbon content, and the presence or absence of calcareous microfossils.

#### *Facies 1. Silt and Silt-Mud Turbidites. (F1)*

Facies 1 consists of sharp-based, fining-upward beds of gray to dark-gray silt, or less commonly sandy silt, that grade up through silty clay to clay. Internally the beds are massive, or rarely display a faint horizontal lamination in the basal few centimeters. Beds of this facies range from 5 to 140 cm thick, averaging 40 cm. Silt to clay fractions are very micaceous (5–15%), generally quartz-rich (50–70%), and often slightly calcareous (2–10% calcite). Plant debris occurs scattered throughout the coarser portion of this facies and, rarely, forms 1- to 3-mm thick layers. Bioturbation and calcareous microfossils are rare.

#### *Facies 2. Organic-poor Mud Turbidites. (F2)*

Facies 2 consists of sharp-based, light greenish gray to gray silty clay that grades upward into clay. Bed thicknesses range be-

**Table 1. Coring summary for Holes 718A, 718B, 718C, 718D and 718E.**

Core No.	Date July 1987	Time	Sub-bottom top (mbsf)	Sub-bottom bottom (mbsf)	Meters cored (m)	Meters recovered (m)	Percent Recovery
1H	20	1600	0.0	9.5	9.5	9.42	99.1
					9.5	9.42	
1H	20	1650	0.0	9.5	9.5	9.26	97.5
					9.5	9.26	
1X	20	1955	9.3	18.8	9.5	0.01	0.1
2X	20	2100	18.8	28.3	9.5	0.27	2.8
3X	20	2250	28.3	37.8	9.5	4.91	51.7
4X	21	0025	37.8	47.3	9.5	0.96	10.1
5X	21	0140	47.3	56.8	9.5	0.00	0.0
6X	21	0320	56.8	66.3	9.5	0.00	0.0
7X	21	0530	66.3	75.8	9.5	0.00	0.0
8X	21	0950	75.8	85.3	9.5	0.00	0.0
9X	21	1115	85.3	94.8	9.5	0.10	1.1
10X	21	1250	94.8	104.3	9.5	0.24	2.5
11X	21	1430	104.3	113.8	9.5	5.47	57.6
12X	21	1900	113.8	123.3	9.5	3.38	35.6
13X	21	2025	123.3	132.8	9.5	3.22	33.9
14X	21	2200	132.8	142.3	9.5	8.23	86.6
15X	22	0215	142.3	151.8	9.5	3.95	41.6
16X	22	0620	151.8	161.3	9.5	9.07	95.5
17X	22	0810	161.3	170.8	9.5	9.29	97.8
18X	22	1315	170.8	180.3	9.5	0.54	5.7
19X	22	1500	180.3	189.8	9.5	6.90	72.6
20X	22	2100	189.8	199.3	9.5	2.86	30.1
21X	22	2240	199.3	208.8	9.5	0.04	0.4
22X	23	0020	208.8	218.3	9.5	0.05	0.5
23X	23	0140	218.3	227.8	9.5	0.04	0.4
24X	23	0310	227.8	237.3	9.5	0.08	0.8
25X	23	0445	237.3	246.8	9.5	2.18	22.9
26X	23	0635	246.8	256.3	9.5	0.65	6.8
27X	23	0820	256.3	265.8	9.5	1.42	14.9
28X	23	1000	265.8	275.3	9.5	0.70	7.4
29X	23	1120	275.3	284.8	9.5	1.90	20.0
30X	23	1320	284.8	294.3	9.5	0.78	8.2
31X	23	1510	294.3	303.8	9.5	0.07	0.7
32X	23	1700	303.8	313.3	9.5	3.70	38.9
33X	23	1815	313.3	322.8	9.5	0.40	4.2

tween 2 and 25 cm. Typically silt comprises no more than 10% of this facies. Beds are often marked by a 0.5- to 3.0-mm thick, quartz-rich, basal silt laminae. The upper portion of beds is generally bioturbated. Calcareous microfossils are largely absent.

#### **Facies 3. Organic-rich Mud Turbidites. (F3)**

Facies 3 is characterized by moderate amounts (2-10%) of plant debris and consists of very dark-gray to black, sharp-based, 3-35 cm thick (avg. 15 cm), fining-upward beds of silty clay grading into clay. Typically the basal few centimeters exhibit a silty horizontal lamination that passes upward into faint wispy laminations and finally a massive interval. Pyrite is found locally as concretions, or after burrows, in the clay, as well as silt-sized framboids(?) in the basal layer. The tops of the beds are commonly bioturbated.

#### **Facies 4. Biogenic Silt-mud Turbidites. (F4)**

This facies consists of sharp-based, fining-upward, light yellowish gray to olive-gray calcareous silt (rarely), silty clay and clay. Beds range in thickness from 2 to 30 cm. This facies occurs most commonly as massive calcareous silty clay to clay. Rarely, a faint horizontal lamination is discernible and in some cases the basal silt layer (0.5-4 cm thick) is cross-laminated (Fig. 4). Calcareous microfossils (mainly nannofossils, but with common foraminifers) are abundant, making up to 20% of the sediment. Unidentified calcareous silt and clay-sized material accounts for an additional 20-30% of the sediment.

#### **Facies 5. Pelagic Clays. (F5)**

This facies consists of gradationally based beds of clay 10-30 cm thick, varying in color between reddish brown, mottled red-green, and gray. Slight to moderate bioturbation is characteristic of this facies. Common trace fossils include Chondrites, Planolites, and Zoophycos. Ferro-manganiferous (?) chemical fronts characterize the gray clays of this facies. Calcareous microfossils are very rare or absent; those that remain show evidence of extreme dissolution.

#### **Facies 6. Pelagic Calcareous Clays and Oozes. (F6)**

Facies 6 consists of pale yellowish green to light gray, bioturbated, calcareous clay with a silt content generally 5% or less. This facies is characterized by an abundant fauna of nannofossils (up to 50%) and foraminifers (up to 5%). Minor bioturbation is common.

#### **Facies 7. Structureless Muds. (F7)**

Facies 7 consists of 10- to 190-cm thick beds of massive, gray, silty clay to clay that have indistinct lower bed boundaries. Beds generally exhibit light bioturbation throughout. Ferro-manganiferous (?) chemical fronts are absent, and calcareous microfossils are rare.

These facies (F1-F7) are similar to those found at Site 717, but with some significant differences. In particular, the greenish gray, nannofossil-rich, biogenic turbidites (F4), which characterize Unit III at Site 717, are not found at Site 718. The bio-

Table 1 (continued).

Core No.	Date July 1987	Time	Sub-bottom top (mbsf)	Sub-bottom bottom (mbsf)	Meters cored (m)	Meters recovered (m)	Percent Recovery
34X	23	1930	322.8	332.3	9.5	0.00	0.0
35X	23	2140	332.3	341.8	9.5	0.04	0.4
36X	23	2350	341.8	351.3	9.5	1.75	18.4
37X	24	0205	351.3	360.8	9.5	2.04	21.5
38X	24	0410	360.8	370.3	9.5	1.35	14.2
39X	24	0555	370.3	379.8	9.5	0.17	1.8
40X	24	0745	379.8	389.3	9.5	0.83	8.7
41X	24	1000	389.3	398.8	9.5	9.79	103.0
42X	24	1200	398.8	408.3	9.5	1.90	20.0
43X	24	1345	408.3	417.8	9.5	1.03	10.8
44X	24	1515	417.8	427.3	9.5	1.45	15.2
45X	24	1705	427.3	436.8	9.5	2.28	24.0
46X	24	1900	436.8	446.3	9.5	2.88	30.3
47X	24	2045	446.3	455.8	9.5	2.10	22.1
48X	24	2220	455.8	465.3	9.5	0.90	9.5
49X	25	0115	465.3	474.8	9.5	2.48	26.1
50X	25	0310	474.8	484.3	9.5	2.63	27.7
51X	25	0520	484.3	493.8	9.5	2.20	23.1
52X	25	0705	493.8	503.3	9.5	2.93	30.8
53X	25	0900	503.3	512.8	9.5	1.39	14.6
54X	25	1550	512.8	522.3	9.5	1.36	14.3
55X	25	1730	522.3	531.8	9.5	3.36	35.3
56X	25	1920	531.8	541.3	9.5	5.67	59.7
57X	25	2100	541.3	550.8	9.5	7.56	79.6
58X	25	2240	550.8	560.3	9.5	0.90	9.5
59X	26	0125	560.3	569.8	9.5	5.54	58.3
60X	26	0315	569.8	579.3	9.5	2.06	21.7
61X	26	0505	579.3	588.8	9.5	3.87	40.7
62X	26	0725	588.8	598.3	9.5	4.93	51.9
63X	26	1005	598.3	607.8	9.5	9.64	101.0
64X	26	1250	607.8	617.3	9.5	9.80	103.0
65X	26	1435	617.3	626.8	9.5	7.91	83.2
66X	26	1615	626.8	636.3	9.5	3.96	41.7
67X	26	1815	636.3	645.8	9.5	4.44	46.7
68X	26	2000	645.8	655.3	9.5	2.45	25.8
69X	26	2155	655.3	664.8	9.5	3.39	35.7
70X	26	2325	664.8	674.3	9.5	1.64	17.2
71X	27	0130	674.3	683.8	9.5	7.26	76.4
72X	27	0430	683.8	693.3	9.5	9.79	103.0
73X	27	0700	693.3	702.8	9.5	4.77	50.2

genic turbidites (F4) at Site 718 are thinner, whitish colored, and show a much higher percentage of silt. These biogenic turbidites are also found at a much lower stratigraphic level (in Unit V, below 630 mbsf). The thick-bedded, very dark-gray to black, organic-rich turbidites (F3) found in Units III and IV at Site 717, are lighter colored (less organic-rich?), occur less frequently, and are much thinner at Site 718. The absence of green biogenic turbidites and the limited occurrence of thick-bedded black organic-rich mud turbidites at Site 718 suggests that they were not deposited, or were eroded, as the combined thickness of Units III and IV is considerably thinner at Site 718 (85.5 m) than at Site 717 (381.6 m).

### Lithologic Units

To facilitate correlation between sites, the sedimentary sequence recovered at Site 718 is divided into five units corresponding to the five lithologic units defined at Site 717 (Fig. 5). These units are very similar to those found at Site 717, differing primarily in thickness and the number of subdivisions.

#### Unit I. Core 116-718B-1H; 0 to 2.0 mbsf

Unit I is only 2.0 m thick and is composed of clay and calcareous clay. The unit is capped by a 35-cm thick calcareous clay sequence (F6) which contains abundant calcareous and siliceous microfossils. The entire unit is disturbed by the initial core penetration so that it is difficult to interpret the origin of the brownish and grayish colored, biogenic-poor clays. By analogy with

the muds in Unit III (below), they are most likely of turbidite origin. Both the calcareous and siliceous microfossils in the uppermost layer show signs of dissolution, indicating that the seabed currently lies close to the lysocline and that the geochemical environment is not conducive to silica preservation.

#### Unit II. Cores 116-718B-1H, 116-718C-2X-10X; 2.0 to 100 mbsf

Unit II is approximately 98.0 m thick. The lower boundary is not well defined, but must occur somewhere between 95 and 104.3 mbsf. Very poor recovery (15%) was obtained from this interval. Cored sediments consist mainly of silt and silt-mud turbidites (F1). In the two cores with the best recovery (Core 116-718B-1H, 97.5%, and Core 116-718C-3X, 51.7%) the turbidite beds attain a maximum thickness in excess of 70 cm (40 cm silty base), but generally range from 10 to 30 cm thick (2- to 6-cm silty base). The silty layers at the base of the turbidites in these cores form only about 10–15% of the section, with silty clay and clay without bioturbation constituting the majority of the turbidite beds. Approximately 20% of the section is either bioturbated or apparently structureless mud. These mud sequences may represent *pelagic* clays (F5), or, more probably, they represent bioturbated tops of thin mud turbidites (F2).

The lack of recovery throughout the rest of the unit, together with some core-catcher samples of similar gray silt and clays, indicates the continuation of this facies to about 100 mbsf. It is probable that the recovery voids represent sections with a higher silt-to-mud ratio, or with coarser and cleaner silt.

Table 1 (continued).

Core No.	Date July 1987	Time	Sub-bottom top (mbsf)	Sub-bottom bottom (mbsf)	Meters cored (m)	Meters recovered (m)	Percent Recovery
74X	27	0915	702.8	712.3	9.5	2.04	21.5
75X	27	1045	712.3	721.8	9.5	0.02	0.2
76X	27	1230	721.8	731.3	9.5	0.63	6.6
77X	27	1400	731.3	740.8	9.5	0.77	8.1
78X	27	1605	740.8	750.3	9.5	7.87	82.8
79X	27	1755	750.3	759.8	9.5	4.25	44.7
80X	27	1945	759.8	769.3	9.5	3.65	38.4
81X	27	2140	769.3	778.8	9.5	3.71	39.0
82X	27	2330	778.8	788.3	9.5	2.54	26.7
83X	28	0115	788.3	797.8	9.5	2.00	21.0
84X	28	0320	797.8	807.3	9.5	1.92	20.2
85X	28	0530	807.3	816.8	9.5	1.48	15.6
86X	28	0735	816.8	826.3	9.5	4.70	49.5
87X	28	0915	826.3	835.8	9.5	2.25	23.7
88X	28	1150	835.8	845.3	9.5	5.28	55.6
89X	28	1345	845.3	854.8	9.5	0.83	8.7
90X	28	1540	854.8	864.3	9.5	2.46	25.9
91X	28	1730	864.3	873.8	9.5	1.13	11.9
92X	28	1920	873.8	878.0	4.2	0.36	8.6
93X	28	2140	878.0	887.5	9.5	0.91	9.6
94X	28	2340	887.5	897.0	9.5	9.72	102.0
95X	29	0200	897.0	906.5	9.5	1.22	12.8
96X	29	0420	906.5	916.0	9.5	1.08	11.3
97X	29	0615	916.0	925.5	9.5	0.95	10.0
98X	29	0815	925.5	935.0	9.5	0.43	4.5
					925.7	274.05	
Aug. 1987							
1X	02	0355	71.0	80.5	9.5	0.17	1.8
2X	02	0750	80.5	90.0	9.5	0.00	0.0
					19.0	0.17	
1R	12	1310	933.1	942.6	9.5	2.22	23.3
2R	12	1515	942.6	952.1	9.5	4.50	47.3
3R	12	1810	952.1	961.6	9.5	3.20	33.7
					28.5	9.92	

**Unit III-IV. Cores 116-718C-10X-19X; 100 to 189.8 mbsf**

Identification of a Plio-Pleistocene hiatus (which occurs within Unit III at Site 717) between Cores 116-718C-11X and -718C-12X indicates that at least 5.5 m of Unit III is present at Site 718. However, no clear lithologic distinction is found between Units III and IV at Site 718; the green biogenic turbidites which characterize Unit III at Site 717 are absent at Site 718. Therefore, these two units are described together below, and referred to as Unit III-IV.

Unit III-IV is 89.8 m thick and consists dominantly of interbedded thin- to medium-bedded, dark-gray, organic-rich mud turbidites (F3) and thin- to medium-bedded, gray, organic-poor mud turbidites (F2). The organic-poor mud turbidites become increasingly more abundant toward the bottom of Unit III-IV. This increased abundance is coincident with the presence of thin-bedded silt-mud turbidites (F1) which occur as a minor facies in the lower half of the unit. Facies 4 is present as one 11-cm thick white, biogenic turbidite bed (Sample 116-718C-17X-6, 15-26 cm). "Pelagic" clays (F5) tend to occur as thin "caps" on the turbidite facies. In addition, medium- to thick-bedded structureless muds (F7) are found interbedded with the facies above between the following intervals: 104-117 mbsf, 133-140 mbsf, and 161-168 mbsf.

**Unit V. Cores 116-718C-20X to -98X, 189.8 to 935.0 mbsf; 116-718E-1R to -718E-3R, 933.1 to 961.6 mbsf**

Unit V is 771.8 m thick and is dominantly a monotonous sequence of silt and silt-mud turbidites, based on the limited re-

covery. This unit has been subdivided into two subunits based on the abundance of red pelagic clays (F5), and the presence of biogenic turbidites (F4).

**Subunit VA. Cores 116-718C-20X to -718C-63X; 189.8 to 605.0 mbsf**

Subunit VA is 415.2 m thick and yielded particularly poor recovery (22%). Recovered sediments consist of silt to silt-mud turbidites (F1) with thin, sporadic interbeds of organic-poor mud turbidites (F2) and pelagic clays (F5). Turbidite thicknesses range from a maximum of >80 cm (40 cm silty base) to a minimum of about 1 cm (1- to 2-mm silty base), and average 3-15 cm thick (1- to 5-cm thick silty base). Within a given turbidite sequence the silt-size fraction averages 20-30%. Within the limitations of recovery, it appears that there are alternating zones of thicker and thinner turbidites sometimes showing thickening-upward and thinning-upward trends over a few meters of section. Wireline log interpretations provide additional evidence for these trends (see "Logging" section).

**Subunit VB. Cores 116-718C-63X to -718C-98X, 605 to 935 mbsf; 116-718E-1R to -3R, 933.1 to 961.6 mbsf**

Subunit VB is 356.6 m thick and yielded relatively better recovery (38.5%) than Subunit VA. Facies types represented are similar to Subunit VA, mainly silt and silt-mud turbidites (F1), with minor mud turbidites (F2) and pelagic clays (F5). Subunit VB shows more abundant mud-rich intervals which range from 1 m to 20 m in thickness and commonly contain thin, white biogenic turbidites below 630 mbsf (Fig. 4).

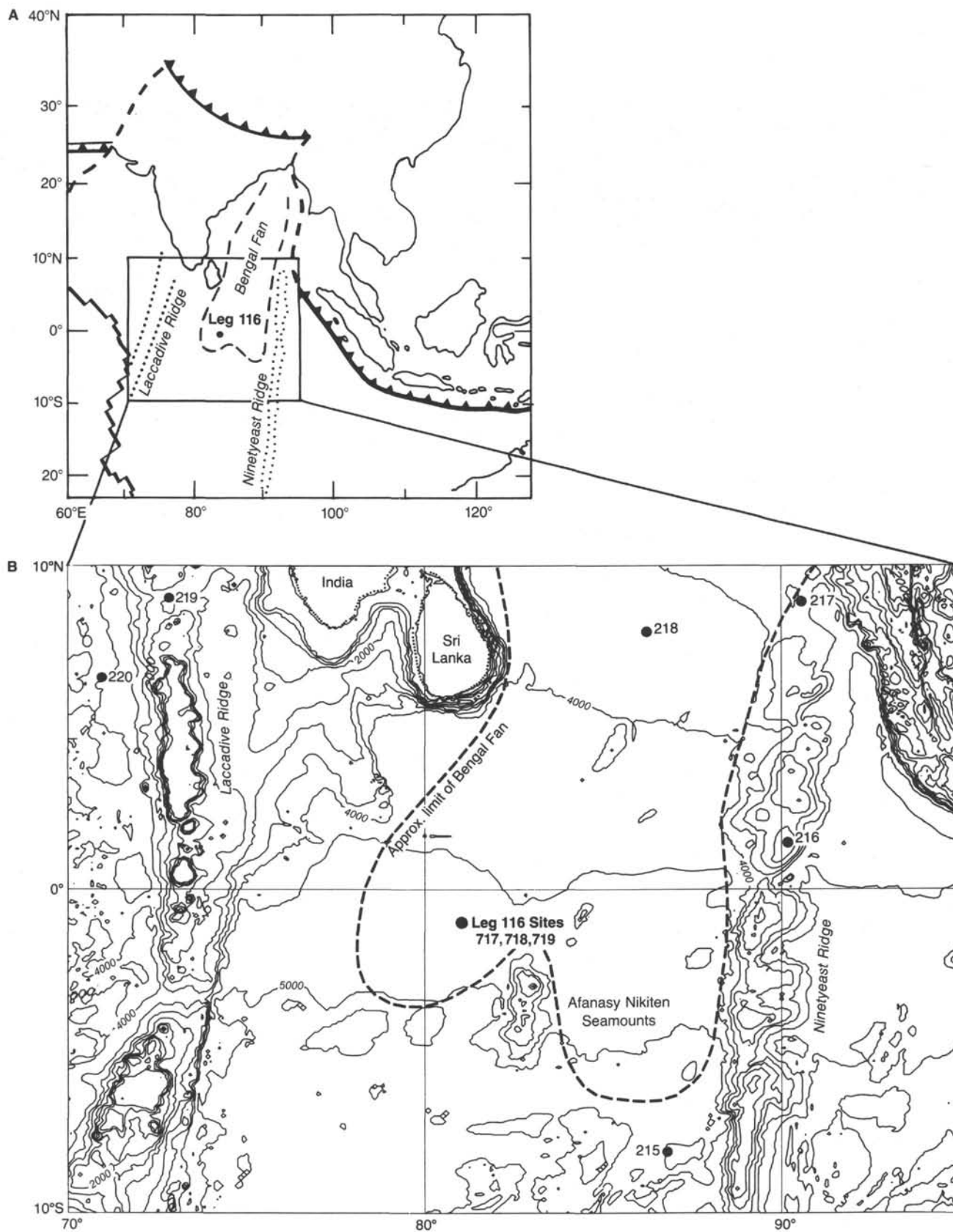


Figure 1. Location maps for the Leg 116 sites. A: Setting of the Leg 116 sites relative to tectonic elements of the eastern Indian Ocean. Heavy solid line represents mid-ocean ridge axes, dashed lines are transform plate boundaries, and sawtooth pattern shows convergent plate boundaries. B: Setting of Leg 116 sites within the north central Indian Ocean. Bathymetry is machine-contoured DBDB10 gridded data at 500-m intervals. Location of DSDP drill sites within the region is also shown.

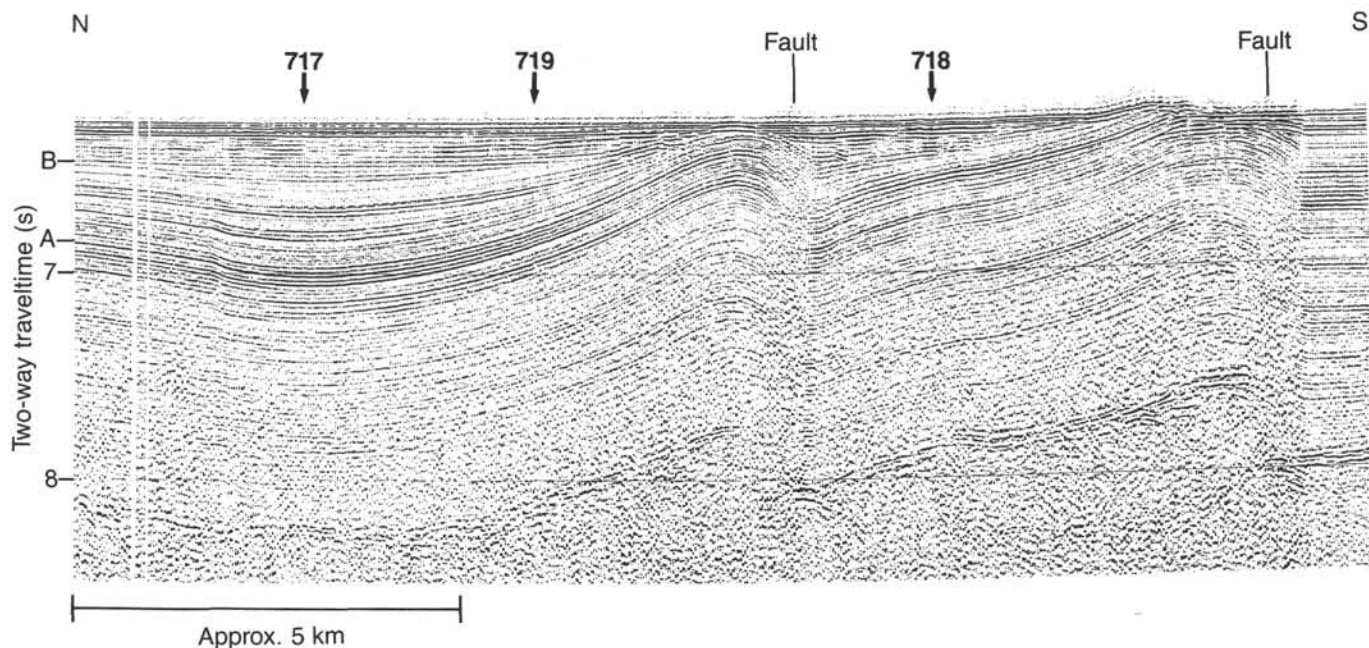


Figure 2. North-south seismic reflection profile across the Leg 116 drill sites. Locations of Sites 717, 718, and 719 are shown. Also noted are the locations of the faults bounding the tilted blocks and prominent unconformities A and B.

The mud-rich intervals comprise very thin-bedded, greenish gray silt-mud turbidites that generally grade upward into reddish brown clay. Thin zones of bioturbated and featureless chocolate red-brown clays that appear more pelagic in nature also occur, becoming more frequent with depth. No more than 20% of the clay section can be considered pelagic and deposition was probably influenced by a significant amount of turbidite clay suspension.

#### Maximum Quartz Grain Size

Maximum grain size was determined at approximately 10-m intervals at Site 718. In each case the coarsest lithology in the individual core (generally from the base of the coarsest turbidite) was chosen for smear-slide examination and the largest equant quartz grain measured. Results are shown graphically in Figure 6.

Maximum grain size ranges from 30 to 610  $\mu\text{m}$  (coarse silt to medium sand on the Wentworth Scale). Not surprisingly, the coarsest maximum grain size corresponds to the sandy silt and silt turbidites of Facies 1 within Units II, IV, and V. In addition, the analysis shows that grains at least as coarse as 600  $\mu\text{m}$  reached Site 718 via turbidity currents since the early Miocene (700–935 mbsf, Fig. 6).

#### Carbonate Content

The downhole carbonate content from selected intervals at Site 718 is shown in Figure 7. There is an overall increase in carbonate content with depth, with maximum values just below 15% from 0 to 500 mbsf, and maximum values in the 15–25% range below 500 mbsf. The *noisy* appearance of the plot is largely a facies effect, with coarser grained facies tending to possess higher carbonate contents than finer grained facies. The 45% value at 750 mbsf corresponds to a biogenic turbidite facies (F4). The increase in carbonate content with depth may reflect a source change, or diagenetic effects.

## BIOSTRATIGRAPHY

### General

Site 718 yielded usable siliceous microfossils only from the youngest sediments immediately below the seafloor. Radiolarians, diatoms and silicoflagellates are present in some abundance, but disappear rapidly downcore and are represented below this level only as rare, pyrite-replaced specimens. Calcareous microfossils, too, are most abundant near the seafloor and disappear rapidly downcore. Planktonic foraminifers are particularly scarce and occur, with rare exceptions, predominantly as fragmented or diminutive specimens in the occasional chalky layers in the sediment column. Benthonic foraminifers occur more consistently, but this group also is represented for the most part by small specimens of little utility. Calcareous nannofossils occur sporadically throughout the core, in specimen-rich and species-poor residual assemblages in white, chalky, and some green and gray calcareous clay, layers. However, through most of the section they are present in such low concentrations—a few to a few tens of specimens per slide—as to be regarded as little more than *background noise*. It is this poor record, nevertheless, that forms the backbone of the biostratigraphy, indeed the entire chronological framework, for this site. This type of record hardly inspires confidence, but the rationale for using it is that it is the best available.

### Radiolarians

Well-preserved radiolarian assemblages at Site 718 are limited to the uppermost core at each of the three holes. Below the top, only a few specimens of radiolarians occur sporadically down to Core 116-718C-11X. Core 116-718C-41X yielded pyritized radiolarians. The remainder of samples did not contain any radiolarians, even though the total number of samples processed at this site was approximately 170, including core-catcher and shipboard paleontology samples.

Sample 116-718B-1H-1, 5–10 cm, the topmost sediments of reddish brown and light gray mottled clay, contains a moder-

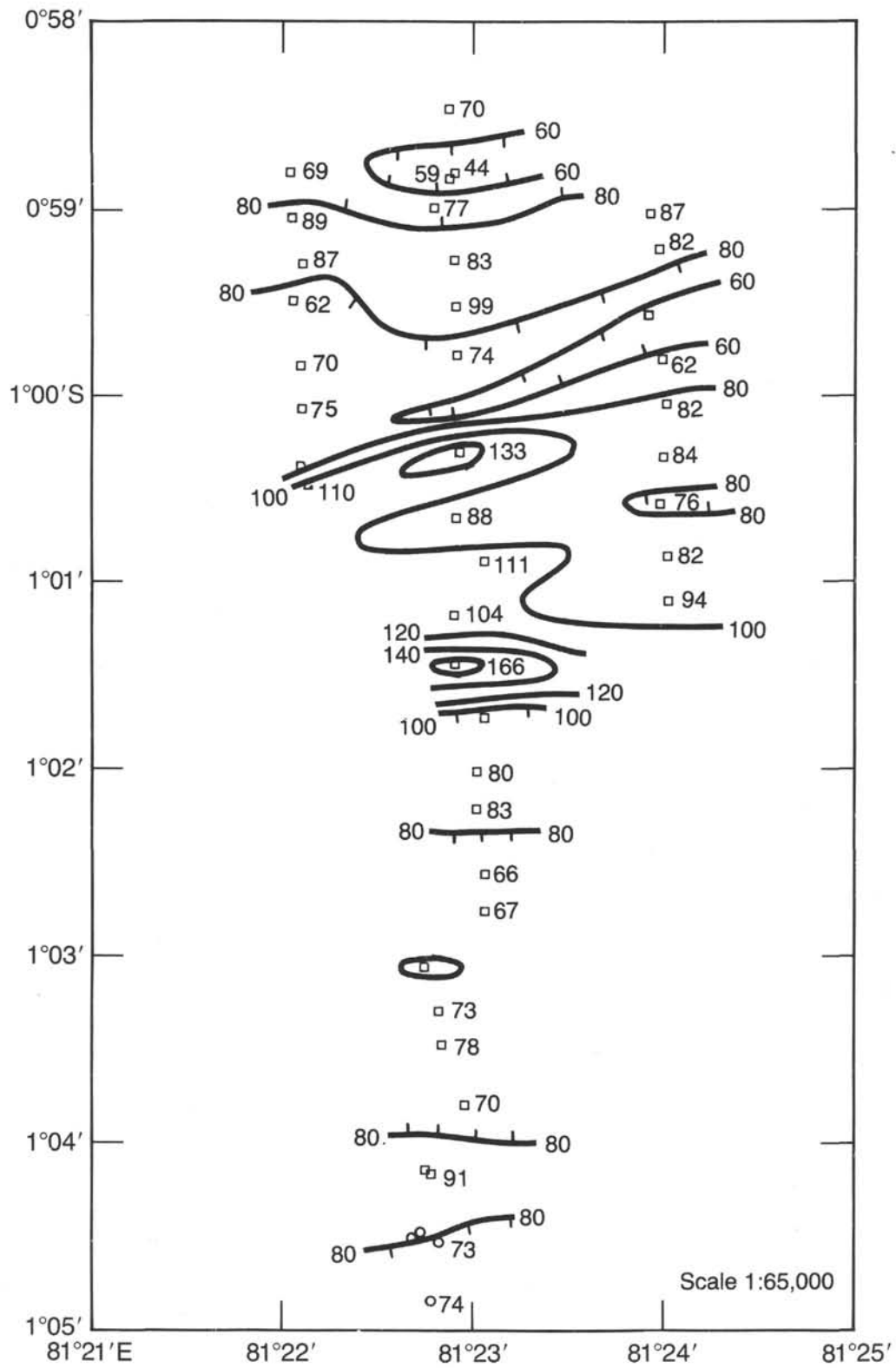


Figure 3. Detailed contour map of heat-flow measurements. Squares and circles are heat-flow stations with their values in  $\text{mW}/\text{m}^2$  (after J. K. Weissen, unpublished data).

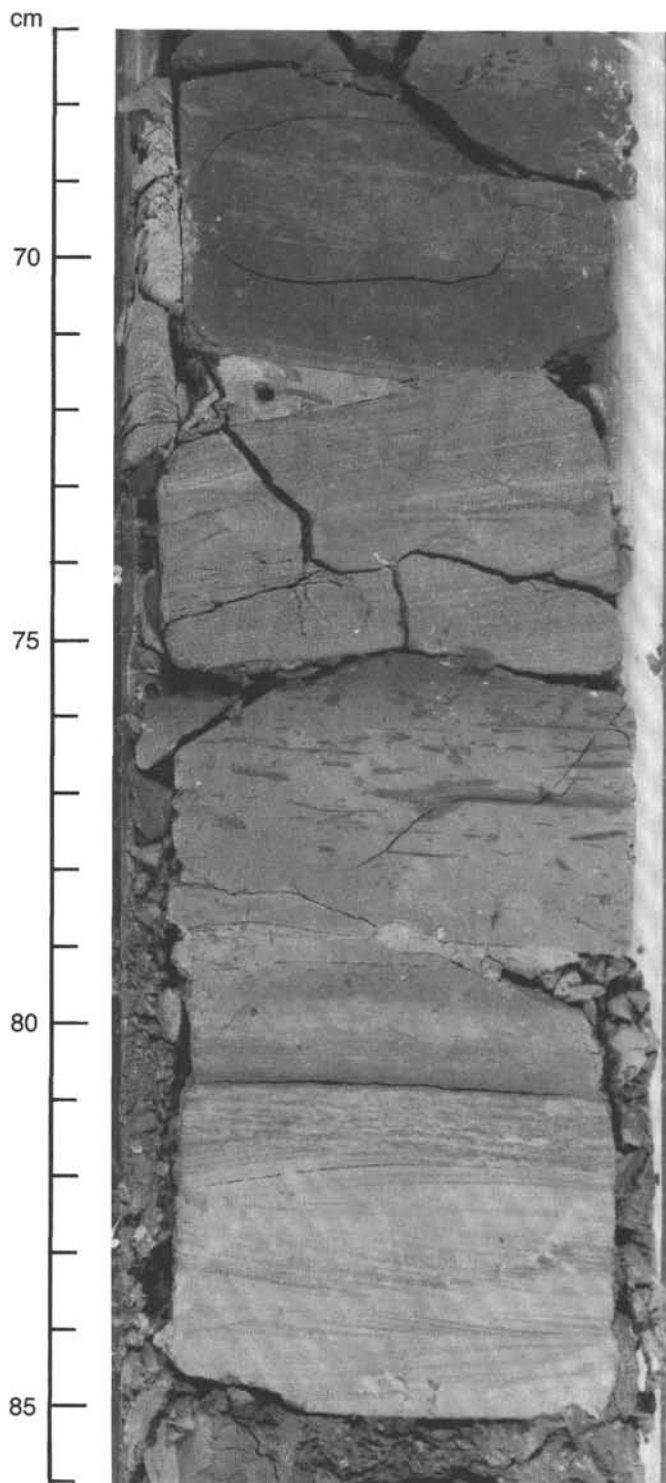


Figure 4. Photograph of two successive facies 4 biogenic silt-mud turbidite beds (Core 116-718C-94X, 75–78 cm and 66–74 cm), showing low-angle cross-bedded silty bases grading up into bioturbated clay.

ately preserved radiolarian assemblage of Quaternary age including *Acanthodesmia vinculata*, *Octopyle tetrapyle*, *Euchitonia elegans*, *Heliodiscus asteriscus*, *Spirocyrtilis scalaris*, *Hymeniastrum euclidis*, *Ommatodiscus fragilis*, and several other species.

Sample 116-718B-1H-1, 22–27 cm, a pinkish gray clay, contains an abundant well-preserved and diversified (> 50 taxa) radiolarian fauna similar to the biocoenosis reported from the tropical Atlantic and Pacific (Takahashi and Honjo, 1981). Diagnostic species in the sample include *Amphispyris costata*, *Anthocyrtilidium ophirensis*, *A. zanguebaricum*, *A. maritalis*, *Acrosphaera spinosa*, *A. murrayi*, *Acanthodesmia vinculata*, *Botryostrobus aquilonaris*, *Botryocyrtilis scutum*, *Collosphaera tuberosa*, *C. huxleyi*, *Carpocanarium papillosum*, *Didymocyrtilis tetrathalamus tetrathalamus*, *Euchitonia elegans*, *Eucyrtilidium acuminatum*, *Heliodiscus asteriscus*, *Hymeniastrum euclidis*, *Hexacanthium axotrias*, *Lamprocyrtilis nigrinae*, *L. hannai*, *Lithopera bacca*, *Phormosticoartus corbula*, *Pterocanium praetextum praetextum*, *P. trilobum*, *Pterocorys campanula*, *P. zancleus*, *P. hertwigi*, *Rhodosphaera* group, *Siphonosphaera polysiphonia*, *Spongaster tetras tetras*, *S. pentas*, *Stylochamydium asteriscus*, *Theocorythium trachelium trachelium*, *Theocalyptra davisiana cornutoides*, and many more species. All of the listed species occur in the plankton biocoenosis. However, dissolution-susceptible species of the biocoenosis (> 100 taxa) are not present in the sample, apparently lost due to dissolution. The taphocoenosis is considered to be of Holocene age.

*Spongaster pentas* is found in Sample 116-718B-1H-1, 22–27 cm. In the geologic record this taxon is known to occur only in the middle Pliocene *S. pentas* Zone. However, this species is found in the modern oceans (McMillen and Casey, 1978; Takahashi and Honjo, 1981). The modern form of *S. pentas* may be different from the Pliocene form in the patterns of its five or six characteristic spongy lobes (D. Johnson, pers. commun. 1986). In any case, *S. pentas* has never been recorded from either late Pliocene or Pleistocene marine sediments. Thus, the presence of this species in the sample is another indication of the Holocene age as there is no Pliocene or older marker species present.

The Holocene productivity of Site 718 must be high, based on the morphology of several radiolarian species. For example, skeletons of *E. elegans* have well-developed patagium, an auxiliary spongy skeletal meshwork, that is known to occur in highly productive areas such as the Panama Basin (Takahashi and Honjo, 1981).

Somewhat less diversified but similar Quaternary assemblages were encountered in Sections 116-718B-1H, CC, -718A-1H, CC, -718C-1X, CC, and in Samples 116-718A-1H-3, 140–150 cm, and -718A-1H-4, 140–150 cm. Whether these samples are of Holocene or Pleistocene age is unclear and requires further work to determine.

The following sections contained several radiolarian specimens, but they were not enough to assign ages: 116-718C-4X, CC, *Octopyle tetrapyle*; 116-718C-10X, CC, *Zygocircus* spp. and a spumellarian, gen. et. sp. undet.; and Sample 116-718C-11X-1, 2–4 cm, *Zygocircus* spp. and a spumellarian, gen. et. sp. undet.

Sample 116-718C-41X-3, 20–26 cm, contained a few specimens of pyritized radiolarians. Because of the pyritization all examinations were done with the scanning electron microscope, but this did not yield much useful information. Eight different taxa are recognized but most of them are identified only to generic or family levels. Among these, three specimens are nearly conformable with either *Acrosphaera spinosa fasciculopora* or *A. spinosa hamospinosa* which were described from the western South Pacific by Caulet (1986) in DSDP Leg 90. Unfortunately, all three specimens lack the tips of their spines, which are one of the key features of the subspecies identification. Apparently, they have been broken off. Caulet states that these two subspecies are very abundant near the end of *Stichocorys peregrina* Zone (lower Pliocene), but timings of the first occurrences of these two subspecies are not known.

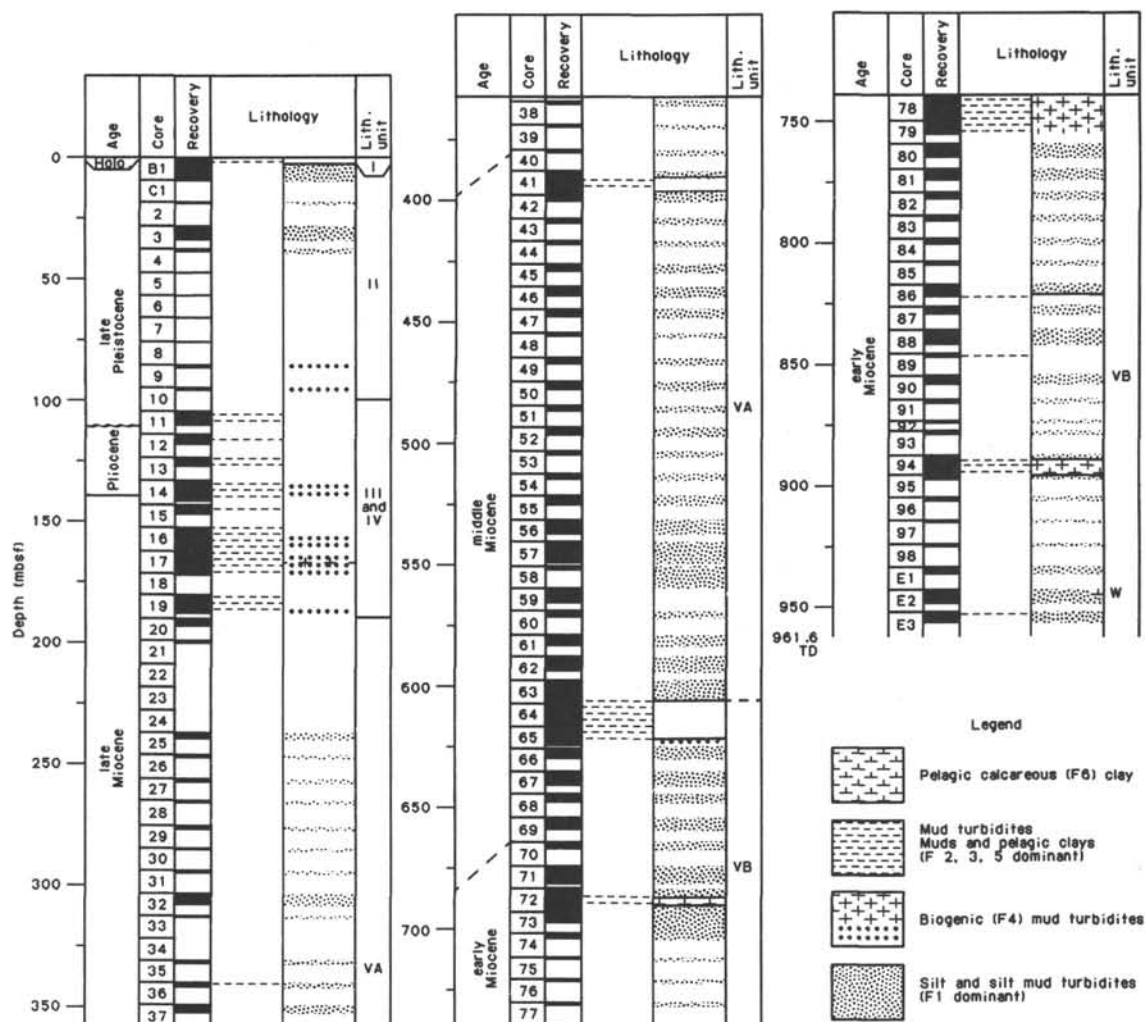


Figure 5. Summary of lithostratigraphy at Site 718.

### Silicoflagellates

Only several specimens of *Dictyocha* sp. were preserved in the topmost Holocene sediments and they did not yield any useful information concerning biostratigraphy of the Site. Silicoflagellates were not encountered in any of the remaining cores, probably due to dissolution and dilution with enormous amounts of terrigenous material.

### Diatoms

In 166 samples examined, isolated specimens of diatoms were present only in 15 of them (from Cores 116-718C-1H, -3X, -4X, -10X, -11X, -13X to 18X, -24X, -29X and -51X). *Thalassiosira oestrupii*, a Plio-Pleistocene, low-latitude diatom, is present in Sections 116-718C-1H, CC and 718C-3X-3, 51 cm.

In all other samples the diatoms recovered were nearly always much older and apparently redeposited into the strata in which they occur. For example, *Actinocyclus ingens* (Section 116-718C-4X, CC) is known from the middle Miocene (approximately 13–15.5 m.y.). The few other species which were present have long stratigraphic ranges (Late Cretaceous–Holocene) and could not reveal even the age of the eroded source sediments.

### Foraminifers

Foraminifers were sporadic to absent throughout the section with the exception of the top of Holes 718A, 718B, and 718C,

which contain a rich planktonic assemblage. In what appear to be pelagic ooze layers (crypto-turbidites, pseudo-crypto-turbidites or paraturbidites?) at several levels in the section, the planktonic foraminifers were represented by only the most resistant species and by highly fragmented tests, or were absent. Benthic foraminifers in these samples, however, were more diversified and fairly well preserved. Sandy and silty layers were mostly barren or contained few displaced benthic species. The assemblages were always rare and rarely diagnostic. Consequently the zonal or age assignment given at several depths in the hole was not very reliable. Moreover the residual assemblages were severely affected by downhole contamination and reworking. For zonal designation reference is made to Bolli et al. (1985).

### Biostratigraphic Evaluation of Foraminifers

A Holocene age was recognized in Sample 116-718B-1H-1, 15–17 cm, which contains a rich foraminiferal assemblage with *Bolliella adamsi*. Further below, and based on the occurrence of *Globorotalia hessi*, Section 116-718C-10X, CC can be referred to Zone N22. Therefore Cores 116-718C-1X to -718C-10X have been assigned to the Pleistocene.

Cores 116-718C-14X to -55X seem to span the basal middle Pliocene to late Miocene based on the occurrence of *Sphaeroidinellopsis seminulina*, which ranges from Zone N16 to the basal

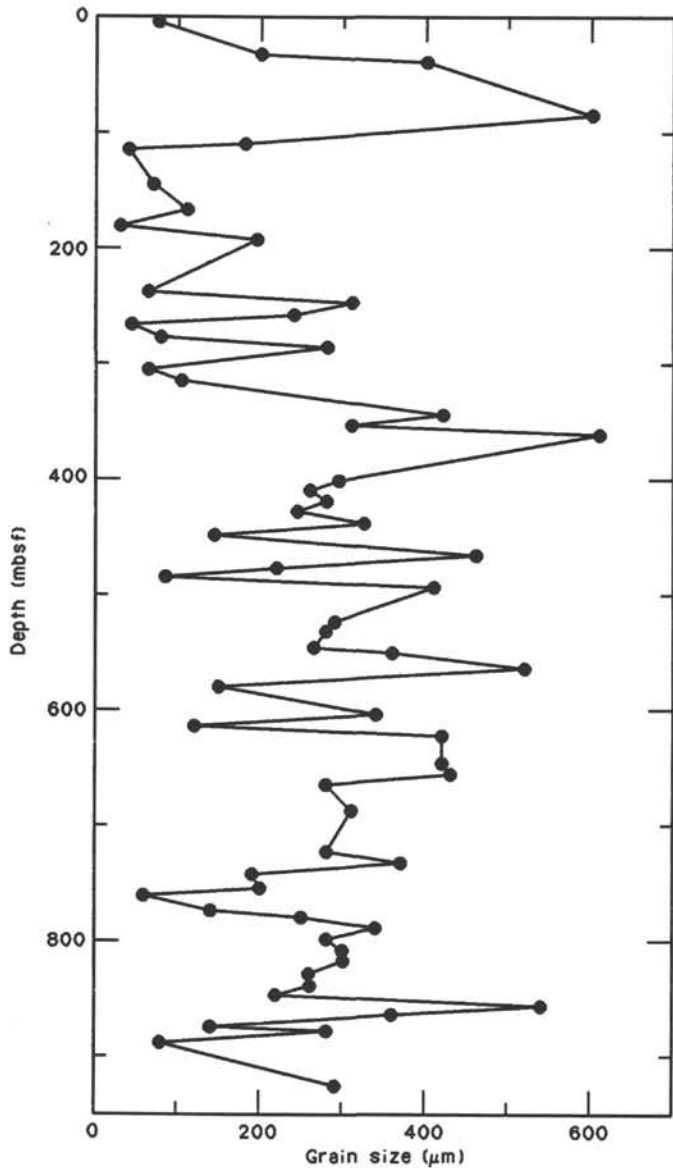


Figure 6. Graph of maximum grain size vs. depth, Site 718.

part of Zone N20. However, the samples from this interval do not contain *Sphaeroidinella dehiscentes*, a species that normally occurs in residual assemblages and which first appears in the early Pliocene (Zone N19). The occurrence of only one specimen of *Sphaeroidinella dehiscentes* in Section 116-718C-39, CC, is judged to be due to downhole displacement. For this reason a late Miocene age assignment is considered more reasonable.

From Core 116-718C-60X downward there is no additional indication of a late Miocene age. In Section 116-718C-67X, CC the co-occurrence of *Globorotalia mayeri* and *Globigerinoides subquadratus* is indicative of a middle Miocene age. Zone N11/12, recognized by the presence of *Globorotalia foehsi* s.l. and *G. foehsi lobata*, is identified in Sample 116-718C-72X-3, 110-112 cm.

An early Miocene age is presumed from Sample 116-718C-79X-2, 57-59 cm downward. Evidence for this is the occurrence in Sample 116-718C-94X-5, 64-66 cm of *Globorotalia peripheroronda* and *Praeorbulina* sp., which indicates that this sample is referable to Zone N8. Sample 116-718C-94X-6, 117-119 cm

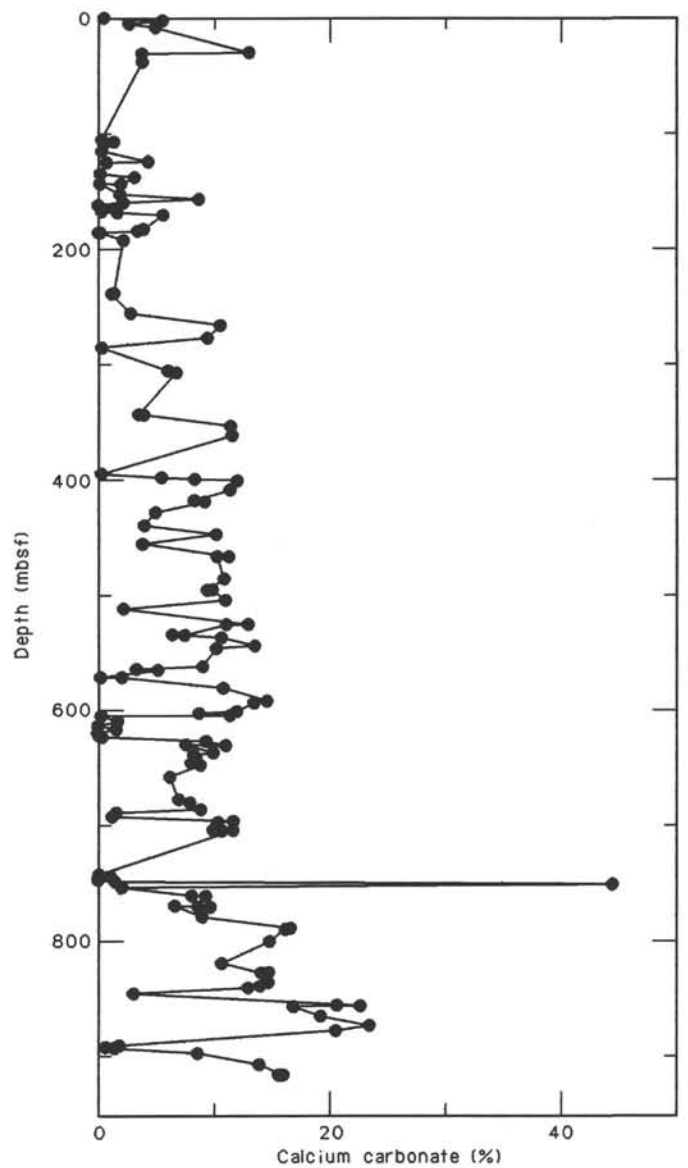


Figure 7. Graph of calcium carbonate content vs. depth, Site 718.

is assigned to Zone N7 based on the presence of *G. peripheroronda* and *Globigerinoides bisphericus*.

### Calcareous Nannofossils

Coccoliths and other calcareous nannofossils occur at irregular intervals, and in widely varying abundances, in the cores recovered at Site 718. Nannofossils are predictably rare in the silty intervals. At best, rare specimens of only the most durable species are present and much of the silty sediment is largely barren. As at Site 717, the most nearly complete nannofossil assemblages were recovered only at, and immediately below, the seafloor, and these are essentially late Pleistocene assemblages. At burial depths of more than a few meters only residual assemblages were recovered, from which all but the most solution-resistant species have been removed by dissolution. Nannofossils occur in considerable abundance in the several white, chalky layers as well as in certain green, clayey and black, clayey layers in the generally more silty sediment section. In all cases, however, even these fossil-rich layers yielded only residual assem-

blages. Some of these fossiliferous layers show distinct graded bedding and the fossils from them are clearly redeposited. In others graded bedding is not obvious, but there is the distinct possibility, based on the frequency of redeposited older materials, that all of the nannofossils have been redeposited except the Pleistocene assemblages near the seafloor. It is all the more remarkable that a distinct zonal succession can be recognized in the section. Apparently all redeposition of fossiliferous sediments was penecontemporaneous with formation of those sediments.

Normally ubiquitous redeposited Cretaceous coccoliths constitute a remarkably small proportion of the coccoliths, and their presence is most noticeable in the very sparsely fossiliferous, silty turbidites. Rare Eocene and Oligocene nannofossils also occur among the older redeposited forms, although these are so scarce as not to present a real problem.

All age assignments are based on the Okada and Bukry (1980) numerical zonal designation, as at Site 717. The numerical ages assigned to various biohorizons or datums are taken almost entirely from Berggren et al. (1985), with the exception of the age of the *Sphenolithus heteromorphus* highest occurrence datum, which is clearly younger in tropical latitudes (e.g., the Caribbean) than the age assigned to it in the Berggren et al. (1985) compilation.

#### Biostratigraphic Evaluation of Nannofossils

Holes 718A and 718B, each consisting of one core, yielded late Pleistocene nannofossils, a rather poor assemblage from the former and a more nearly representative, though still impoverished (residual), assemblage from the latter. *Emiliania huxleyi* is present only in Core 116-718B-1H-1, and part of this core is, therefore, assigned to the late Pleistocene Zone CN15, with an age less than 0.28 m.y. The next lower marker, *Pseudoemiliana lacunosa*, occurs sporadically from the core catcher of this same core on down but may be reworked in the upper part of its occurrence. Consequently, no precise level can be assigned to the highest occurrence of this species. Undifferentiated Pleistocene nannofossils continue to the bottom of Core 116-718C-11X, though in much reduced numbers and as assemblages of a few, solution-resistant, species with an occasional sprinkling of older contaminants. Very poor core recovery as well as unfavorable lithology contribute to the inadequate biostratigraphy. A short interval with no core recovery between Cores 116-718C-11X and -718C-12X may contain a hiatus. Sample 116-718C-12X, 40–42 cm, yielded only a single specimen of *Discoaster*, but core 116-718C-13X immediately below yielded a reasonably diverse early to mid-Pliocene assemblage containing abundant *Reticulofenestra pseudumbilica* and *Sphenolithus abies*. This level (Section 116-718C-13X-2, 126 cm) is succeeded below by an essentially late Pliocene succession to Sample 116-718C-15X-1, 44–46 cm, and the early to mid-Pliocene assemblage above is considered redeposited (and may be exactly equivalent to a similar-age redeposited assemblage in Section 116-717C-35X-CC). Mid- to late-Pliocene assemblages continue to the level of Section 116-718C-16X-1, 68 cm, but the next sample below, (Section 116-718C-16X-5, 148 cm) contains *Discoaster quinqueramus*, a late Miocene marker that occurs consistently from this level downward, thus implying a greatly attenuated early Pliocene section or a hiatus. The Pliocene/Miocene boundary is placed between the last two samples and is assigned an age of 5.6 m.y.

Late Miocene nannofossils were recovered sporadically downward through Core 116-718C-40X and to the top of a clayey interval in Core 116-718C-41X. The middle Miocene marker *Discoaster hamatus* is present in Section 116-718C-41X-2, 64 cm and again in Section 116-718C-41X-3. The age assigned to this level is 10 m.y. (It should be noted here that placement of the late Miocene/middle Miocene boundary remains debatable. In

two recent compilations the late Miocene/middle Miocene boundary is placed variously at 11.1–11.3 m.y. (Bolli et al., 1985), i.e., within Zone CN7, the *Discoaster hamatus* Zone; and at about 10.5 m.y. (Berggren et al., 1985), i.e., within Zone CN6, the *Catinaster coalitus* Zone. Clearly, there is a wide choice of dates available.)

The next lower datum is the lowest occurrence of *Catinaster coalitus*, a surprisingly persistent and durable middle Miocene species in Sample 116-718C-59X-1, 100–102 cm. This datum corresponds to the boundary between Zones CN5 and CN6, and the age associated with it is 10.8 m.y. Below this datum the nannofossils are notably rare and unremarkable—generalized Miocene species with few distinguishing characteristics—down to the highest occurrence of *Sphenolithus heteromorphus* in Sample 116-718C-72X-3, 110–112 cm, which marks the top of Zone CN4. The age assigned to this level, based on primary data from low-latitude DSDP sites, is approximately 13.7 m.y., which is substantially different from the ages assigned to it in the previously cited two recent compilations. However, both of those compilations imply nannofossil to planktonic foraminifer correlations that are incompatible with published data on the ranges of marker species. The middle Miocene/early Miocene boundary is placed, albeit again rather arbitrarily, in the largely barren interval of about 40 m immediately above the highest occurrence of *Sphenolithus heteromorphus*. This is stratigraphically close to where Bolli et al. (1985) place the boundary, although the age given here is substantially younger. However, is well above the level at which Berggren et al. (1985) place the middle Miocene/early Miocene boundary.

Only one additional datum was encountered in Hole 718C and that is the highest occurrence of *Helicosphaera ampliaperta* in Section 116-718C-81X, CC. This datum marks the top of Zone CN3 and has an associated age of 16.2 m.y. Although this latter species was recorded from only one core, *Sphenolithus heteromorphus*, whose lowest occurrence marks the lower limit of Zone CN3, occurs down to Section 116-718C-96X, CC. In the remaining two cores below this no further diagnostic nannofossils were recovered. It is reasonable to infer, therefore, that the base of Zone CN5 probably was not penetrated and that the maximum age for the bottom of the core hole is something less than 17.1 m.y., the age associated with the *Sphenolithus heteromorphus* first (lowest) occurrence.

#### Sediment Accumulation Rate

The ages derived from paleontological analysis—chiefly nannofossils—and the corresponding depths are given in tabular form in Table 2. They are also given on a depth vs. age plot on Figure 8 in the form of a sediment accumulation rate curve. The following discussion should be preceded by the caveat that paleontological control over much of the cored interval is not as good as could be desired; consequently, the sedimentation rate plot could be significantly distorted over certain segments. The plot suggests a high sedimentation rate during the late Pleistocene (0–<1 m.y.), during the late middle Miocene (10.0–10.8 m.y.), and during the latest early Miocene (16.2–<17.1 m.y.). Sediment accumulated at the rate of 122, 226, and 174 m/m.y., respectively, in each of these three intervals. Extremely low sediment accumulation rates are indicated for the early Pleistocene and for the late Pliocene. However, this interval contains a major hiatus; very little early Pleistocene and late Pliocene sediment was identified, and it is reasonable to surmise that sediments of that age are either much attenuated or nonexistent at this site. It is not surprising that these same intervals are represented by similarly low sedimentation rates at Site 717. Clearly there seems to have been a period—the first million years (more or less) of the Pleistocene and much of the early Pliocene—during which detrital sediments were not deposited in this particu-

**Table 2. Depths and ages of Neogene nannofossil biohorizons at Site 718.**

Depth (mbsf)	Age (m.y.)
113.8	<0.93
126.0	3.5
151.3	5.6
391.5	10.0
572.3	10.8
686.9	13.7
778.8	16.2
935	17.1

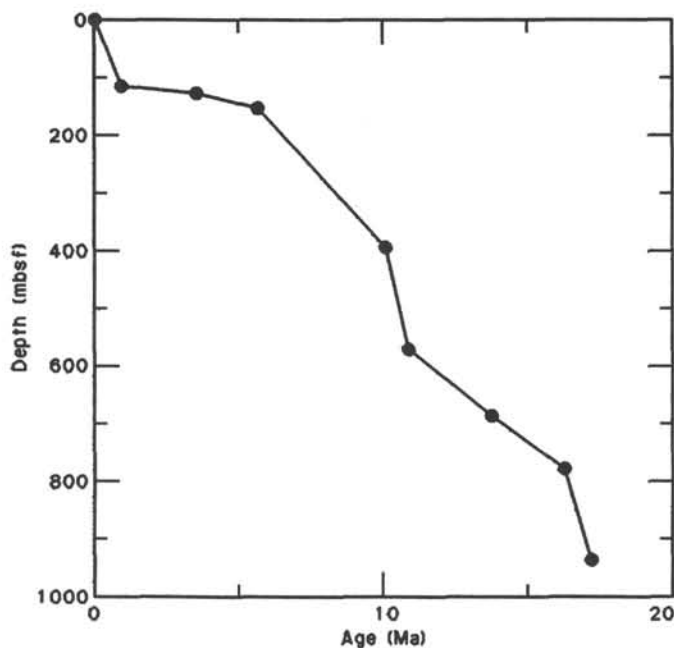


Figure 8. Sediment accumulation rate at Site 718.

lar region of the distal Bengal Fan. It is unclear whether this lack of deposition should be attributed to blocking or diversion of the turbidity current-transported sediment as by an intervening barrier, raised by regional tectonics, or whether the supply of sediment was curtailed in the source area in the Ganges-Brahmaputra delta system or even beyond by relative tectonic quiescence in the Himalayas.

## ORGANIC GEOCHEMISTRY

Hydrocarbon gases, organic carbon, and organic material characteristics of samples from Site 718 were routinely monitored. Details of the methods and procedures are given in the Site 717 chapter. Instrumentation is described in the Explanatory Notes.

### Hydrocarbon gases

#### Vacutainer Gases

No samples were obtained for Vacutainer gas analysis at any depths due to the apparent lack of gas in the cores. The sedimentary at Site 718 sequence is extremely poor in organic carbon, which occurs as amorphous, hydrogen-rich Kerogen (Tissot et al., 1974).

### Extracted Gases

As a whole,  $C_1$  concentrations at all depths are considerably lower than at Site 717. However,  $C_2$  values, although low, are similar to those at Site 717; consequently, the ratio of  $C_1$  to  $C_2$  at Site 718 is generally lower. The results are shown in Table 3 and Figure 9.  $C_1$  concentrations are very low, under 10 ppm, above 300 mbsf. Microbiological gases were apparently not generated in spite of the presence of organic carbon. This is reflected by the fact that sulfate in the interstitial water is greater than 10 mmol/L.  $C_1$  concentrations increase abruptly at the depth of 360 mbsf and remain constant (300–600 ppm) between 400 and 600 mbsf. They become very much lower (under 40 ppm) between 660 and 750 mbsf. However, the organic carbon content does not show a similar change with depth. The reason for this is not clear, but it may be due to a lack of active organic material. Below 800 mbsf,  $C_1$  concentrations show a scattered increase with depth.  $C_2$  contents range from 0 to 8.3 ppm; these low amounts are most likely derived from microbial sources. The ratios of  $C_1/C_2$  (Fig. 10) are less than 10 above 300 mbsf and increase rapidly to about 300 at 400 mbsf. The ratios are nearly constant with depth between 400 and 600 mbsf and become lower (i.e., 15 to 90), from 600 to 750 mbsf. The ratios show a scattered increase below 750 mbsf. This variation of the  $C_1/C_2$  ratio with depth reflects variation in the total  $C_1$  concentration. Rice and Claypool (1981) suggest that the amount of  $C_2$  appears to be proportional to both the temperature and the age of the sediment, and Claypool and Kvenvolden (1983) point out that an exponential increase in  $C_2$  content with depth is commonly observed in oceanic sediments. At Site 718,  $C_2$  concentrations do not increase with depth, which suggests that the sediments are relatively young and contain nonmarine organic matter.

### Carbon

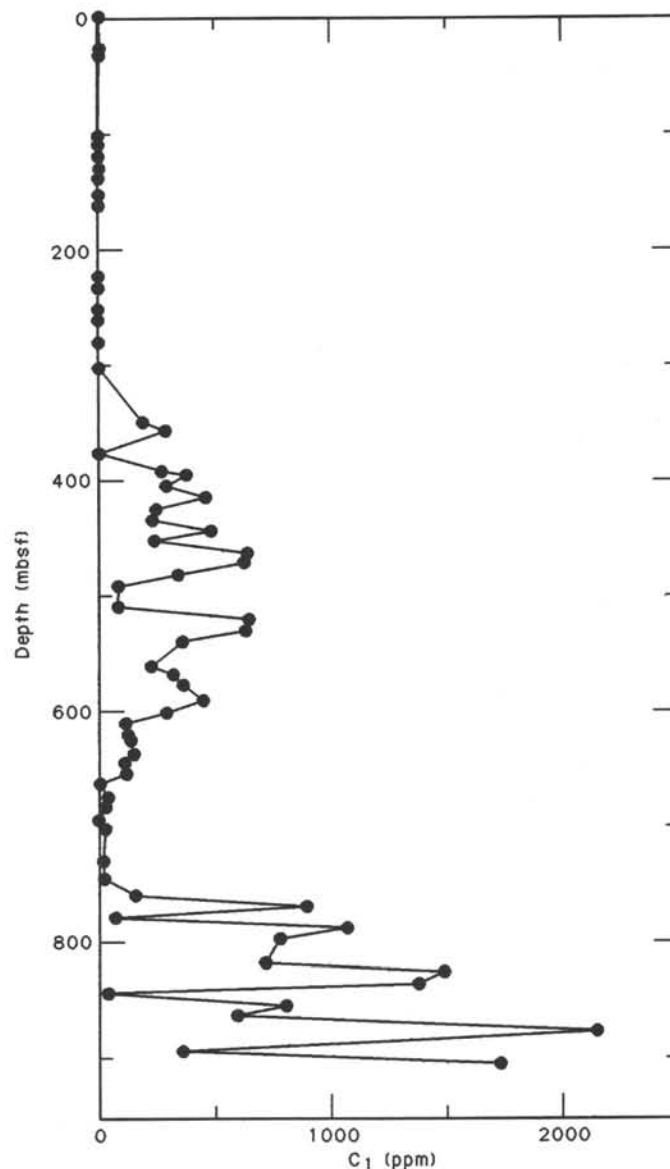
The inorganic carbon (IC) was determined using the Coulometrics Carbon Dioxide Coulometer. The total carbon (TC) was obtained by means of Coulometrics 5030 carbonate carbon apparatus. The organic carbon (TOC) was obtained from Rock Eval. Table 4 gives the values of total carbon displayed in Figure 11. The upper 175 m of sediment is moderately rich in organic matter (average organic carbon content of 1.0%), whereas below 175 mbsf the total organic carbon ranges from 0.1 to 0.5% (average 0.25%). The sulfate reduction is not complete, because sulfate content of pore water remains at more than 10 mmol/L through the upper 175 m. Therefore, bacterial activity in the upper part is higher than that at depth, where sulfate reduction was finished. This fact suggests that the supply of organic carbon or the sedimentation rate was higher in the shallower position of the section than in the deeper part. The boundary corresponds to the lithological boundary between Unit IV and Unit V, and indicates that the organic carbon content of the more clayey sediment is higher than that of the silt and silt-mud turbidites. There appears also to be a cyclic change of organic carbon concentration at Site 718 similar to that observed in the upper 500 m as at Site 717. This cyclicity may result from variations in paleoclimatic paleoceanographic or depositional factors, but requires a more detailed evaluation of closely-spaced samples and measurements on stable isotopes of carbon before more definite conclusions can be reached.

### Rock Eval

Data from Rock-Eval pyrolysis are listed in Table 4 for the 55 samples from Site 718. Hydrogen Index (HI) and Oxygen Index (OI) values are plotted on a van Krevelen-like diagram (Tissot and Welte, 1984) (Fig. 12). All samples have  $T_{max}$  values less

Table 3. Headspace gases at Site 718. Concentrations in ppm.

Section	Int bot	Int top	SBD (m)	C <sub>1</sub> (ppm)	C <sub>2</sub> (ppm)	C <sub>3</sub> (ppm)	C <sub>1</sub> /C <sub>2</sub>
<b>HOLE 718A</b>							
1H-5	0	5	6.00	7.1	1.2		5.9
<b>HOLE 718C</b>							
3X-3	0	5	31.30	5.9	1.2		5.0
4X-1	0	5	37.80	6.1	1.1		5.5
11X-3	0	5	107.30	3.2	0.5		6.4
12X-2	0	5	115.30	3.1	0.8		3.9
13X-2	0	5	124.80	2.8			3.9
14X-3	0	5	135.80	6.2	1.4		4.4
15X-2	0	5	143.80	3.6	1.5		2.4
16X-5	0	5	157.80	2.9	0.5		2.4
17X-5	0	5	167.30	2.0	0.8		2.5
19X-4	0	5	184.80	3.4	0.9		2.8
20X-2	0	5	191.30	2.8	2.4	0.3	1.2
24X-1	0	5	227.80	2.9	2.0	1.5	
25X-2	0	5	238.80	1.0	1.0	1.0	
27X-1	0	5	256.30	2.4	2.4	0.2	1.0
28X-1	0	5	265.80	2.5	0.9	2.8	
30X-1	0	5	284.80	2.8		0.6	
32X-3	0	5	306.80	4.9	3.5		1.4
37X-2	0	5	352.80	191.8	4.1		46.8
38X-1	0	5	360.80	286.1	3.3		86.7
40X-1	0	5	379.80	5.0	1.6	3.1	
41X-5	0	5	395.30	273.0	1.2		227.5
42X-1	0	5	398.80	378.0	3.0		126.0
43X-1	0	5	408.30	292.0	1.0	0.5	292.0
44X-1	98	103	418.78	461.0	4.4		105.0
45X-2	0	5	428.80	247.0	3.0		82.3
46X-2	0	5	438.30	232.0	0.8		290.0
47X-2	0	5	447.80	483.5	0.9		537.0
48X-1	0	5	455.80	239.7	1.9		126.0
49X-2	0	5	466.80	638.3	1.7		376.0
50X-1	0	5	474.80	625.6	2.5		250.0
51X-2	0	5	485.80	343.0	2.5		137.0
52X-2	45	50	495.75	86.0	3.6		23.9
54X-1	96	101	513.76	85.0	0.3	0.3	243.0
55X-2	0	5	523.80	647.0	0.1		6470.0
56X-2	0	5	533.30	631.0	3.4		186.0
57X-2	0	5	542.80	363.5	3.7		98.2
59X-4	0	5	564.80	225.0	0.8	1.3	281.0
60X-1	145	150	571.25	322.3			
61X-2	0	5	580.80	363.6	1.5	0.8	242.0
62X-3	135	140	593.15	449.0	1.5		300.0
63X-5	0	5	604.30	291.0	0.4	0.2	437.5
64X-5	0	5	613.80	117.0	3.3	0.2	35.5
65X-5	0	5	623.30	126.0	2.0		63.0
66X-2	0	5	628.30	138.0	1.6	0.6	85.5
67X-3	0	5	639.30	151.0	5.0	0.2	32.0
68X-2	0	5	647.30	111.6	2.1		53.0
69X-2	0	5	656.80	120.0	2.0		60.0
70X-1	0	5	664.80	6.2	0.4		15.5
71X-3	0	5	677.30	39.9			
72X-2	0	5	685.30	26.6	0.8		33.0
73X-3	0	5	696.30	0.0			
74X-2	0	5	704.30	26.0		0.2	
77X-1	0	5	731.30	19.0	5.1	0.9	5.8
78X-5	0	5	746.80	25.5	0.9		28.3
80X-2	0	5	761.30	159.0	5.8	0.7	27.4
81X-2	0	5	770.80	893.2	7.1		125.8
82X-2	0	5	780.30	72.6	1.7	0.5	42.7
83X-1	145	150	789.75	1069.3	4.2		254.5
84X-1	135	140	799.15	780.5			
86X-3	0	5	819.80	718.0	2.3		312.0
87X-1	110	115	827.40	1494.0	8.3	0.7	180.0
88X-2	0	5	837.30	1381.0	5.3		261.0
89X-1	0	5	845.30	38.5	3.8	0.5	10.0
90X-2	0	5	856.30	806.0	6.8	0.5	119.0
91X-1	0	5	864.30	596.0	7.5		79.0
93X-1	0	5	878.00	2154.0	11.9	0.8	181.0
94X-6	0	5	895.00	360.0	1.3		278.0
96X-1	0	5	906.50	1737.0	6.1		284.7

Figure 9. Plot of headspace methane concentration, C<sub>1</sub>, vs. depth at Site 718.

than 450°C except Sample 116-718C-12X-2, 60–64 cm (115.9 mbsf) (545°C), suggesting that the organic materials are immature with regard to petroleum generation. The HI and OI values range from 0 to 160 and from 0 to 470, respectively. The samples with HI values less than 160 are believed to have a significant component of terrestrial woody organic materials (Type III, Kerogens). However, the OI in two Samples (116-718C-30X-1, 34–39 cm and 116-718C-78X-4, 140–150 cm) are less than 20, indicating the presence of Types I and II kerogens, which are derived from marine algae and marine plankton, respectively. They have relatively low amounts of organic carbon (0.15 and 0.13%), which indicates that the terrestrial supply was small. Rashid (1985) points out that surface sediment in this area contains organic carbon between 0.5 and 1.0%. However, the organic carbon of the sediment from Hole 718C below the depth of 200 mbsf is less than 0.4%. This fact suggests that the terrestrial supply had been less than that above the depth of 200 mbsf or that there was a geological event during which the terrestrial supply into this area changed.

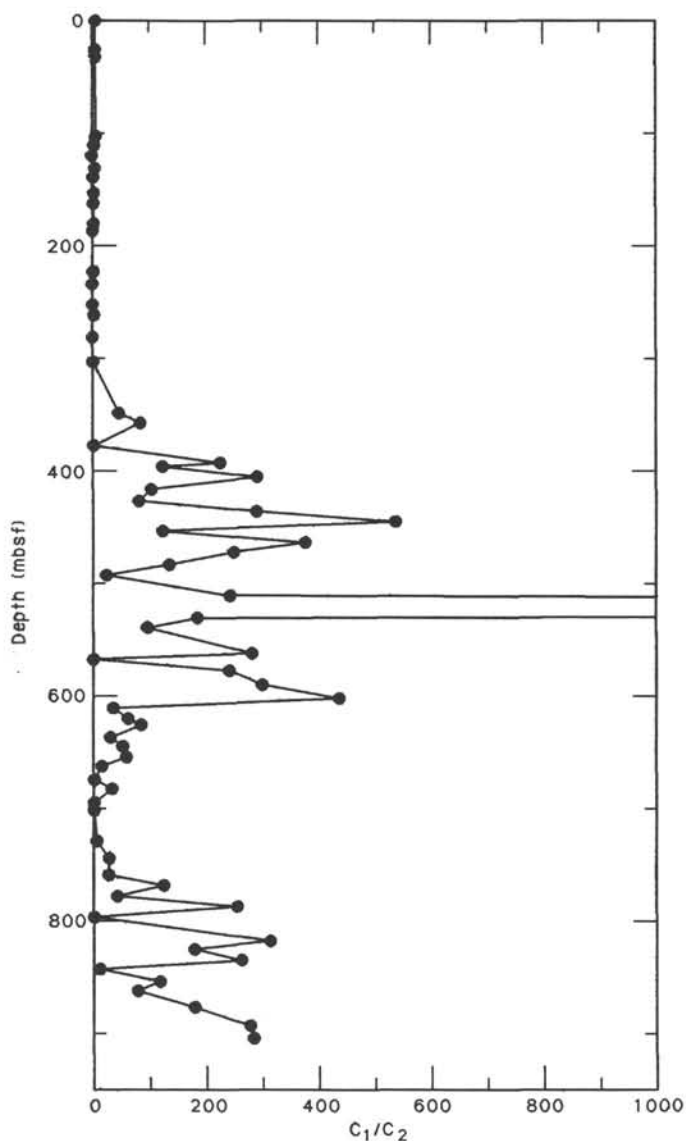


Figure 10. Methane/ethane ( $C_1/C_2$ ) ratios in gas extracted from Site 718 sediments by the headspace procedure.

## INORGANIC GEOCHEMISTRY

One of the purposes of drilling at Site 718 was to study the possibility of fluid circulation in relation to intraplate deformation. Anomalous heat flow was recorded in the vicinity of the site, leading to expectations of active hot fluid circulation.

### Sampling and Methods

Fluid sampling was carried out at both Holes 718A and 718C. Core 116-718A-1H was devoted to checking if a gradient in the upper 9 m could indicate upward flow. Cores from Hole 718C were sampled at regular intervals when recovery enabled good-quality sampling. In several cases there was no sediment recovery; this circumstance is believed due to a high proportion of unconsolidated silt layers, particularly at depths of 30–100, 195–235 and 700–730 mbsf. In several cases the sediment sample was quite indurated and composed mostly of compacted clays, in which case a limited volume of pore water (less than 7 cm<sup>3</sup>) was recovered. In one instance, near 747 mbsf, no water was obtained upon squeezing the mud to 12 MPa.

In addition, two *in-situ* water samples were obtained from Hole 718D utilizing the Barnes-Uyeda probe. The purpose of Hole 718D was to obtain more information about the 70–100 m depth range where previous sampling was unsuccessful and where previous temperature measurements indicated the advection of a hot fluid. The Core (116-718D-2I) obtained at 80.5 mbsf most probably came from a silt layer and had a composition identical to the drilling fluid. This can be explained by the permeation of the drilling fluid into the silt following the washing operation that preceded the *in-situ* water sampling. We will not discuss this sample further. The Core (116-718D-3I) obtained at 90 mbsf, most probably near the silt/clay boundary (lithological Units II and III) had a composition different from the drill fluid and will be discussed in the following section.

The analytical methods and procedures employed for interstitial waters (IW) are the same as for Site 717 and are described in the Explanatory Notes chapter (this volume).

## Results

### Chloride (Cl), Sodium plus Potassium (Na + K)

The concentrations of Cl and Na + K show large variations (Fig. 13). Here again, as observed at Site 717, the contrasting effect of compaction on the composition of fluids associated with clay and silt-sand layers can be seen on Cl and Na + K depth profiles. In the clay layers there is a decrease of Cl and Na + K, whereas in the silt-sand layers there is an increase of Cl and Na + K. The bulk effect of compaction is toward a slight increase of Cl and Na + K.

From a depth of 30 mbsf there is a decrease in the (Na + K)/Cl ratio, which reflects the effect of clay diagenesis on the composition of IW as depth increases. This effect is larger in the clay-rich layers (110–195, 390–397, 605–625, 740–750, and 855–895 mbsf) than in the silts.

### Calcium (Ca)

As shown in Figure 13, the Ca vs. depth trend is almost linear with  $dCa/dz = 9 \text{ mmol}/(\text{L} \times \text{km})$ . This could be due to conservative behavior of Ca. However, since the porosity is not constant, this trend cannot be so simply interpreted. The increase may be partly due to the effect of Ca-Mg exchange in clay minerals.

The local variations of Ca are often correlated with alkalinity (shown by dotted lines in Fig. 13) and may be related to carbonate precipitation and to variations in end-member fluids. Micrite formation as well as carbonate cements have been observed extensively at Site 718.

### Magnesium (Mg)

As shown in Figure 13, the concentration-depth profile of Mg can be divided in three parts:

- 0–30 mbsf: Mg is about the same as in sea water.
- 107–240 mbsf: there is an almost linear decrease of Mg with depth together with a good correlation with  $\text{SO}_4$  characterized by  $dMg/d\text{SO}_4 = 1$ .
- 240–930 mbsf: There is a smooth decrease of Mg with increasing depth. Significant variations are almost all enveloped by two parallel linear trends (curves a and b on Fig. 13). This zone can be characterized by  $dCa/dMg = -0.55$ , and by a positive correlation with  $\text{SO}_4$ .

The decrease of Mg with depth, mostly in zone 3, could be characteristic of conservative behavior. However, because the porosity is not constant this is probably partly due to Ca-Mg exchange during clay diagenesis. There is no clear correlation of Mg with Cl. However, it seems that there is a positive correla-

Table 4. Rock-Eval data summary, Site 718.

Section	Int top	Int bot	Depth (mbsf)	Wt (mg)	TMAX	S1	S2	S3	PI	S2/S3	PC	TOC	HI	OI
HOLE 718A														
1H-1	40	44	0.40	103.5	397	0.17	0.78	1.81	0.18	0.43	0.07	1.96	40	92
1H-2	140	150	2.90	99.5	334	0.05	0.12	0.85	0.31	0.14	0.01	0.55	22	155
HOLE 718C														
3X-2	145	150	31.25	98.3	408	0.02	0.00	0.00	1.00		0.00	0.41	0	0
4X-1	44	46	38.24	103.1	315	0.06	0.11	1.51	0.37	0.07	0.01	0.48	22	314
11X-2	140	150	107.20	102.1	340	0.07	0.31	1.05	0.18	0.29	0.03	0.97	32	108
11X-4	60	64	109.40	98.8	393	0.22	0.88	2.32	0.20	0.37	0.09	2.41	37	96
12X-2	60	64	115.90	98.5	545	0.03	0.23	0.20	0.12	1.15	0.02	0.21	109	95
13X-1	140	150	124.70	102.6	440	0.08	0.54	1.07	0.13	0.50	0.05	0.46	117	233
15X-1	140	150	143.70	101.9	380	0.06	0.13	0.80	0.33	0.16	0.01	0.56	23	142
16X-6	79	82	160.09	102.7	379	0.22	0.21	3.66	0.52	0.05	0.03	2.19	9	167
17X-4	140	150	167.20	103.0	450	0.07	0.49	1.33	0.12	0.36	0.04	1.80	27	73
18X-cc	22	25	171.02	99.4	319	0.08	0.11	1.04	0.44	0.10	0.01	0.55	20	189
19X-3	140	150	184.70	99.2	412	0.02	0.06	1.73	0.25	0.03	0.00	0.12	50	1441
20X-2	80	84	192.10	101.6	394	0.00	0.03	0.21	0.00	0.14	0.00	0.17	18	124
25X-1	140	150	238.70	97.2	307	0.02	0.02	0.16	0.50	0.12	0.00	0.16	12	100
25X-2	20	24	239.00	101.3	371	0.04	0.26	0.43	0.13	0.60	0.02	0.14	186	307
27X-1	67	71	256.97	99.3	277	0.02	0.01	0.31	1.00	0.03	0.00	0.32	3	97
28X-cc	0	4	266.22	99.8	358	0.03	0.03	1.15	0.50	0.02	0.00	0.33	9	348
29X-cc	4	8	276.79	98.9	277	0.04	0.06	0.92	0.40	0.06	0.00	0.32	19	288
30X-1	34	39	285.14	102.0	431	0.05	0.17	0.02	0.23	8.50	0.01	0.15	113	13
32X-cc	12	15	307.24	96.6	244	0.04	0.05	0.44	0.50	0.11	0.00	0.32	16	138
36X-1	130	140	343.10	100.8	277	0.03	0.02	0.47	0.75	0.04	0.00	0.23	9	204
36X-cc	5	9	343.25	101.1	340	0.02	0.00	0.46	1.00	0.00	0.00	0.17	0	271
37X-cc	4	8	353.01	102.7	299	0.03	0.05	1.49	0.37	0.03	0.00	0.41	12	363
38X-1	26	30	361.06	101.1	252	0.01	0.00	0.95		0.00	0.00	0.35	0	271
41X-2	147	150	392.27	100.9	381	0.02	0.08	0.33	0.20	0.24	0.00	0.16	50	206
41X-4	140	150	395.20	100.2	437	0.06	0.32	0.21	0.16	1.52	0.03	0.28	114	75
42X-1	95	98	399.75	100.7	277	0.03	0.01	0.70	0.75	0.01	0.00	0.34	3	206
43X-1	65	68	408.95	100.2	428	0.02	0.02	0.83	0.50	0.02	0.00	0.43	5	193
44X-1	80	84	418.60	98.8	301	0.05	0.09	1.16	0.36	0.07	0.01	0.40	23	290
44X-1	103	113	418.83	102.2	323	0.01	0.02	1.74	0.50	0.01	0.00	0.37	5	470
45X-2	18	22	428.98	101.0	220	0.00	0.00	0.76		0.00	0.00	0.29	0	262
46X-2	100	104	439.30	99.0	276	0.05	0.09	0.37	0.36	0.24	0.01	0.23	39	161
47X-2	10	14	447.90	103.4	282	0.05	0.11	0.96	0.31	0.11	0.01	0.29	38	331
48X-1	11	15	455.91	102.7	244	0.04	0.10	0.53	0.29	0.18	0.01	0.20	50	265
49X-1	140	150	466.70	98.0	301	0.03	0.07	0.86	0.30	0.08	0.00	0.50	14	172
49X-2	12	16	466.92	102.8	247	0.01	0.01	0.90	0.50	0.01	0.00	0.30	3	300
50X-1	82	85	475.62	103.7	235	0.00	0.01	0.63		0.01	0.00	0.21	5	300
51X-cc	3	7	486.12	97.5	329	0.01	0.01	0.78	0.50	0.01	0.00	0.23	4	339
52X-2	8	12	495.38	97.2	220	0.01	0.00	0.75		0.00	0.00	0.27	0	278
53X-cc	4	7	504.44	98.5	276	0.07	0.21	1.05	0.25	0.20	0.02	0.37	57	284
54X-1	0	4	512.80	96.8	384	0.07	0.22	0.68	0.25	0.32	0.02	0.34	65	200
55X-cc	16	20	525.46	102.7	276	0.01	0.03	1.22	0.25	0.02	0.00	0.33	9	370
56X-1	118	122	532.98	96.8	274	0.02	0.00	0.60	1.00	0.00	0.00			
59X-3	140	150	564.70	99.7	352	0.02	0.02	0.40	0.00	0.14	0.00	0.11	18	364
63X-4	140	150	604.20	96.3	305	0.04	0.10	0.67	0.29	0.14	0.01	0.22	45	304
71X-2	133	143	677.13	98.4	328	0.04	0.00	0.55	1.00	0.00	0.00	0.31	0	177
74X-1	140	150	704.20	98.4	217	0.03	0.00	0.44	1.00	0.00	0.00	0.25	0	176
78X-4	140	150	746.70	97.9	380	0.03	0.21	0.00	0.12		0.02	0.13	161	0
81X-1	140	150	770.70	98.7	308	0.05	0.06	0.84	0.50	0.07	0.00	0.29	21	290
84X-1	140	150	799.20	101.7	276	0.03	0.00	0.34	1.00	0.00	0.00	0.18	0	189
87X-1	140	150	827.70	101.1	320	0.02	0.00	0.19	1.00	0.00	0.00	0.10	0	190
90X-1	140	150	856.20	97.1	276	0.02	0.02	0.56	0.50	0.03	0.00	0.27	7	207
94X-4	140	150	893.40	103.0	367	0.01	0.02	0.03	0.50	0.66	0.00	0.09	22	33
97X-1	71	81	916.71	100.9	305	0.02	0.07	0.41	0.25	0.17	0.00	0.23	30	178

tion in the range 240–400 mbsf and a negative correlation in the range 420–930 mbsf.

#### Sulfate (SO<sub>4</sub>)

SO<sub>4</sub> concentrations have large variations with depth (Fig. 13). There is a rapid decrease of SO<sub>4</sub> in the top 30 m which can be attributed to biological sulfate reduction. At 107 mbsf there is a high value of SO<sub>4</sub> followed by a steep decrease down to 240 mbsf. At greater depths the variations are large and cannot be attributed to the effect of oxidation of sulfides upon recovery of the sediments. The low values of SO<sub>4</sub> are more often found in clays but there is no systematic relationship.

The most important feature is the excellent correlation of SO<sub>4</sub> and Mg over the depth range 100–930 mbsf, except in between 675 and 771 mbsf. This correlation is found in the absence of significant chemical fractionation, hence it can only be attributed to the mixing of two types of fluids. One fluid should have high Mg and SO<sub>4</sub>, and it is most probably bottom sea water; the other fluid should have low Mg and SO<sub>4</sub>. This point will be discussed further below.

#### Alkalinity (Alk), Carbonate saturation

As shown in Figure 13 there is a large increase of Alk in the upper 30 m that can be attributed to decomposition of organic

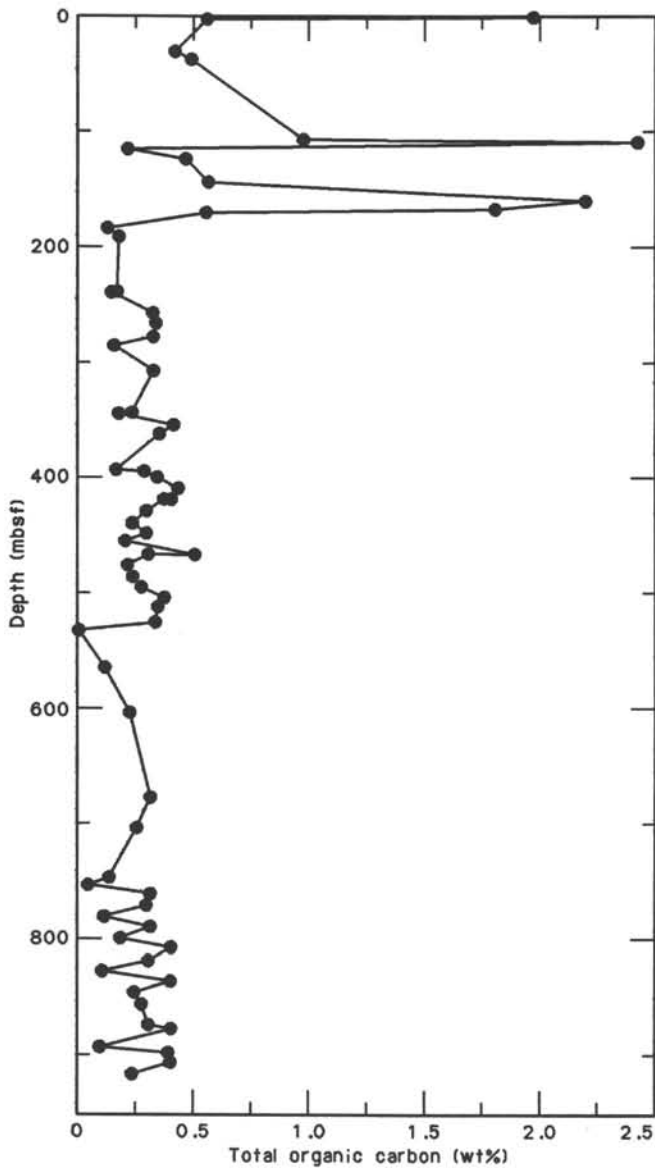


Figure 11. Plot of total organic carbon (TOC) vs. depth at Site 718.

matter. Alk values decrease linearly with depth between 105 and 185 mbsf and between 185 and 270 mbsf. From 270 to 675 mbsf there is a general decrease, but with large local variations. In the range 675 to 930 mbsf there is a slight increase with a very large maximum near 771 mbsf and another near 830 mbsf.

From 240 toward 930 mbsf the overall variation of Alk at Site 718 can be compared with that found at Site 717. This reflects control by diagenetic factors. Alk values are positively correlated with Cl in the samples where  $CH_4 > 0.5$  mmol/L and it is negatively correlated with Cl in the samples where  $CH_4 < 0.03$  mmol/L. This can be attributed to a diagenetic effect combined with a lithological effect (clays vs. silt and sands).

Undersaturation with aragonite and a slight undersaturation with calcite are found in most of the samples from 107 mbsf downward. In the clay layers equilibrium with calcite is reached. This is partly controlled by clay diagenesis because these observations correlate with  $(Na + K)/Cl$  ratios. Most of the silt layers are close to equilibrium with 3%-Mg calcite. This may be the carbonate phase that actually precipitates.

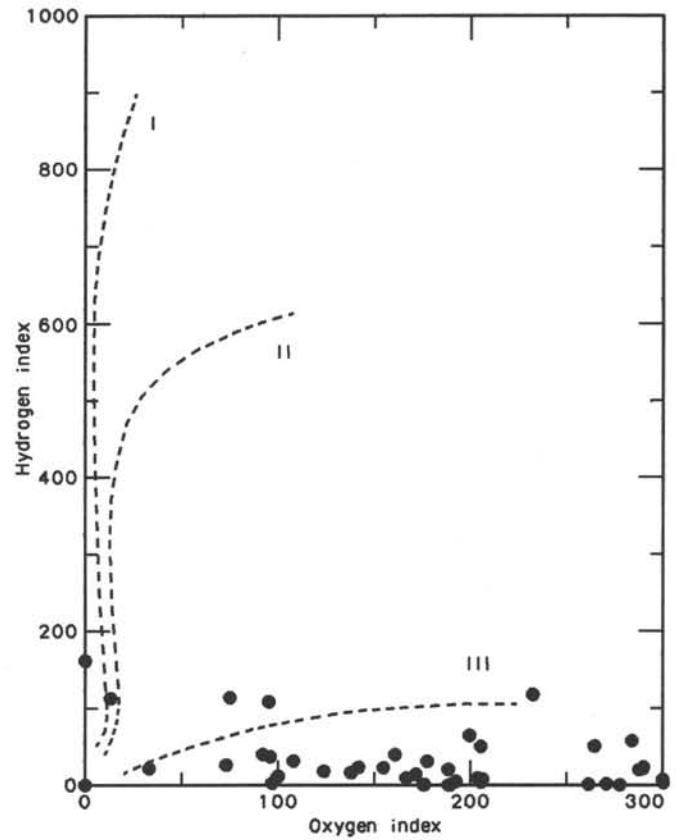


Figure 12. Hydrogen and oxygen indexes (HI and OI) obtained from Rock-Eval pyrolysis of sediments from Site 718.

**Silica ( $SiO_2$ )**

Silica shows large variations in the top 10 mbsf (see Fig. 13), which can be related to degradation of siliceous tests. In the range 107 to 675 mbsf  $SiO_2$  has almost constant values; but, below 675 mbsf there is an increase.

There is a good correlation of  $SiO_2$  and Alk below 400 mbsf. There is no clear relation of  $SiO_2$  to other biologically derived components such as  $PO_4$  and  $NH_4$  at depths below 30 mbsf.

**Phosphate ( $PO_4$ ), and Ammonia ( $NH_4$ )**

$NH_4$  and  $PO_4$  have large concentrations in the upper 30 m, as expected from biological decomposition of organic matter (see Fig. 13).  $PO_4$  has a maximum in the oxic zone where  $NH_4$  is almost zero.

Below 107 mbsf  $PO_4$  is almost constant (approximately 0.002 mmol/L). A maximum, reaching about 0.0045 mmol/L is, however, observed near 140–190 mbsf, corresponding to a clay layer and a minimum of  $NH_4$ . This may be due to a local increase in biological activity or to the input of water derived from the surface of the sediments.

$NH_4$  values are nearly constant (0.6 mmol/L) with large variations (ranging up to 0.3 mmol/L) from 107 mbsf downward.

**In-Situ Water Samples**

The sample collected at 90 mbsf has slightly different Ca and Alk values than those of the IW samples collected at 30 and 107 mbsf. On the other hand, Cl for this sample is about the same as at 30 and 107 mbsf and larger than in bottom sea water. Because anomalous heat flow was found at the depth range of the

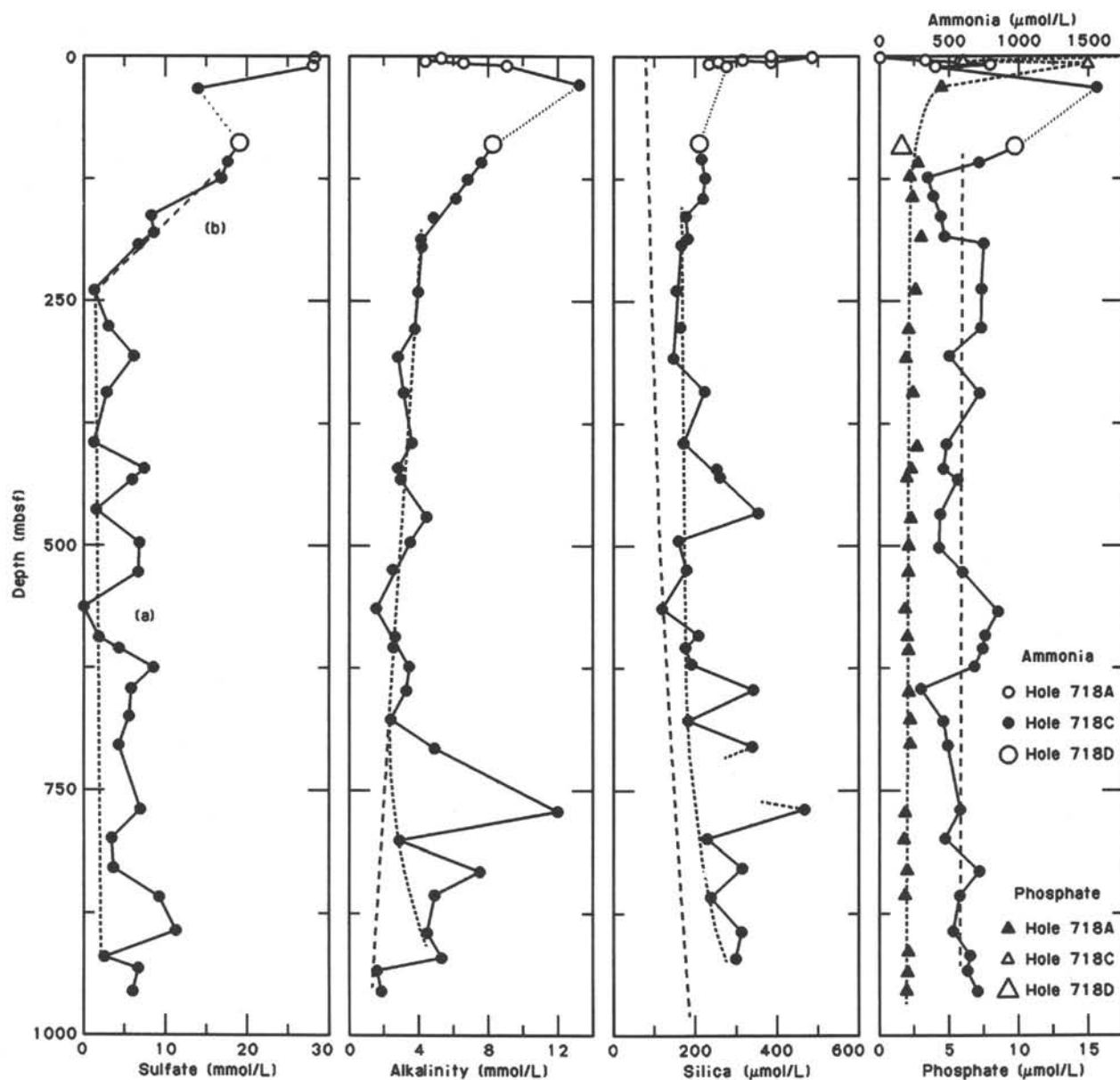


Figure 13. Concentrations of Cl, Na + K, Ca, Mg, SO<sub>4</sub>, alkalinity (Alk.), SiO<sub>2</sub>, PO<sub>4</sub>, and NH<sub>4</sub> vs. depth at Site 718.

sample, these differences can be interpreted in terms of a mixing between a warm fluid component flowing upward and a downward-flowing bottom sea water. Some of the characteristics of the warm fluid component, as compared to bottom sea water and pore water in the 0–100 mbsf depth range, are: increase of Ca, Alk, SiO<sub>2</sub>, possible increase of Cl, and decrease of SO<sub>4</sub>. In spite of its association with a rather silty layer, the *in-situ* sample is in equilibrium with calcite and oversaturated with respect to aragonite. CaCO<sub>3</sub> may precipitate, which may explain the lack of the expected decrease of Mg as compared to Ca. The concentration of CH<sub>4</sub> is 2500 nL/L, larger than at 30 mbsf (1000 nL/L) and at 107 mbsf (650 nL/L). At Site 718 such CH<sub>4</sub> concentration is only found at depths below 305 mbsf. The CH<sub>4</sub> concentration can be related to the upward advection of a warm fluid.

### Discussion

First the IW results from Site 717 and Site 718 are compared and then the reasons for similarities and discrepancies are dis-

cussed. The second point discussed will be the origin of the chemical composition of the IW and the possibilities of the circulation of fluids.

Sites 717 and 718 have only two features in common with respect to IW composition.

1. The large variations of Cl and Na + K and the decrease of (Na + K)/Cl ratios with increasing depths. These are due to the effects of compaction and clay diagenesis.

2. The large increase of Alk within meters below an indurated clay-rich layer found near 747 mbsf at Site 718 and near 790 mbsf at Site 717. It is correlated with increases of Ca and SiO<sub>2</sub> and decrease of Mg. It has previously been attributed to the upward flow of pore water within a convective circulation system.

Apart from the two above points the lack of similarity between Sites 717 and 718 is quite remarkable as they are located only a few miles apart. This can be attributed to the possibility of extensive flow of fluid in the larger part of the sediment col-

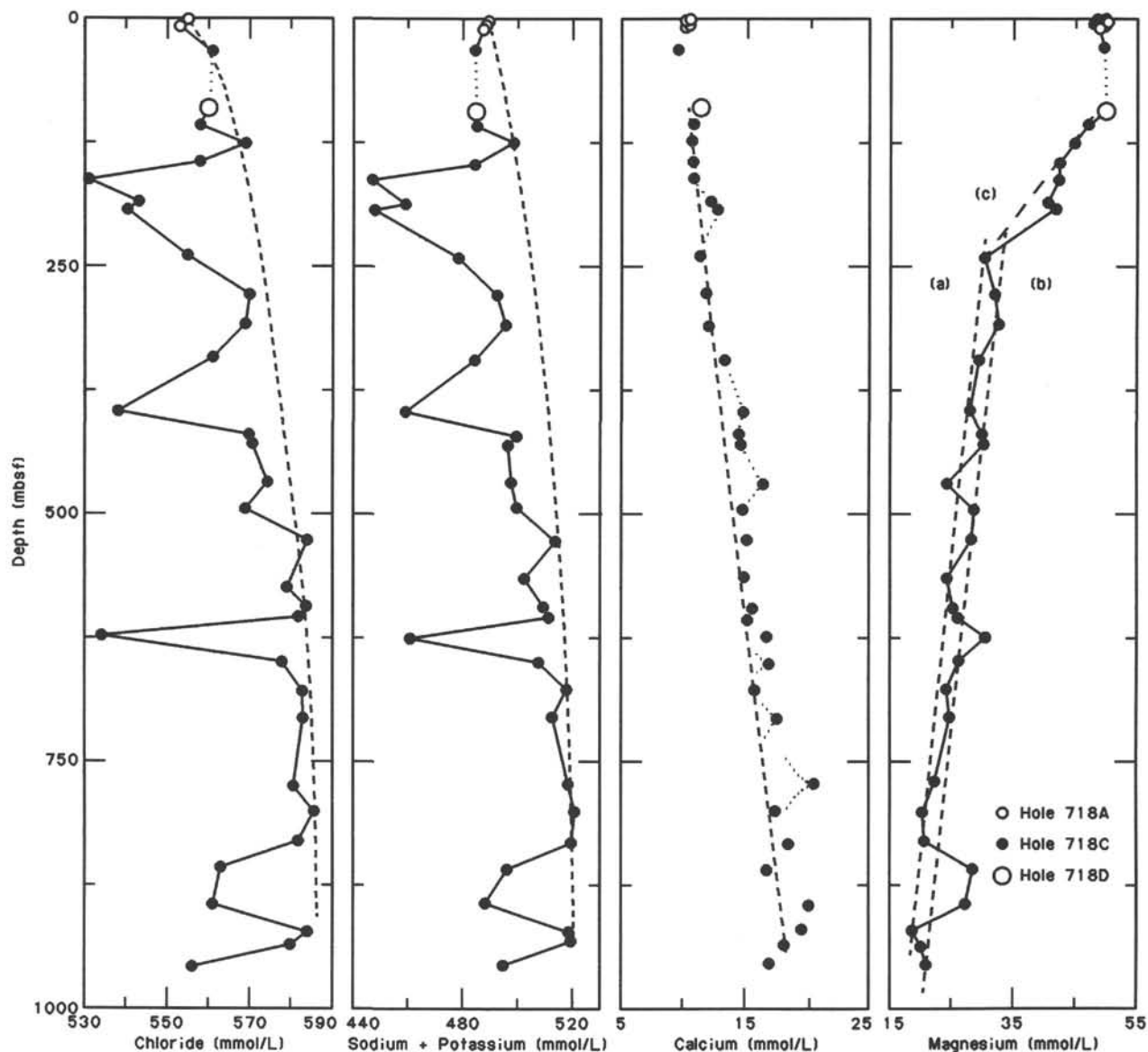


Figure 13 (continued).

umn at Site 718. Such a possibility was first inferred from measurements of heat flow. The temperature measurements carried out during Leg 116 at Site 718 may show an anomalously high temperature near 75 mbsf and show anomalously low temperatures, about 3 to 7°C respectively, at 140 and 190 mbsf. This suggests an upward flow of hot water expanding in the upper part of the core (30–80 mbsf?), overlying a downward flow of cold bottom sea water (140–190 mbsf).

In spite of the poor recovery of IW at the location of inferred expansion of hot water, the IW chemistry is indeed in agreement with a mixed origin for the IW over most of the sediment column. This is indicated by the correlation between Mg and  $\text{SO}_4$  found over almost the entire depth scale at Site 718. This unique correlation can be due to the mixing of one end-member fluid with high Mg and  $\text{SO}_4$ , which can be identified as bottom sea water, and a second end member with low Mg and  $\text{SO}_4$ , which can be either a hot-water component or pore water after extensive modifications due to diagenesis. In the latter case Mg and  $\text{SO}_4$  should have been depleted owing to clay diagenesis and organic matter diagenesis, respectively. However, considering the low organic content and its mostly terrestrial origin in

lithologic Unit V, this is quite unlikely. The hot-water end member should have low Mg and  $\text{SO}_4$  and high Ca concentrations as compared with sea water, which can be acquired owing to Ca-Mg exchange during water-rock-sediment interactions and deposition of  $\text{CaSO}_4$  upon increase in temperature of the Ca-enriched fluid. It is difficult to differentiate between the two possibilities for the second end-member fluid without additional information on the solid phase with which it has interacted during the acquisition of its composition. Such information should be acquired from Sr isotopic ratios.

By combining the chemical information with the temperature data, we can give an account of the origin of IW composition for the main sediment layers found at Site 718. This is presented in Figure 14. In this account some uncertainty exists owing to the lack of IW recovery in several large depth intervals. The upward flow of hot water is probably expanding in the sand unit between 30 and 100 mbsf. The downward flow of bottom sea water is found in the predominantly clay-rich layers between 110 and 190 mbsf owing to the possible intercalations of silt layers (suggested by the low recovery of part of the corresponding cores), and in the probable sand layer between 190 and 240

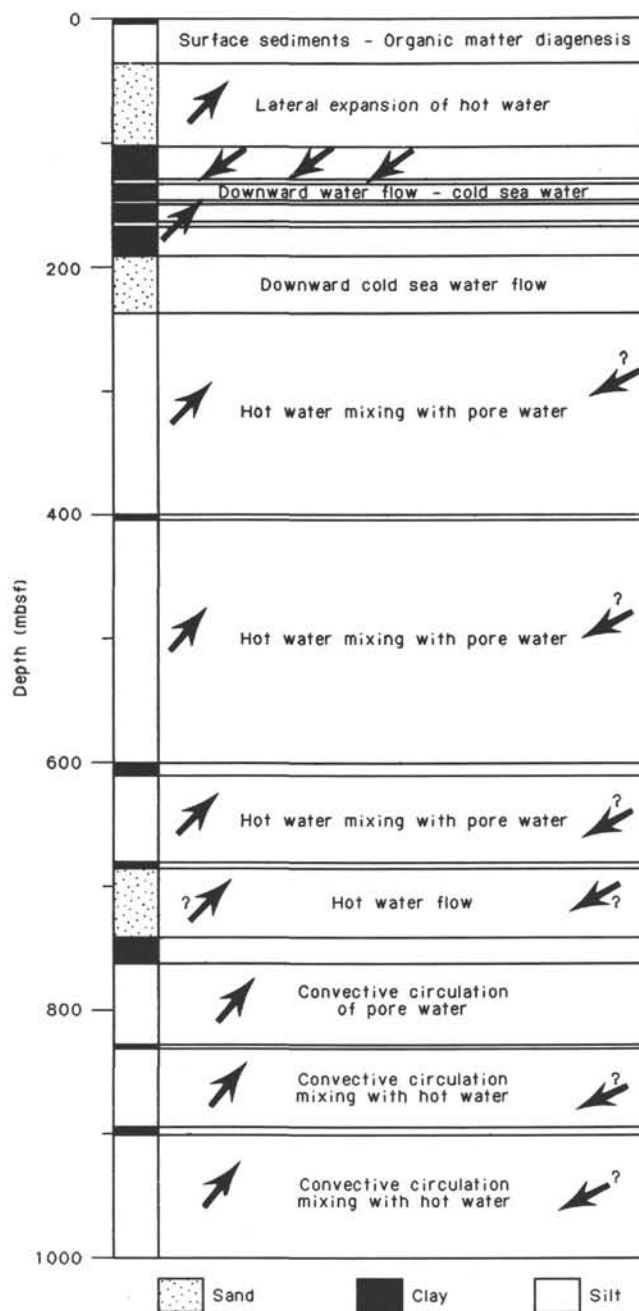


Figure 14. Schematic model of the origin of the compositions of the IW samples. See text for comments.

mbsf. At depths below 240 mbsf one can find the hot-water end member mixing with pore water. At depths below 770 mbsf the pore water is probably part of a convective system, as already inferred from the comparison of IW compositions at Sites 717 and 718 in this depth range. A possible flow pattern in agreement with the above discussion is shown in Figure 15.

Over the 240- to 930-mbsf depth range it is necessary to introduce a cold sea-water component mixing with pore water and hot water to explain the chemistry of the IW samples. This input of sea water is probably not contemporaneous with the hot water flux and its mixing with pore water, for obvious hydrodynamic reasons. It may have occurred during a preceding stage of circulation of fluids. This is a quite recent event as the characteristics of this sea-water component have not been completely

erased by diagenesis and diffusion. Such oscillatory behaviour of the flow has been modeled in sandstone aquifers in relation with mineralizing hot fluids ascending along fault zones (D. Turcotte, pers. commun.).

Chemistry as well as heat flow give results which suggest lateral as well as vertical anisotropy of the pattern of the flow path of the fluid. It has often been recognized that a fluid ascending along a fault plane tends to form coalescent conduits when near an area of lateral expansion or near the outlet. This is probably what is happening in the case of the area of Site 718 and may explain the difference in chemical data 10 m apart (distance between Holes 718C and 718D). Upon its expansion in the sediment, one should expect that the flow will also be limited to an area near the intersections of the conduits of the upward flow

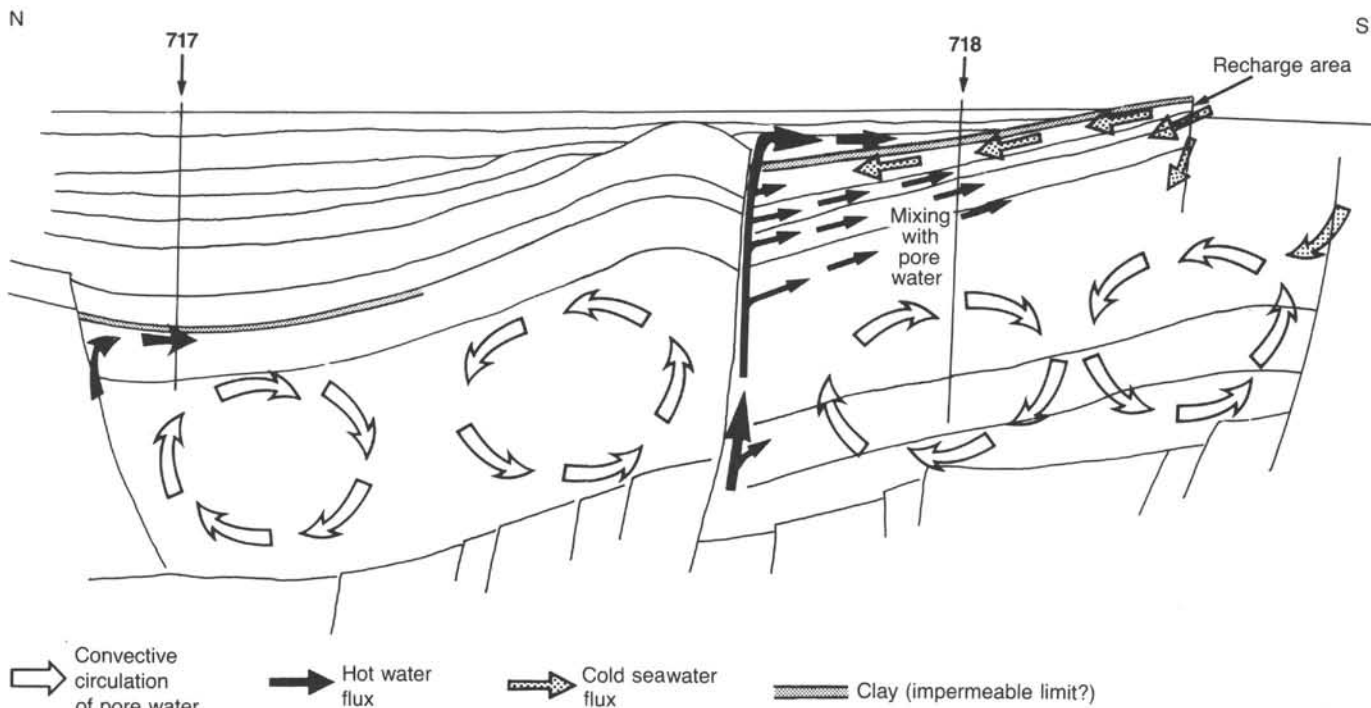


Figure 15. Schematic geological section of the area of Sites 717 and 718 (after single-channel seismic line of R/V *Conrad* cruise 2706, see "Site Survey" chapter). The pattern of the different flow circulations discussed in the text are given with the same symbols as in Figure 14.

with the coarser sediment layers. Hence, one should expect to have lateral anisotropy in chemical as well physical properties.

Core 116-718D-21 was found to consist of drilling fluid. The implication is that the flow of warm water in the silt layer at 80.5 mbsf may be quite limited as it did not replace the drilling fluid after the washing operation preceding the *in-situ* sampling.

Fluids expelled from deformation areas off Japan have been shown to be able to transport enough nutrients ( $\text{CH}_4$ ,  $\text{N}_2$ ,  $\text{H}_2\text{S}$ ) to sustain large colonies of clams with bacterial chemoautotrophic symbionts for primary energetic and biological growth requirements (Boulegue et al., 1987; Dron et al., 1987). The slightly anomalous composition of the fluid collected at 90 mbsf with the *in-situ* sampler does not permit us to suggest that such colonies should be found at the sea-floor outlet of the upward fluid. Methane concentration most probably remains low in the warm end-member fluid because the sediment cover is only about 1500 m. Deeper penetration at Site 718 may help to confirm this interpretation.

### Conclusion

The main conclusions from the study of the IW at Site 718 are as follows.

1. As at Site 717, the effect of compaction and clay diagenesis has led to a differentiation between the Cl, Na+K, and (Na+K)/Cl ratios of the clay-rich layers and the silt-sand layers. The effect of clay diagenesis can also be seen in the bulk decrease of Mg and the bulk increase of Ca.

2. Most of the chemical composition of the IW is controlled by the mixing of the pore waters with two end-member fluids: (a) upward flow of hot water, most probably resulting from the interaction of sea water with basement rocks and their overlying sediments. The effect of this interaction is mostly to decrease Mg and  $\text{SO}_4$ , increase Ca,  $\text{SiO}_2$ ,  $\text{CH}_4$ , and possibly Alk. (b) Downward flow of cold bottom sea water. The recharge area for the cold fluid is most probably located where lithologic Units

III, IV, and the upper part of V outcrop at the surface, about 2–3 miles south of Site 718.

3. The lower part of the sediment, below about 747 mbsf, may be part of a large-scale convective circulation of the pore fluid as already inferred at Site 717.

## PALEOMAGNETISM

### Remanent Magnetic Intensity

The natural remanent magnetization (NRM) of the archive half of each core from Holes 718B, 717C, and 718E was measured using a 5-cm spacing. No measurements were made on the single core from Hole 718A. Approximately 11% of the sections at this site contained sediment too strongly magnetized to measure with the cryogenic magnetometer. The observed NRM intensities spanned a wide range of values with a logarithmic mean of 37 mA/m (Fig. 16). Remanent intensities usually followed a log-normal distribution (Tarling, 1983), but as seen in Figure 16 the values were skewed toward lower intensities. This difference was due to the fact that the higher intensity sections which exceeded the range of the magnetometer were not included in Figure 16. The true mean value is therefore probably somewhat larger than 37 mA/m. After alternating field (AF) demagnetization with a 9-mT field, the intensity distribution was closer to log-normal (Fig. 16), with only two sections (i.e., 1%) still too magnetic to be measured.

The mean intensity of the demagnetized sections (viz. 7.4 mA/m) is significantly larger than at Site 717, where the mean intensity after demagnetization was only 2.5 mA/m (Table 5). Logarithmic means for lithostratigraphic Units II through V (see "Lithostratigraphy" section) were determined and are shown in Table 5 together with the corresponding values for Site 717. It can be seen that Units II and V had similar values for both sites while Units III and IV were substantially lower at Site 717. Unit III is only about 50 m thick at Site 718 but more than 150 m thick at Site 717. The disparity in remanent intensities may therefore be due to the absence at Site 718 of the upper, more

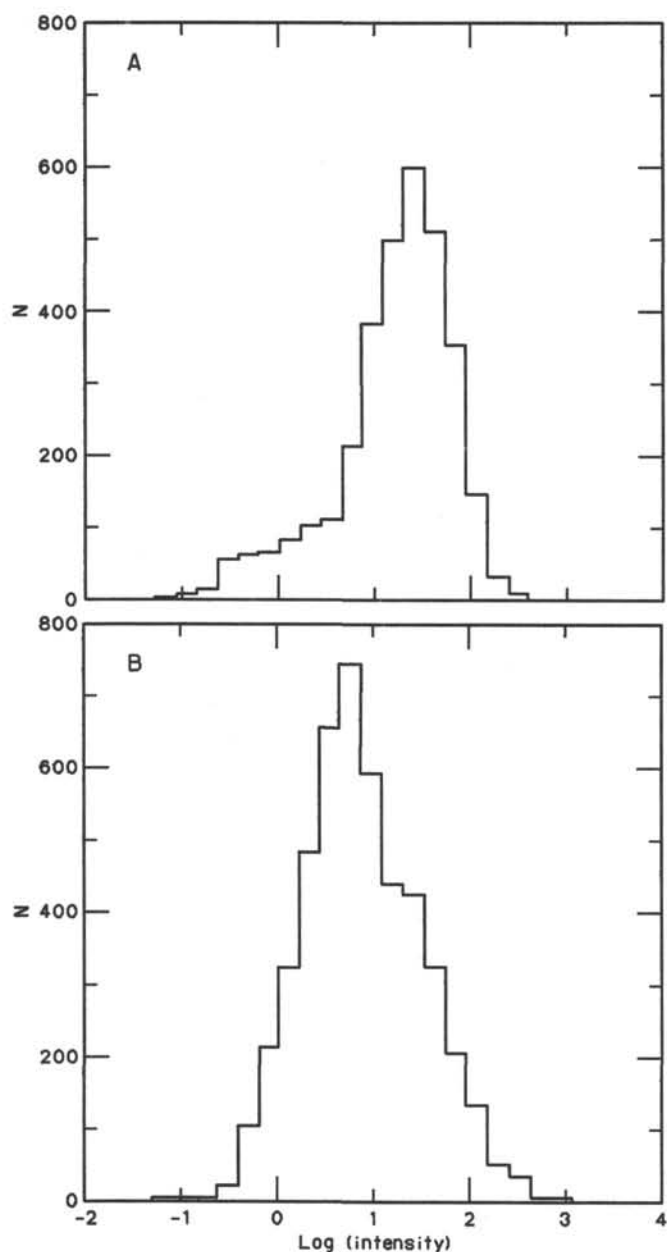


Figure 16. Histogram of logarithmic intensity of remanence for (A) NRM, and (B) 9-mT AF demagnetization measurements for Holes 718B, 717C, and 718E.

weakly magnetized portion of Unit III. In the case of Unit IV, the thickness was also substantially smaller at Site 718, but the remanent intensities suggest that the upper, more strongly magnetized portion of Unit IV (corresponding to Unit IVa of Site 717) was present and the lower, more weakly magnetized portion was either absent or very condensed. Seismic reflection data, however, indicated that the upper few tens of meters of Unit V are also absent at Site 718 (see "Seismic Stratigraphy section), suggesting that the lower part of Unit IV is more likely absent than condensed. An alternative explanation is that the lithostratigraphic units identified at both sites do not correspond in the manner suggested.

Comparison of the remanent intensities with the magnetic susceptibility displays a relatively good correlation, as was the case at the previous site. However, the correlation is not perfect

Table 5. Logarithmic mean remanent magnetic intensity (mA/m) after 9-mT AF demagnetization.

Site 718			Site 717		
Unit	Subunit	Mean	Unit	Subunit	Mean
II		24.5	II		20.1
III		6.7	III		1.3
IV		18.2	IV	all	1.2
				A	4.5
				B	1.0
				C	0.6
V	all	6.0	V		7.4
	A	6.0			
	B	6.0			
I-V		7.4	I-V		2.5

and susceptibility peaks were noted that exhibited no corresponding intensity peak and vice-versa. The cause of these differences is difficult to determine without more detailed lithologic information and careful analysis of the results. It is likely, however, that variations in ferromagnetic grain size or the presence of paramagnetic materials were responsible for these differences.

### Magnetic Inclination

A statistical study of the NRM inclination data from Site 718 showed a clear bias towards negative inclinations, confirming the suspected influence of the drill pipe and core barrel as discussed in the Site 717 chapter. A comparison of the histograms and arithmetic means for the inclination data before and after AF demagnetization (Fig. 17) demonstrated that this bias is reduced but not completely removed by the demagnetization process. To determine the magnitude of the remaining bias, the negative and positive inclinations were analyzed separately. This analysis gives mean negative and positive inclinations of  $-32.4^\circ$  and  $+22.1^\circ$ , respectively; both have standard deviations of approximately  $20^\circ$ . The average inclination after demagnetization, therefore, was approximately  $27^\circ$  with a mean bias of about  $-5^\circ$ . The  $27^\circ$  value was somewhat larger than the expected dipole inclination at Site 718, but has associated with it a large standard deviation and was therefore not considered particularly reliable. Taking into account the northward tectonic drift of the Indian plate, the anticipated magnetic inclination for sediments at the bottom of Hole 718C was about  $\pm 17^\circ$ . Although the difference between this and the observed value can be explained by the large scatter, some of which may have been due to secular variation, there are at least two other factors that may have contributed to an inclination larger or smaller than expected. The first is the northward dip of the sedimentary strata caused by tectonic deformation, and the second, the influence from *far-sided* effects of long-term nondipole components of the geomagnetic field. The former amounts to about  $3^\circ$  and should decrease the observed inclinations. Conversely, the latter should steepen the observed inclinations by a variable amount that can be as much as  $10^\circ$ – $12^\circ$  in the early and middle Miocene (Epp et al., 1983). Accounting for these factors, we expected early Miocene inclinations of about  $24^\circ$ – $26^\circ$ , not very different from the observed mean inclination of  $27^\circ$ .

A study was also made of changes in the mean inclination with depth in the hole by calculating a mean value at approximately 100-m intervals (i.e., about every 800 values). No statistically significant increase in inclination was apparent even though the difference in age between the top and bottom of the hole should give rise to an  $10^\circ$ – $15^\circ$  difference. It is believed, however, that the scatter in the data is too large to discern such a modest increase, especially in light of the vertical overprint caused by

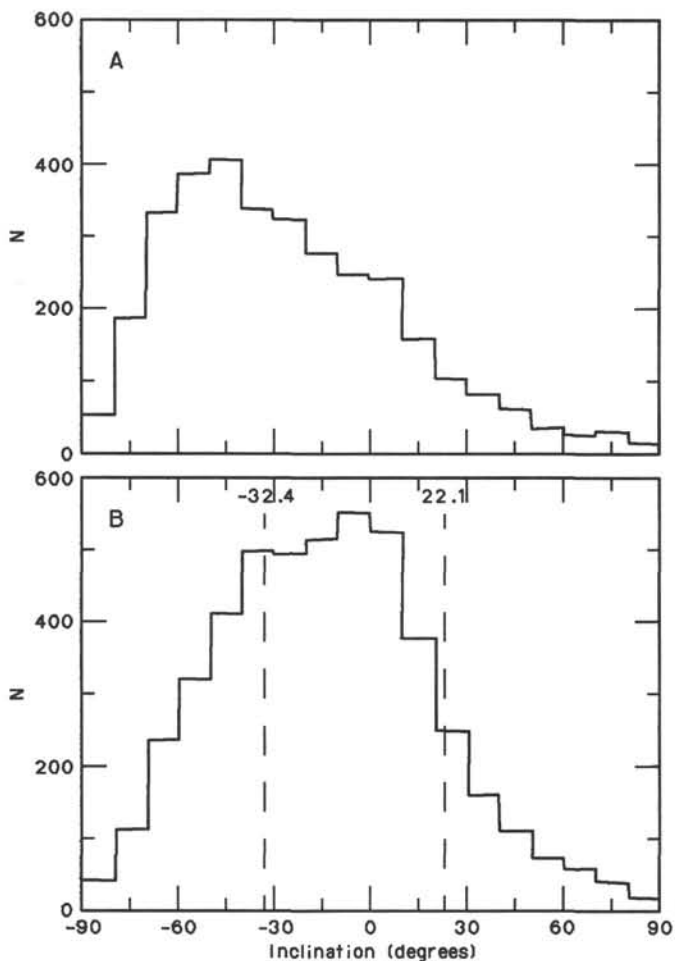


Figure 17. Histogram of magnetic inclinations for (A) NRM, and (B) 9-mT AF demagnetization measurements for Holes 718B, 718C, and 718E. Dashed lines in (B) show the arithmetic mean values of positive and negative inclinations.

the core barrel or drill pipe which appears to vary from core to core.

### Magnetic Declination

At this site, as at Site 717, the hole was cored using the XCB, with the result that biscuiting was again very prevalent throughout the cores. Because of this, it was anticipated that the declination values would show no preferred orientation but rather would be randomly distributed between  $0^\circ$  and  $360^\circ$ . A histogram of the NRM declination values, however, showed a significantly peaked rather than random distribution (Fig. 18). This azimuthal bias was rather puzzling, as individual cores should be situated in the core barrel with no preferential orientation. It is therefore difficult to explain the peak in the declination values as an overprint from the core barrel or drill pipe. Apparently, this overprint was acquired during the handling process or NRM measurement. A comparison of declinations before and after AF demagnetization showed that the peak was reduced, implying that the azimuthal bias was partially removed by the demagnetization. The origin of this declination anomaly is unknown but should be investigated further. Because the cores were not oriented, the declination values were not used to define reversals of the geomagnetic field. The declination information, however, if used, should be treated with caution.

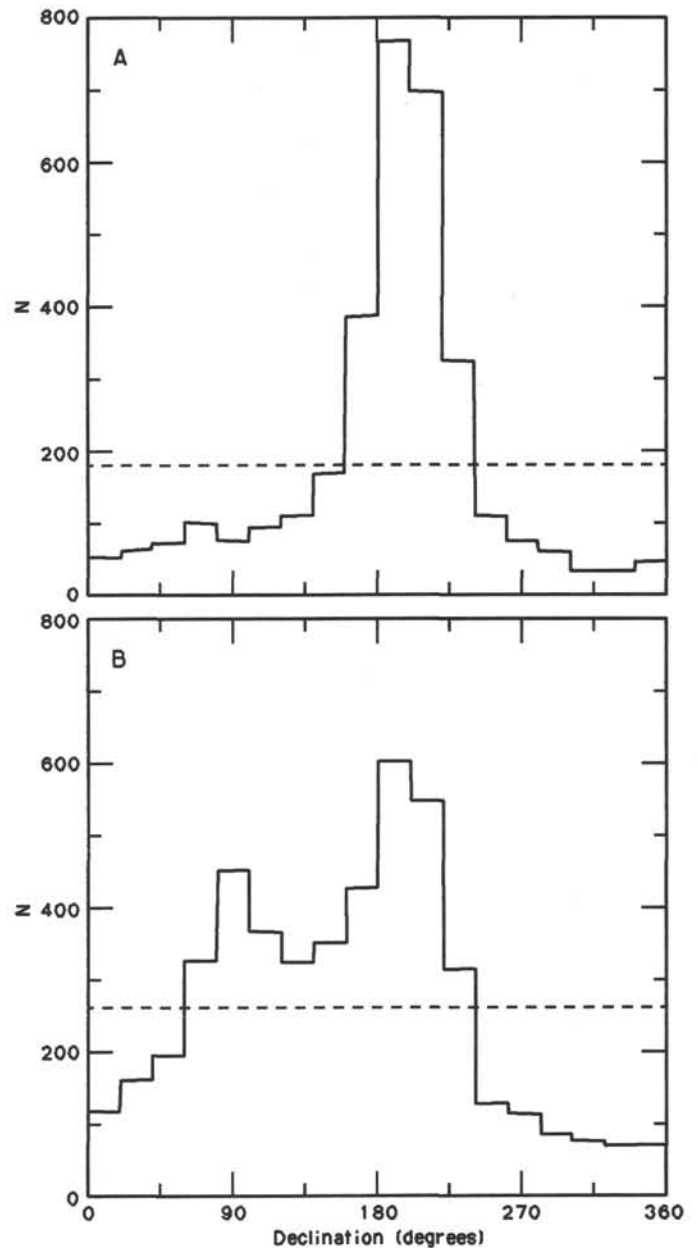


Figure 18. Histogram of magnetic declinations for (A) NRM, and (B) 9-mT AF demagnetization measurements for Holes 718B, 717C, and 718E. Horizontal dashed lines show distribution of declinations expected for a random distribution of values.

### Magnetic Susceptibility

As at Site 717, whole core volume magnetic susceptibility measurements were made at 5-cm intervals downcores from Site 718. In all, 5,747 susceptibility readings were taken from Site 718 cores. Of these, 173 were from Core 116-718B-1H, 178 from Cores 116-718E-1R to -718E-3R, and the remainder from Hole 718C cores. No measurements were made of the single core from Hole 718A. As at Site 717, the Site 718 holes were drilled so that the bottom of Hole 718B is approximately coincident with the top of Hole 718C. Furthermore, Hole 718E was drilled to so that its first core begins at the same depth as the bottom of Hole 718C. Consequently, the results from all three holes were combined in the following discussion.

The magnetic susceptibility values measured from Site 718 cores were similar to those obtained at Site 717. The low and high measurements at Site 718 were  $3.0 \times 10^{-6}$  cgs, in Core 116-718C-42X and  $9.4 \times 10^{-4}$  cgs in Core 116-718C-16X, a range nearly identical to that found at Site 717. Most of the susceptibility values, 66%, were between  $2.0 \times 10^{-5}$  and  $6.0 \times 10^{-6}$  cgs, close to the 71% found between these values at Site 717. As at Site 717, the highest susceptibility values were recorded in peaks corresponding to turbidites (Fig. 19).

A few differences in susceptibility were noted between Sites 717 and 718. Most Site 718 cores had slightly higher and more irregular susceptibility values than those of Site 717. Only 0.8%

of the Site 718 susceptibility values fell below  $2.0 \times 10^{-5}$  cgs, contrasted to over 7% at Site 717. Unlike Site 717, there were few cores from Site 718 that displayed a relatively low, constant background susceptibility. Additionally, the susceptibility peaks measured in the Site 718 cores were generally narrower than those found in Site 717 cores. Many peaks measured from Site 718 cores appeared to be only 10 to 20 cm in width and only a few were greater than 1 m in thickness. The narrower peaks seemed to be indicative of thinner turbidite layers in these cores. An interesting difference is the susceptibility characteristics of Cores 116-718C-96X and -718C-97X at the bottom of Hole 718C, and Cores 116-718E-1R to -718E-3R in Hole 718E (see

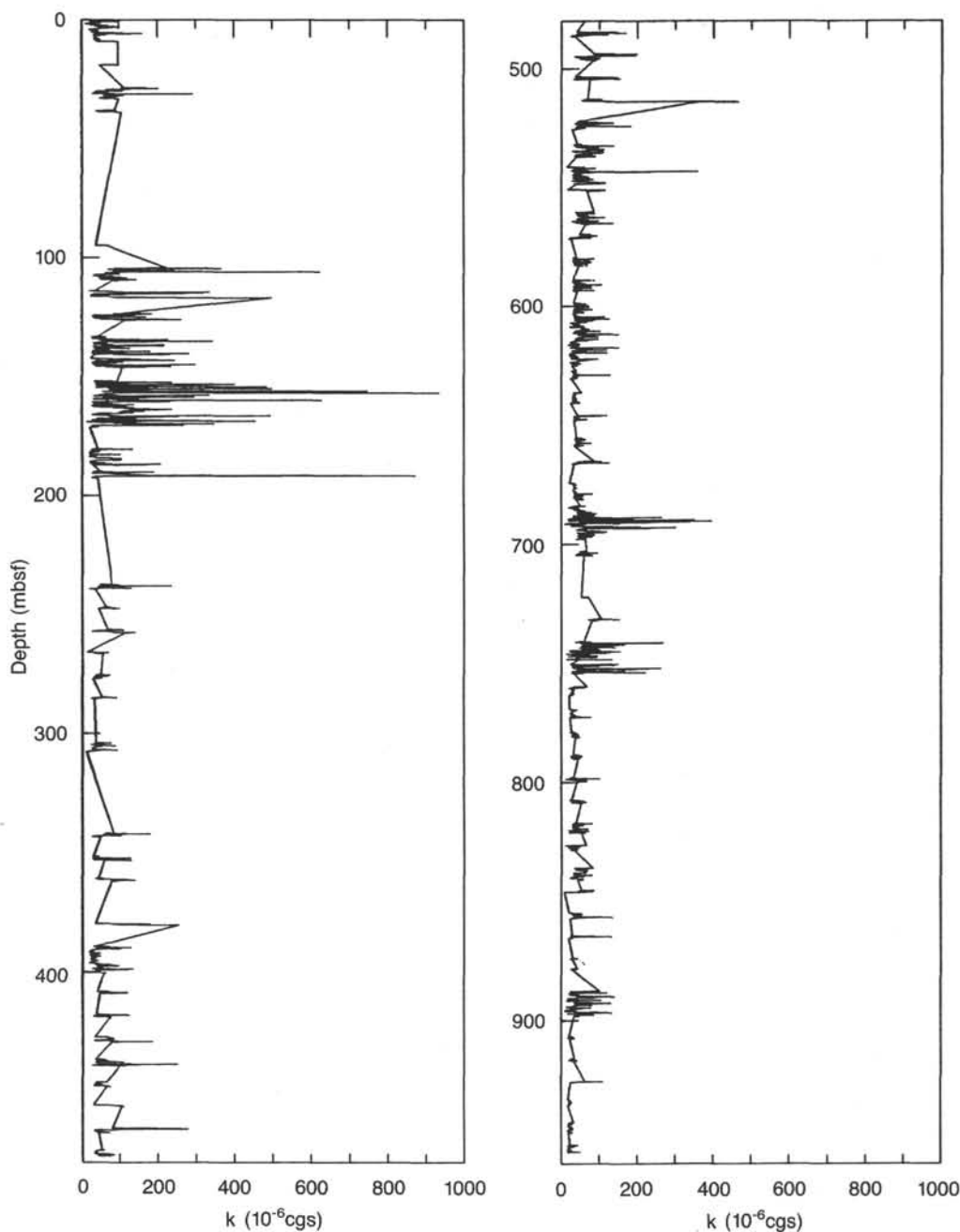


Figure 19. Whole-core volume magnetic susceptibility plotted vs. depth for Site 718. Data from Holes 718B, 718C, and 718E are included. Susceptibility,  $k$ , is given on the horizontal axis. The graph at left shows measurements obtained in cores recovered between 0 and 480 mbsf, and on the right, from 480 to 960 mbsf.

Fig. 19 below 906 mbsf). Unlike any others measured on Leg 116, the susceptibility record in these cores was essentially flat, around  $1.9\text{--}2.4 \times 10^{-5}$  cgs, with no significant peaks.

The larger scale susceptibility characteristics of Site 718 cores also displayed some similarities and differences from those of the previous site. Figure 19, a plot of susceptibility vs. depth at Site 718, resembles Figure 22 of the Site 717 chapter. However, in the latter, several sections of tens of meters in thickness were noted in which high susceptibility values were more commonly encountered. Furthermore, the pulses of high susceptibility observed at Site 717 did not correlate well with the pattern of lithologic units. Figure 19 shows that the cores of Site 718 displayed only one obvious pulse, between 100 and 200 mbsf, that corresponded almost exactly to the gray muds of lithostratigraphic Units III and IV ("Lithostratigraphy" section). However, two other pulses may have been detected at depths of 515–540 mbsf and 680–750 mbsf, but because of poor recovery in these intervals both were uncertain. Biostratigraphic ages (see "Biostratigraphy" section) and sediment characteristics (see "Lithostratigraphy" section) suggest that Units III and IV of Hole 718C correspond to part of Unit IV of Hole 717C. With these constraints, we tentatively correlated the high susceptibility values recorded from cores spanning 100–200 mbsf in Hole 718C with those found in cores from 420 to 480 mbsf in Hole 717C. However, this hypothesis raised a question as to the whereabouts of the other prominent susceptibility pulses that were observed in Site 717 cores. The absence at Site 718 of the pulses between 250 and 310 mbsf and between 580 and 620 mbsf, observed at Site 717, appeared to be a result of the absence at Site 718 of sediments corresponding to those of Unit III, the lower part of Unit IV, and the upper part of Unit V at Site 717. Additionally, the poorly defined pulse seen at the bottom of Hole 717C may correspond to the poorly defined pulse noted between 515 and 540 mbsf in Hole 718C.

## PHYSICAL PROPERTIES

Cores 116-718A-1H and -718B-1H were obtained primarily with the Advanced Piston Core (APC). Cores 116-718C-1X to -718C-98X were recovered by Extended Core Barrel (XCB) operations, and Cores 116-718E-1R to -718E-3R were obtained with a Rotary Core Barrel (RCB). Physical properties measured routinely on all cores recovered at Site 718 include GRAPE density and thermal conductivity from full-round core sections, vane shear strength, compressional wave velocity, and index properties from split sections (the methods used are described in the Explanatory Notes chapter). Results of physical properties measurements at Site 718 are summarized in Tables 6 to 15.

### Index Properties

Index properties include wet-bulk density, water content, porosity, and grain density. The measurements were made mainly on fine-grained deposits (Figs. 20 to 23). The scatter of data points is attributed to disturbance by drilling and variations in sediment composition. Below 500 mbsf, drilling disturbances affected the tested *drilling biscuits* only to a minor degree, and index properties are believed to be mainly related to sediment composition. Those relations are discussed in detail for the porosity data. As the other physical properties are closely related to each other, the same discussion applies for wet-bulk density and water content.

### Porosity

Porosity decreases nearly linearly from an average of 60% at the seafloor to an average of 38% at 700 mbsf with a rate of 3.14%/100 m. Below 700 mbsf this rate decreases to 1.3%/100 m. An average porosity of 35% was observed at the bottom of the hole (Fig. 20).

### Wet-Bulk Density

The wet-bulk density increases nearly linearly from 1.70 g/cm<sup>3</sup> to 2.05 g/cm<sup>3</sup> at 550 mbsf with a rate of 0.064 g/cm<sup>3</sup>/100 m (Fig. 21). Below 550 mbsf the increase is also approximately linear, but the rate of increase decreases to about 0.054 g/cm<sup>3</sup>/100 m. At the bottom of the hole an average wet-bulk density of 2.25 g/cm<sup>3</sup> was determined.

### Water Content

The water content (related to wet weight) shows a similar, but inverse, pattern downhole to the wet-bulk density, with a change in the rate of decrease at 550 mbsf. The water content decreases from 38% at the mud line to about 20% at 550 mbsf, with a rate of 3.27%/100 m. Farther down, this rate decreases to 0.81%/100 m. An average water content of 17% is observed at the bottom of the hole (Fig. 22).

### Grain Density

The average grain density ranges between 2.7 and 2.8 g/cm<sup>3</sup>, which is normal for clayey sediments (Fig. 23).

### Compressional Wave Velocity

Sonic velocity measurements range from 1.52 km/s at the mud line to about 2.0–2.15 km/s at the bottom of Hole 718C (Fig. 24). Two units seem to be present: (a) a first unit from the mud line to 600 mbsf shows a trend increasing to 1.75 km/s, and (b) a second unit from 600 mbsf to the bottom of the hole corresponding to lithologic Unit Vb. This unit shows an alternation of high (1.9–2.15 km/s) and low (1.7–1.8 km/s) values. This alternation is mostly due to drilling disturbances, as values from the same core and same lithology range from usually 1.6 km/s in Sections 1 to about 1.9–2.15 km/s in Sections 6 and/or Core Catchers. However the presence of high values only below 600 mbsf suggests that such high velocities do not occur above 600 mbsf. Additionally, a systematic anisotropy (up to 8–10%) has been observed on relatively well-consolidated samples, the horizontal velocities being always higher than the vertical velocities.

### Thermal Conductivity

Thermal conductivity measurements were routinely performed on each section from the mud line to a depth of 603.4 mbsf (Fig. 25). Below that depth, drilling disturbances induced a lack of coherence in the measurements. Thermal conductivities measured were used for the evaluation of the heat flow in connection with temperature measurements in Hole 718C and 718D (see "Heat Flow" section). The conductivities measured vary between 1.86 and 7.81  $10^{-3}$  cal/(°C × cm × s). Two main thermal conductivity units can be distinguished: (a) the interval from the mud line to about 200 mbsf is characterized by relatively homogeneous values with an average of  $3.2 \times 10^{-3}$  cal/(°C × cm × s); this interval corresponds to lithologic Units I, II, III, and IV. Below that depth, lithologic Unit Va is characterized by highly variable data (2.82 to  $7.81 \times 10^{-3}$  cal/(°C × cm × s) with an average thermal conductivity of about  $4.6 \times 10^{-3}$  cal/(°C × cm × s).

### Undrained Shear Strength

Undrained shear strength was measured in Hole 718C down to 398.6 mbsf, after which depth the core material was too stiff or too disturbed to make valid measurements. In any case, because of low core-recovery and high drilling disturbances, only a few measurements were carried out. Values obtained for undrained shear strength are presented in Tables 14 and 15, and are shown plotted vs. depth in Fig. 26. Shear strength in the natural state varies between 21.3 kPa (0.39 mbsf) and 496.5 kPa

Table 6. Index physical properties from Hole 718B.

Core	Section or core catcher (CC)	Top interval (cm)	Bottom interval (cm)	Sub-bottom depth (m)	Water content (% wet weight)	Porosity (%)	Wet-bulk density (g/cm <sup>3</sup> )	Grain density (g/cm <sup>3</sup> )
1H	1	40	44	0.40	57.97	74.83	1.39	2.16
1H	2	95	99	2.45	35.19	60.04	1.76	2.80
1H	3	85	89	3.85	33.60	58.20	1.80	2.79
1H	4	60	64	5.10	38.12	63.49	1.70	2.86
1H	5	113	117	7.13	33.11	58.35	1.77	2.87
1H	6	63	67	8.13	32.87	57.08	1.84	2.75

(398.62 mbsf). Figure 26 also shows that the shear-strength profile can be subdivided into four major intervals.

1. 0.39–30.41 mbsf: the values obtained for undrained shear strength are fairly constant between 21.8 kPa (7.2 mbsf) and 33.1 kPa (30.41 mbsf). This interval corresponds to lithologic Units I and II.

2. 105.5–166.81 mbsf: the shear-strength data for this interval show considerable scatter, but appear to increase slightly with depth. This interval corresponds to lithologic Units III and IV. The boundary between lithologic Units II and III is marked by a sharp increase in shear strength to 139.5 kPa at 105.5 mbsf. The boundary between lithologic Units IV and V is marked by a distinct decrease in shear strength from 307.4 kPa at 166.81 mbsf to 125.3 kPa at 189.98 mbsf.

3. 190–238 mbsf: the shear-strength data for this interval are very low compared to the upper and lower intervals. The values range from 118.2 kPa at 238 mbsf to 158 kPa at 192 mbsf.

4. 239–398.6 mbsf: the two measured values within this interval show an increase of shear strength from 264.8 kPa at 238.97 mbsf to 496.5 kPa at 398.62 mbsf.

#### State of consolidation

The effective overburden pressure ( $P_o$ ) was calculated for every depth interval with the equation which Richards (1962) applied to marine sediments:

$$P_o = \alpha_w \times \Delta d \text{ (kPa)} + P_i,$$

where  $P_o$  is effective overburden pressure,  
 $\alpha_w$ , buoyant unit weight (wet-bulk density-density of water),  
 $\Delta d$ , depth interval from the above sample, and  
 $P_i$  is effective overburden pressure of the above sample.

To estimate the state of consolidation, a method described by Bjerrum and Simons (1960) and Skempton (1970) was applied. This method relates undrained shear strength ( $cu$ ) to effective overburden pressure ( $P_o$ ). Skempton (1970) established that the ratio of shear strength to effective overburden pressure in normally consolidated marine sediments ranges between 0.2 and 0.5. All values of shear strength/overburden pressure ratio less than 0.2 are assumed to be underconsolidated and those greater than 0.5 are considered to be overconsolidated.

Figure 27 shows the ratio of shear strength to effective overburden pressure plotted vs. depth for the sediments of Site 718, down to 400 mbsf. It shows that the upper 5 m of sediments appeared to be overconsolidated, but the sediments below 5 m are normally to slightly underconsolidated.

The observed overconsolidation of the near-surface sediments and the high values of  $cu/P_o$  between 109 and 167 mbsf at Site 718 are most likely caused by the erosion of a small amount of overburden or cementation.

#### HEAT FLOW

Site 718 is located on a large local heat-flow high determined by the R/V *Robert D. Conrad* site survey. Heat-flow measure-

ments in the survey area show both a great range of values (44–166 mW/m<sup>2</sup>) and very large variations between adjacent measurements (Fig. 3). These two characteristics suggest the presence of a vigorous hydrothermal circulation system, probably related to the faulting and deformation. Another surprising aspect of the heat-flow survey is that the fault trace is not associated with heat-flow highs as might be expected if water was ascending along the fault. Values recorded very near the fault trace are actually depressed by 20 to 30 mW/m<sup>2</sup> with respect to surrounding values. The highest values appear to be consistently located 2–3 km south of the fault. This suggests that water is not reaching the surface along the fault, but rather may ascend to a certain level along the fault and then flow laterally along a permeable sediment layer. Among the factors in deciding to locate Site 718 on the heat-flow high was the opportunity to investigate both the hydrothermal circulation associated with the deformation and the effect of the higher thermal gradient on diagenesis and mineralization.

Downhole temperature measurements were made in the sediment at the bottom of Hole 718C preceding Cores 116-718C-8X (75.8 mbsf), -718C-12X (113.8 mbsf), -718C-15X (142.3 mbsf), -718C-16X (151.5 mbsf), -718C-18X (170.8 mbsf), and -718C-20X (189.8 mbsf). Hole 718D was drilled specifically to investigate further the possibility of hydrothermal circulation suggested by the data from Hole 718C. Specifically, it was designed to obtain pore-water samples and heat flow measurements from the region between 50 and 100 mbsf where core recovery had been very poor in what was interpreted as unconsolidated silty turbidites. Temperature measurements were obtained preceding Cores 116-718D-1X (71 mbsf), -718D-2X (80.5 mbsf), and from the bottom of the hole (90 mbsf). In this section the individual temperature measurements will be referred to by the number of the core with which they are associated. The measurement at the bottom of hole 718D, associated with Core 116-718D-3X will be referred to as D3X.

Temperature measurements were made mainly using the Uyeda/Kinoshita temperature probe described in the Explanatory Notes chapter, or with the Barnes/Uyeda probe, which uses a similar temperature probe but is also designed to obtain a pore-water sample and pressure measurement. The dual-channel recorder on the Barnes/Uyeda probe malfunctioned on measurement C12X, resulting in no data being recorded in spite of a successful deployment of the instrument. The Barnes/Uyeda tool was thereafter used with a single-channel recorder, which did not permit a pressure measurement.

Plots of temperature vs. time for each measurement run are shown in Figures 28 to 35. The temperature vs. time curves have a characteristic shape. The lowering of the probe through the water column is marked by a rapid cooling followed by a relatively constant temperature while it is held at the mud line prior to insertion. Insertion into the formation at the bottom of the hole is marked by a rapid frictional heating followed by a gradual cooling back toward the equilibrium temperature of the sediments. Pullout is sometimes accompanied by another frictional spike and the temperature profile obtained on lowering is reversed on raising the probe to the surface. The section of the

plot when the probe was inserted into the formation at the base of the hole is indicated on each appropriate plot. The temperature does not fully return to equilibrium during the time that the probe is at the bottom, but the temperature vs. time values can be extrapolated to find the asymptotically approached equilibrium value.

Instrumental problems were encountered for a number of the measurements. For measurement D1X where no frictional spike is observed and the temperature increases slowly through the measurement (Fig. 33), it appears that the probe was slowly pushed into the sediments rather than being firmly implanted. Although the final temperature of about 3.1°C is probably close to the actual sediment temperature, it is not considered reliable enough to use for interpretation. Readings terminate at 58 min on measurement C15X (Fig. 29), when an internal switch on the instrument was tripped during pull out, turning it off. The amount of data collected, however, was sufficient to define a cooling curve that could be extrapolated to obtain a temperature equilibrium value. Measurements C8X and C16X both recorded sudden increases of about 7°C that appear to result from an instrument malfunction (Figs. 28, 30). In addition, no measurements were obtained during a portion of measurement C16X due to an intermittent short circuit. Temperature run C18X (Fig. 31) was apparently disturbed during the reading, but the undisturbed section was sufficient to obtain a reliable value.

The temperature measurements extrapolated to equilibrium are listed in Table 16 and plotted as a function of depth in Figure 36. They obviously do not demonstrate a simple increase in temperature with depth. The measurements obtained between 140 and 190 mbsf do show a consistent pattern with a steady temperature increase with depth. A straight line can be fit to those three points with a slope of 92.9°C/km, although one could argue the temperature gradient through that region is actually not linear but rather increases with depth. It is also apparent that these temperatures can not be in equilibrium with sea water at the sea bottom, but rather require that a temperature similar to that of sea water (1.7°C) be found at a depth of about 124.5 mbsf. The 0°C intercept is at 106.24 mbsf.

The two measurements obtained between 75 and 90 mbsf both give temperatures that are higher than obtained for measurement C15X at 142.3 mbsf. The temperature inversion between 90 mbsf and 142.3 mbsf implies that warm water is flowing laterally through the silty layers making up stratigraphic Unit II. In fact, not only must there be a flow of warm water at that level, but there must also be an inflow of colder water below to maintain the cooler temperatures below. A simple heat-diffusion calculation shows that the temperature of 3.2° measured at 142 mbsf could not be maintained for more than a few hundred years in the absence of a steady inflow of cold water.

The seismic reflection line across the site ("Seismic Stratigraphy" section, Figs. 38–39) shows that the nose of the fault block on which Site 718 is located breaks the sea surface and that the tilted reflectors characteristic of lithologic Unit III (104.5–190 mbsf) come close to or may reach the sea bottom. Thus, permeable layers within Unit III may serve as recharge zones with cool sea water flowing down them to the north. A preliminary model which fits the available data is that the warmer temperatures encountered in Unit II result from an upward flow of water from depth along the fault to the north of Site 718. This water can then be assumed to spread laterally in the relatively permeable silty turbidites of Unit II and to reach the surface south of the fault trace producing the observed band of high heat flow observed on the site survey (Fig. 3). This flow must be separated from a northward and downward flow of colder seawater within Unit III by impermeable clay layers near the top of Unit III. The flow must be quite vigorous to maintain the observed temperature structure.

This model, based on the temperature measurements, is supported by geochemical studies of the interstitial waters (see "Inorganic Geochemistry" section) which appear to require the mixing of two end-member fluids. One must have high Mg and SO<sub>4</sub> concentrations and can be identified as bottom sea water. The other must be low in Mg and SO<sub>4</sub> and could be a hot water component that has interacted with basement rocks and the immediately overlying sediments.

## SEISMIC STRATIGRAPHY

Site 718 was chosen on the basis of single-channel seismic reflection data acquired with a water gun source during a site survey by R/V *Robert D. Conrad* on cruise C2706 (Figs. 3, 37). The *Conrad* seismic line was filtered using a time varying band-pass filter, and single-channel migration was employed to improve the resolution and to precisely locate the fault surfaces. The processing greatly improved the amount of detail that could be observed in the acoustic stratigraphy and removed most of the diffractions associated with the faults (Fig. 2).

The site chosen was located at 1451 UTC, 11 July 1986, on the *Conrad* seismic record (Fig. 2). An alternative site was also chosen at 1257 UTC, 11 July 1986, 3.9 km away on a parallel seismic line. The site is located on the next fault block south from Sites 717 and 719 on a pronounced local heat-flow high observed during the site survey (Fig. 37). The site is located approximately 2 km south of the fault separating the two blocks, about one third of the way up the fault block. The sediment thickness at the site is 1.58 s of two-way traveltime.

The seismic stratigraphic section in the region studied on Leg 116 can be divided into two first-order acoustic units separated by a prominent seismic unconformity labeled "A" on Figs. 2 and 38. The lower unit is consistently 1.15 to 1.35 s thick and reflectors within it are parallel and follow the basement. This unit appears to represent the predeformation sedimentary section. Drilling at Site 717 suggested that unconformity A lies within a sequence of upper Miocene silty turbidites. It was assigned an age of about 7.5 Ma by interpolation between reliable paleontological dates. It thus probably corresponds to the "Upper Unconformity" noted by Curray and Moore (1971) further up the fan, which was also assigned an upper Miocene age based on drilling results from Site 218, DSDP Leg 22 (Moore et al, 1974).

The fault block on which Site 718 is located sits higher than that under Sites 717 and 719 and the difference in basement depth is reflected by a thinner postunconformity A section. Unconformity A is found at a depth of about 290 ms at the site chosen for Site 718. The upper portion of the seismic section throughout the Leg 116 study area consists of a nearly flat-lying sequence of reflectors 100–200 ms thick which unconformably overlie and truncate the deeper reflectors. This reflector sequence corresponds to a series of silty turbidites deposited very rapidly during the Holocene and late Pleistocene at Site 717. The same sequence of reflectors is observed on the fault block containing Site 718, although it is thinner than to the north (about 130 ms compared to 200 ms at Site 717) and the unconformity at its base is less well developed. The section between unconformities A and B, which is 500 ms (443 m) thick at Site 717, is thus compressed into about 105 ms at Site 718.

*JOIDES Resolution* approached the site from the north, obtaining a line over the location of Site 717 and the proposed location of Site 719 as well as of Site 718. The beacon was dropped as the ship passed over the site and the line was continued about 8 km to the south to obtain a seismic profile completely across the fault block. However, the data-logging computer malfunctioned during the seismic line and only the analog record is available. This record is shown in Fig. 39 with the lithologic section inserted at the location of Site 718. Because the great vertical exaggeration of the analog monitor record makes

Table 7. Index physical properties from Hole 718C.

Core	Section or core catcher (CC)	Top interval (cm)	Bottom interval (cm)	Sub-bottom depth (m)	Water content (% wet weight)	Porosity (%)	Wet-bulk density (g/cm <sup>3</sup> )	Grain density (g/cm <sup>3</sup> )
3X	2	67	70	30.47	37.17	61.08	1.73	2.69
4X	1	44	46	38.24	31.52	55.85	1.79	2.79
11X	1	113	117	105.43	35.46	57.14	1.74	
11X	2	60	64	106.40	40.01	63.81	1.69	2.67
11X	3	110	114	108.40	35.91	59.53	1.73	2.66
11X	4	61	65	109.41	35.46	58.27	1.74	2.57
12X	1	113	117	114.93	33.20	57.33	1.77	2.74
12X	2	60	64	115.90	31.20	55.86	1.86	2.83
13X	1	110	115	124.40	39.27	63.49	1.71	2.72
13X	2	74	78	125.54	33.88	58.94	1.80	2.84
14X	1	130	134	134.10	27.47	51.37	1.93	2.83
14X	2	60	64	134.90	38.46	62.95	1.70	2.75
14X	3	115	119	136.95	33.11	55.50	1.80	
14X	4	72	76	138.02	30.47	54.91	1.86	2.82
14X	5	114	118	139.94	36.14	60.76	1.74	2.77
15X	1	113	116	143.43	28.31	52.64	1.98	2.86
15X	2	14	17	143.94	36.43	59.31	1.78	
15X	3	2	5	145.32	35.19	58.29	1.80	2.61
16X	1	133	136	153.13	35.35	60.31	1.78	2.82
16X	2	37	40	153.67	29.64	54.56	1.89	2.89
16X	3	110	113	155.90	32.02	55.53	1.82	2.69
16X	4	124	127	157.54	29.17	53.83	1.93	2.87
16X	5	56	59	158.36	35.92	60.98	1.77	2.83
16X	6	80	83	160.10	35.42	58.75	1.75	2.63
17X	1	144	147	162.74	37.75	62.66	1.73	2.80
17X	2	103	107	163.83	36.24	59.84	1.76	2.65
17X	3	140	143	165.70	30.01	54.42	1.86	2.82
17X	4	100	103	166.80	34.99	58.11	1.76	2.61
17X	5	90	93	168.20	26.54	49.84	1.93	2.79
17X	6	108	111	169.88	33.50	58.38	1.78	2.82
18X	CC	22	25	171.02	28.17	52.41	1.90	2.85
19X	2	140	143	183.20	28.96	53.36	1.71	2.85
19X	3	137	140	184.67	34.79	58.70	1.79	2.70
19X	4	137	140	186.17	35.48	59.71	1.78	2.73
19X	5	14	17	186.44	37.35	60.77	1.89	2.63
20X	1	12	17	189.92	28.23	53.47	1.94	2.97
20X	2	80	84	192.10	27.90	52.22	1.94	2.86
25X	1	77	81	238.07	24.02	46.91	2.01	2.84
25X	2	20	24	239.00	31.18	56.48	1.87	2.90
27X	1	67	70	256.97	26.81	50.66	1.94	2.84
28X	CC	0	3	266.22	22.74	44.91	2.04	2.81
29X	CC	5	8	276.80	23.98	47.22	2.00	2.88
30X	1	35	38	285.15	25.68	49.14	1.97	2.84
32X	2	56	59	305.86	51.11	67.05	2.13	2.96
32X	CC	12	15	307.24	52.79	65.66	2.13	2.71
36X	CC	5	9	343.25	23.89	47.18	2.02	2.89
37X	1	129	133	352.59	23.68	46.74	2.01	2.87
37X	CC	5	8	353.02	22.00	44.30	2.07	2.86
38X	1	26	30	361.06	22.27	44.52	2.06	2.84
41X	2	57	60	391.37	28.98	49.10	1.87	
41X	2	147	150	392.27	24.20	47.46	2.00	2.87
41X	3	29	32	392.59	32.14	57.36	1.83	2.88
41X	4	65	68	394.45	31.58	56.60	1.85	2.86
41X	5	70	73	396.00	29.50	51.66	1.86	2.59
41X	6	119	122	397.99	21.75	43.49	2.09	2.81
41X	7	39	42	398.69	19.52	40.45	2.11	2.84
42X	1	95	98	399.75	23.09	45.67	2.00	2.84
42X	CC	0	3	400.52	19.38	40.82	2.15	2.91
43X	1	65	68	408.95	22.53	44.84	2.03	2.84
44X	1	80	83	418.60	23.48	46.27	2.03	2.85
45X	2	19	22	428.99	26.27	49.82	1.97	2.83
46X	1	113	117	437.93	21.47	43.56	2.10	2.87
46X	2	100	104	439.30	22.25	44.46	2.08	2.84
47X	1	11	16	446.41	23.43	45.84	2.03	2.81
47X	2	10	14	447.90	19.96	41.02	2.11	2.83

the details of the seismic stratigraphy difficult to see, the record from the site survey is also shown in Figure 38. This line is almost exactly coincident with the *JOIDES Resolution* line (see Fig. 37).

A synthetic seismogram was calculated using acoustic impedance values calculated from a compressional wave velocity log and a constant bulk-density profile (see "Logging" section). The synthetic program utilizes a 1-D convolution of a digitized

*Conrad* air-gun signature with the log-derived impedance profile; the program includes the effects of internal multiples, but not sea-floor multiples. The calculated acoustic impedance profile and the synthetic seismogram are compared with the lithologic column in Figure 40 and the synthetic seismogram is superimposed on the observed seismic section in Figure 41.

The synthetic seismogram begins at 140 mbsf as the log above that depth is affected by the presence of the drill pipe.

Table 7 (continued).

Core	Section or core catcher (CC)	Top interval (cm)	Bottom interval (cm)	Sub-bottom depth (m)	Water content (% wet weight)	Porosity (%)	Wet-bulk density (g/cm <sup>3</sup> )	Grain density (g/cm <sup>3</sup> )
48X	1	11	15	455.91	24.49	47.61	2.00	2.84
49X	1	88	92	466.18	21.23	42.96	2.08	2.84
49X	2	12	16	466.92	18.83	39.37	2.13	2.84
50X	2	5	9	476.35	20.79	42.18	2.08	2.82
50X	2	82	85	477.15	19.59	40.93	2.14	2.89
51X	1	121	125	485.51	19.19	39.79	2.13	2.83
51X	CC	3	7	486.12	17.38	37.01	2.16	2.84
52X	1	129	133	495.09	22.70	45.23	2.03	2.85
52X	2	8	12	495.38	16.81	35.72	2.17	2.79
53X	CC	4	7	504.44	22.24	44.40	2.05	2.83
54X	1	0	4	512.80	28.11	50.28	1.95	2.62
54X	1	84	88	513.64	22.68	44.96	2.06	2.83
55X	CC	16	20	525.46	20.43	41.93	2.09	2.86
56X	1	22	26	532.02	24.56	47.90	2.00	2.87
56X	2	118	122	534.48	22.19	46.37	2.07	2.81
56X	3	15	19	534.95	26.27	47.94	2.17	2.64
56X	CC	20	24	537.36	23.17	45.19	2.18	2.65
57X	1	146	150	542.76	22.12	44.44	2.06	2.86
57X	2	116	120	543.96	21.70	43.81	2.06	2.86
57X	3	116	120	545.46	22.40	44.90	2.04	2.87
57X	4	50	54	546.30	21.64	43.69	2.06	2.85
57X	CC	14	18	548.56	20.49	42.26	2.13	2.88
59X	1	89	93	561.19	21.65	43.79	2.09	2.86
59X	2	32	36	562.12	22.79	45.55	2.07	2.88
59X	3	103	107	564.33	29.77	54.09	1.89	2.82
59X	4	22	26	565.02	20.03	41.30	2.13	2.85
60X	1	126	130	571.06	20.58	41.88	2.09	2.82
60X	2	7	11	571.37	24.50	46.60	2.06	2.73
60X	CC	6	10	571.66	19.55	40.24	2.11	2.81
61X	1	85	89	580.15	20.80	42.63	2.11	2.87
61X	2	31	35	581.11	17.66	38.46	2.07	2.96
61X	3	7	11	582.37	20.59	42.05	2.09	2.84
62X	1	102	106	589.82	19.75	40.69	2.10	2.83
62X	2	138	142	591.68	20.99	42.69	2.10	2.85
62X	3	102	106	592.82	20.22	41.32	2.10	2.82
62X	CC	16	20	593.46	21.25	42.50	2.11	2.78
63X	1	106	110	599.36	19.64	40.63	2.16	2.84
63X	2	76	80	600.56	18.96	39.32	2.12	2.81
63X	3	70	74	602.00	18.05	38.12	2.15	2.84
63X	4	56	60	603.36	18.79	39.13	2.21	2.82
63X	5	45	49	604.75	20.62	42.24	2.16	2.86
63X	6	44	48	606.24	19.04	39.81	2.21	2.86
64X	1	59	64	608.39	16.40	35.79	2.21	2.89
64X	2	81	85	610.11	16.04	34.54	2.28	2.80
64X	3	44	48	611.24	16.45	35.66	2.22	2.86
64X	4	72	76	613.02	17.15	36.54	2.23	2.83
64X	5	104	108	614.84	17.62	37.45	2.17	2.84
64X	6	92	96	616.22	18.01	38.11	2.22	2.85
65X	1	94	97	618.24	16.92	36.18	2.21	2.83
65X	2	99	102	619.79	18.19	38.54	2.14	2.86
65X	3	99	102	621.29	16.76	35.70	2.25	2.80
65X	4	25	28	622.05	16.10	34.76	2.23	2.82
65X	5	66	69	623.96	18.96	39.36	2.13	2.82
66X	1	20	23	627.00	20.41	41.64	2.10	2.82
66X	2	117	120	629.47	19.74	40.05	2.11	2.76
66X	3	11	14	629.91	18.92	39.09	2.13	2.79
67X	1	101	104	637.31	18.47	38.61	2.16	2.82
67X	2	130	133	639.10	18.44	38.47	2.14	2.81
67X	3	69	71	639.99	18.12	37.52	2.15	2.76
67X	CC	20	23	640.63	17.22	36.51	2.22	2.81
68X	1	1	3	645.81	18.17	37.91	2.25	2.79
68X	1	106	110	646.86	18.79	39.13	2.15	2.82
69X	1	73	78	656.03	18.83	38.93	2.17	2.79
69X	2	143	147	658.23	18.17	38.17	2.17	2.82
69X	CC	17	21	658.47	16.82	35.70	2.23	2.79

The boundary between lithologic Units II and III is thus not recorded in the synthetic section. There is not a well-developed unconformity on this fault block, such as was found on the block containing Sites 717 and 719 (unconformity B). The flat-lying reflectors of lithologic Unit II tend to lap onto rather than truncate the underlying dipping reflectors.

One of the major differences in the section penetrated in Hole 718C compared to that of 717C is the condensed nature of

lithologic Units III and IV. These units extended from 152 mbsf to 533.2 mbsf (a total of 381.2 m) at Hole 717C, but are compressed into 85 m (100–185 mbsf) at Site 718. This difference is reflected in the seismic stratigraphy. The seismic unit corresponding to these two lithologic units, consisting of a sequence of reflectors thinning toward the top of the fault block through pinch-outs, is much thinner than on the block containing Site 717. It has a maximum thickness of 300 ms near the northern

Table 7 (continued).

Core	Section or core catcher (CC)	Top interval (cm)	Bottom interval (cm)	Sub-bottom depth (m)	Water content (% wet weight)	Porosity (%)	Wet-bulk density (g/cm <sup>3</sup> )	Grain density (g/cm <sup>3</sup> )
70X	1	112	116	665.92	16.86	35.50	2.19	2.76
71X	2	8	12	675.88	15.85	34.09	2.23	2.79
71X	3	120	124	678.50	16.80	35.66	2.23	2.79
71X	4	138	142	680.18	18.02	37.30	2.15	2.75
72X	1	65	69	684.45	18.28	37.72	2.13	2.75
72X	2	67	71	685.97	16.44	35.23	2.22	2.81
72X	3	41	45	687.21	16.11	34.11	2.20	2.74
72X	4	131	134	689.61	17.78	37.27	2.18	2.79
72X	5	144	148	691.24	17.28	37.30	2.23	2.89
72X	6	99	103	692.29	16.71	36.07	2.24	2.86
73X	1	79	83	694.09	17.92	37.50	2.15	2.79
73X	2	136	140	696.16	17.83	37.66	2.19	2.83
73X	3	93	97	697.23	17.94	37.64	2.18	2.80
73X	CC	33	37	697.80	16.39	35.31	2.22	2.83
74X	1	122	126	704.02	17.73	37.27	2.18	2.80
74X	CC	9	13	704.54	17.46	36.82	2.14	2.80
78X	1	109	113	741.89	17.21	36.48	2.16	2.81
78X	2	82	86	743.12	19.66	39.85	2.16	2.75
78X	3	79	83	744.59	16.98	36.23	2.23	2.82
78X	4	5	10	745.35	16.04	34.24	2.26	2.77
78X	4	111	115	746.41	16.31	34.51	2.23	2.75
78X	CC	12	16	748.30	14.14	30.64	2.28	2.72
79X	1	99	103	751.29	17.61	36.60	2.20	2.74
79X	2	52	54	752.32	15.64	33.31	2.31	2.74
79X	3	21	25	753.51	15.12	32.92	2.24	2.80
80X	1	109	111	760.89	17.35	36.38	2.20	2.77
80X	2	45	47	761.75	17.05	35.72	2.20	2.75
81X	1	113	115	770.43	16.90	35.84	2.19	2.79
81X	1	34	36	769.64	17.58	36.88	2.17	2.78
82X	1	141	149	780.21	14.15	31.31	2.32	2.81
82X	2	17	20	780.47	17.40	36.67	2.23	2.79
83X	1	66	70	788.96	17.65	36.74	2.17	2.75
83X	CC	35	39	790.15	17.88	37.33	2.16	2.78
84X	1	27	31	798.07	17.16	36.42	2.18	2.81
85X	1	67	70	807.97	16.39	35.29	2.24	2.83
85X	CC	19	22	808.80	15.72	33.87	2.21	2.79
86X	1	50	54	817.30	16.07	34.06	2.20	2.74
86X	2	55	59	818.85	16.72	35.66	2.20	2.80
86X	3	42	46	820.22	16.85	36.03	2.24	2.82
87X	1	102	104	827.32	15.98	34.61	2.23	2.83
87X	2	8	12	827.88	16.78	35.59	2.19	2.78
88X	1	57	61	836.37	20.60	41.37	2.13	2.76
88X	2	127	131	838.57	17.72	36.99	2.16	2.77
88X	3	55	59	839.35	16.53	35.51	2.20	2.82
88X	4	4	8	840.34	17.94	37.66	2.18	2.81
89X	1	29	33	845.59	14.95	33.02	2.27	2.85
90X	1	132	136	856.12	19.33	39.33	2.11	2.75
90X	CC	3	7	856.90	17.16	36.01	2.15	2.76
91X	CC	30	33	865.35	17.25	36.35	2.18	2.78
92X	CC	9	12	873.89	16.40	35.15	2.21	2.81
93X	1	18	20	878.18	15.38	33.14	2.22	2.77
94X	1	31	35	887.81	14.99	32.10	1.81	2.72
94X	2	103	107	890.03	15.49	33.63	2.74	2.81
94X	4	19	23	892.19	13.52	30.00	2.29	2.79
94X	5	75	79	894.25	13.89	30.43	2.38	2.75
94X	6	149	150	896.49	14.23	31.75	2.35	2.85
94X	7	10	14	896.60	15.16	33.04	2.29	2.81
94X	CC	19	21	896.98	13.49	30.41	2.30	2.85
95X	1	25	29	897.25	16.65	35.82	2.21	2.84
95X	CC	1	6	897.85	15.48	33.49	2.25	2.79
96X	1	52	56	907.02	16.91	35.72	2.19	2.77
97X	1	30	34	916.30	17.03	35.63	2.18	2.74

boundary fault and is about 105 ms thick at the location of Site 718. This interval consists of mud turbidites with thin interbedded clays and is of late Miocene to late Pleistocene age. The condensed section is expressed by the very low sediment accumulation rate during the Plio-Pleistocene (Fig. 8).

Unconformity A, which marks the onset of movement on the fault blocks, is found 90 ms (90 m) below the top of lithologic Unit V at Site 717. At Site 718, unconformity A again appears to occur 90 ms below the top of lithologic Unit V at a depth of about 280 m. The biostratigraphic control on the por-

tion of the section around the top of Unit V is not precise as it involves interpolating between an age determined in Unit IV and an age determined in Unit V, and there is a marked difference in accumulation rate for the clay turbidites of Unit IV and the siltier turbidites of Unit V. However, a linear interpolation gives an age of about 8 Ma for unconformity A. This is slightly older, but similar to the age 7.5 Ma determined at Site 717. It is also consistent with the presence of *A. Primus* with a first appearance of about 7 Ma in Core 104-718C-19, a few meters above the base of lithologic Unit IV.

**Table 8. Index physical properties from Hole 718E.**

Core	Section or core catcher (CC)	Top interval (cm)	Bottom interval (cm)	Sub-bottom depth (m)	Water content (% wet weight)	Porosity (%)	Wet-bulk density (g/cm <sup>3</sup> )	Grain density (g/cm <sup>3</sup> )
1R	1	124	128	934.34	17.77	37.31	2.17	2.80
1R	2	42	46	935.02	16.83	36.05	2.20	2.83
2R	1	56	58	943.16	13.05	28.86	2.30	2.74
2R	1	67	71	943.27	14.76	31.90	2.39	2.75
2R	2	79	83	944.89	17.12	36.53	2.20	2.83
2R	3	26	28	945.86	16.01	34.71	2.25	2.83
3R	1	14	18	952.24	17.11	36.34	2.17	2.81
3R	2	9	13	953.69	17.40	36.53	2.21	2.78
3R	CC	1	3	955.11	16.70	35.37	2.19	2.77

Hole 718C penetrated to a depth of 935 m, which corresponds to about 0.95 s on the seismic records using velocity information from the sonic log. The total depth to basement at the site on the seismic sections is 1.55 s, or about 1500–1600 mbsf. There is, however, no convincing evidence from the sediments that Hole 718C penetrated to near the bottom of the fan deposits. In particular, the silt to mud turbidites characterizing distal fan deposition throughout the section continued to the bottom of the hole. Although there are intervals of pelagic red and green clay deposition in Unit VB, they are never more than about 20 m thick and contain a number of small turbidites within them. As a result, they do not represent significant time intervals. The red clay intervals are found during a time of relatively higher sea level in the middle and lower Miocene (Haq et al., 1987) when the supply of sediment to the fan may have been less and the fan building process slower. The sedimentation rate during this time was, however, still relatively high, averaging about 90 m/Ma, and the sediments still reflect a distal fan environment. The pelagic clay intervals probably represent periods of time when the main fan activity had shifted to another lobe. There is also no evidence in the seismic records of a change in the character of the sediments between the base of Hole 718C and the basement (Fig. 38). It is thus entirely possible that the majority of the sediment below the base of Hole 718 consists of Bengal Fan turbidites.

The age of the sediments at the base of Hole 718C is about 17 Ma and, at the sedimentation rate of 90 m/Ma that was estimated for Unit VB, the approximately 600 m of sediment between the base of the hole and the basement could all have been deposited during the lower Miocene. This implies that the sedimentation rates prior to the initiation of fan sedimentation were quite low, with at most a few hundred meters of sediment deposited during a period of 60 Ma. It thus appears that fan building at the Leg 116 sites, 2500 km from the mouth of the Ganges, began at a rapid rate in the early Miocene.

### LOGGING

Two Schlumberger wireline logging tool strings were used in Hole 718C with the objective of providing a continuous record of *in-situ* physical properties of the sediments. Only one of these strings was run in Hole 718E. The logs can provide a correlatable record of the lithostratigraphic as well as the seismic stratigraphic sections vs. true depth. This is essential to the geological reconstruction of the fault-block history.

The first tool string was the seismic stratigraphic combination consisting of three separate instruments: (a) a digital long-spacing sonic log (LSS) measuring interval transit time (slowness) of sound waves in micro seconds per foot; (b) a phasor dual-induction log (DIT) measuring the bulk resistivity of the formation in ohm-meters; and (c) a natural gamma spectral log (NGT) measuring the absolute magnitude of gamma radioactivity of the formation and the relative content of the primary ra-

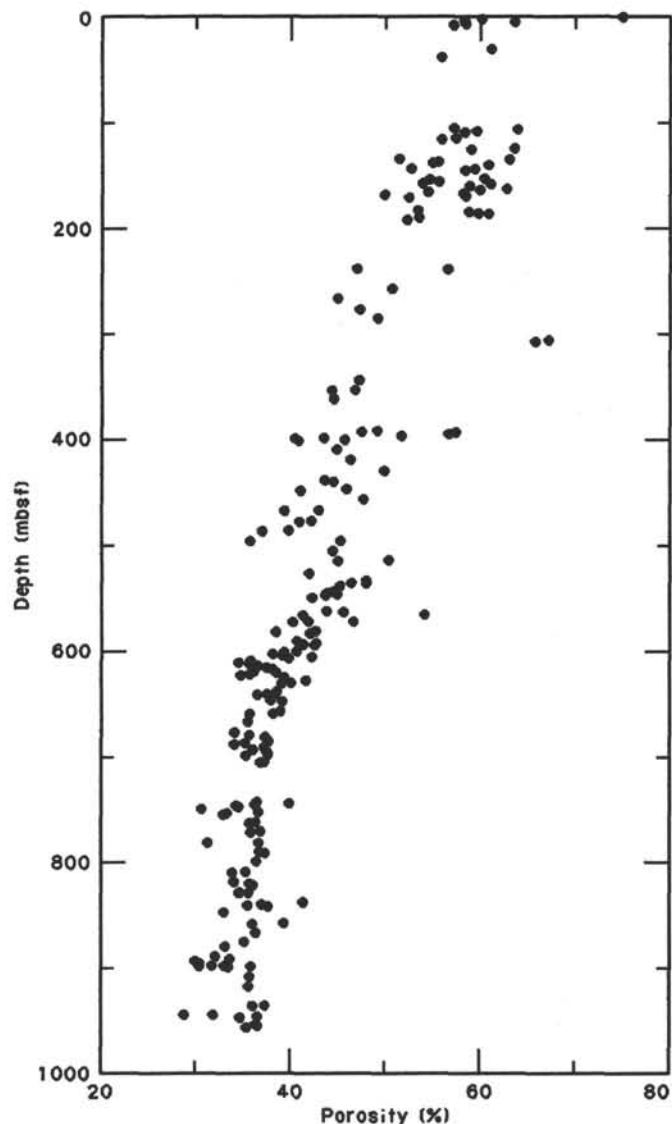


Figure 20. Porosity vs. depth at Site 718, Holes B and C.

dioactive elements potassium (% weight) and uranium and thorium (in parts per million).

The second tool string, the geochemical combination, consisted of four separate instruments: (a) a litho-density log (LDT) measuring bulk density (in g/cm<sup>3</sup>) and the photoelectric absorption cross section of 661 Kev gamma rays in barns/electron, a measurement sensitive to formation chemistry; (b) a gamma

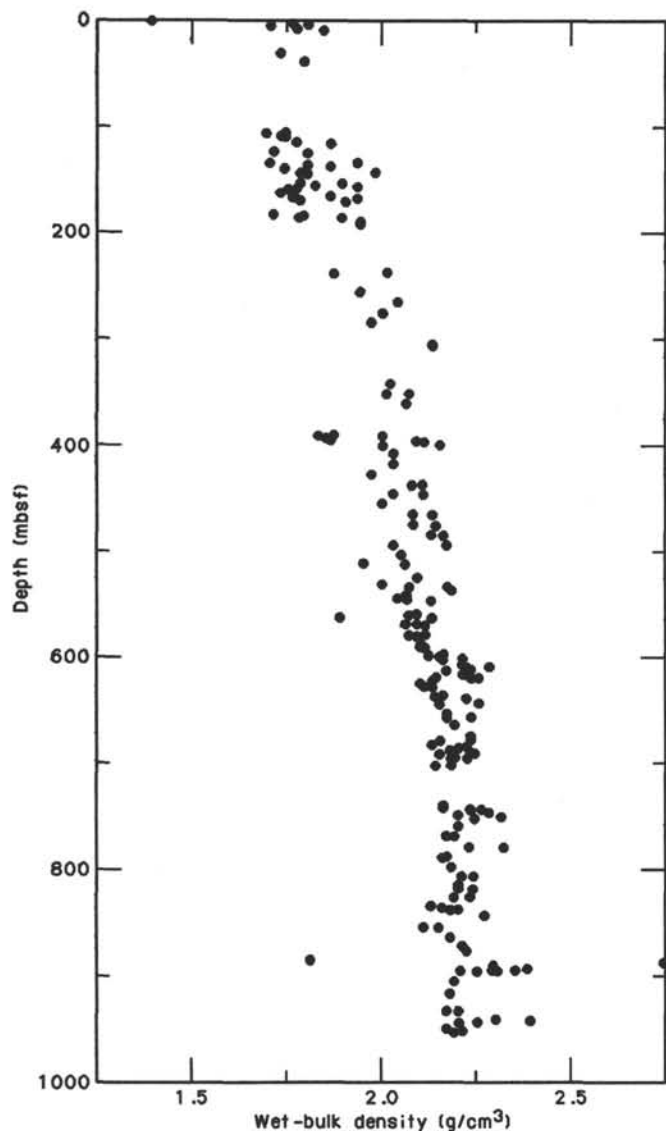


Figure 21. Wet-bulk density vs. depth at Site 718, Holes B, C, and E.

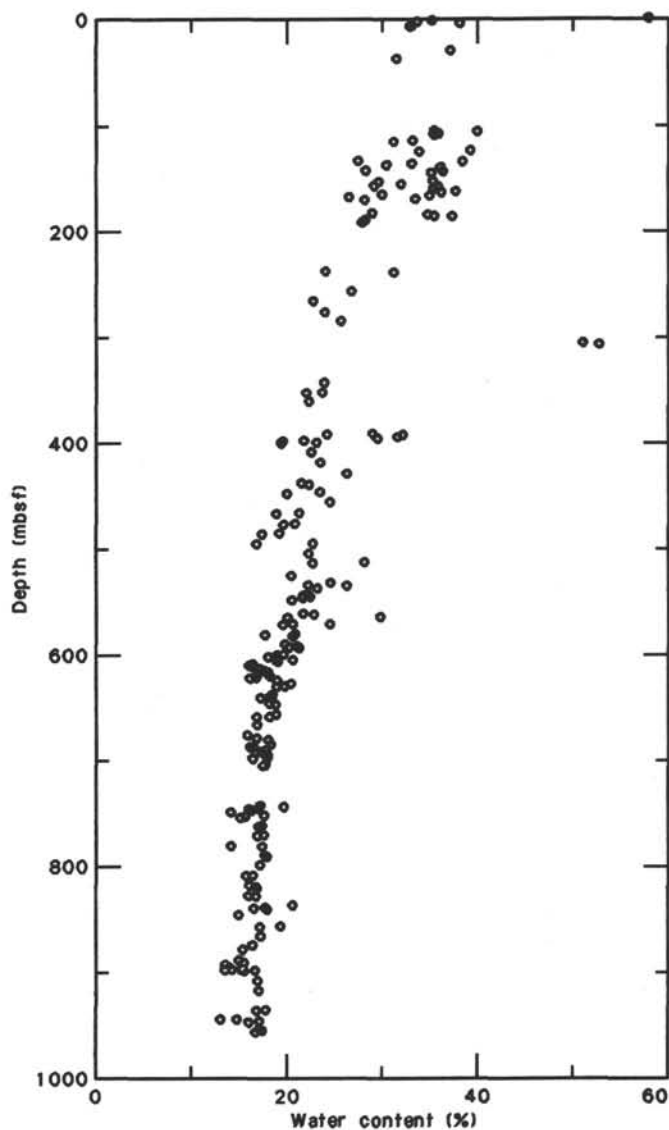


Figure 22. Water content vs. depth at Site 718, Holes B, C, and E.

spectroscopy log (GST), which measures various elemental yields in the sediments using gamma-ray spectra emitted by formation nuclei after bombardment by 14-Mev neutrons; (c) an aluminum activation clay log (AACT), which measures the weight percent of aluminum via neutron capture and subsequent emission of 1.78-Mev gamma rays; and (d) an NGT log to aid in correlating the two logging runs.

A more complete description of the logging measurements can be found in the Explanatory Notes chapter. The original logging data are displayed at the end of this chapter, along with correlations to core locations and recovery.

It should be kept in mind that conventional log interpretation applies to lithified sediments (Doveton, 1986; Schlumberger, 1986; Schlumberger, 1987; Serra, 1985; Borehole Research Group, 1986). In unconsolidated formations, such as were drilled at Site 718, some of the principal ideas presented in the literature may not be valid and so the interpretation of these logs may evolve as more information about the physical properties of shallow sediments accumulates.

Two points should be remembered. First, because the spatial frequency of measurements is 0.15 m and anti-alias filtering is not possible for a spatial sequence such as a wireline log, the Nyquist criterion implies that any spatial variations with a

wavelength less than 0.3 m will appear with a longer wavelength. For this reason a Fourier analysis of spatial variability must be limited in its application. However, in a sequence such as this, such an analysis may be interesting and is planned.

Second, each of the instruments has a different sampling volume and so will have a different impulse response to a step change in physical properties. The response of the resistivity and sonic transit time measurements will be a convolution of this volume with the true formation parameters and will exhibit a more gradual boundary gradient. This property alleviates some of the problems associated with discrete sampling mentioned above. Nuclear measurements generally sample a much smaller volume and the stochastic nature of the measurement produces a sharper impulse response. However, statistical variations in nuclear phenomena can produce spurious log responses.

## Measurements

### Seismic Stratigraphic Combination

#### Hole 718C

This tool string provided good-quality data from just below the pipe at 100 mbsf to 557 mbsf. This interval includes litho-

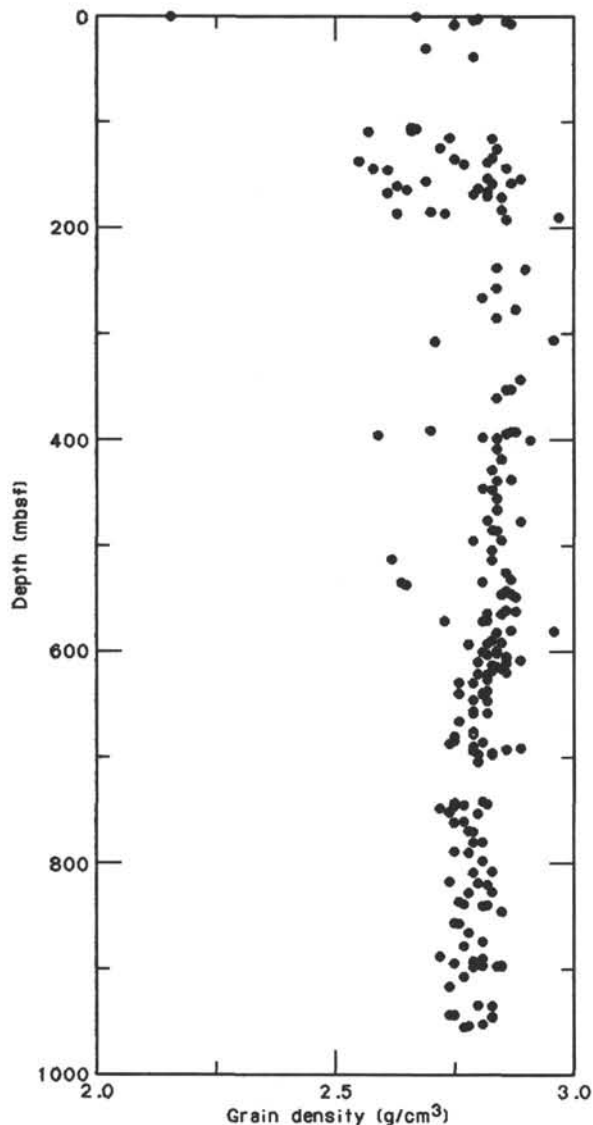


Figure 23. Grain density vs. depth at Site 718, Holes B, C, and E.

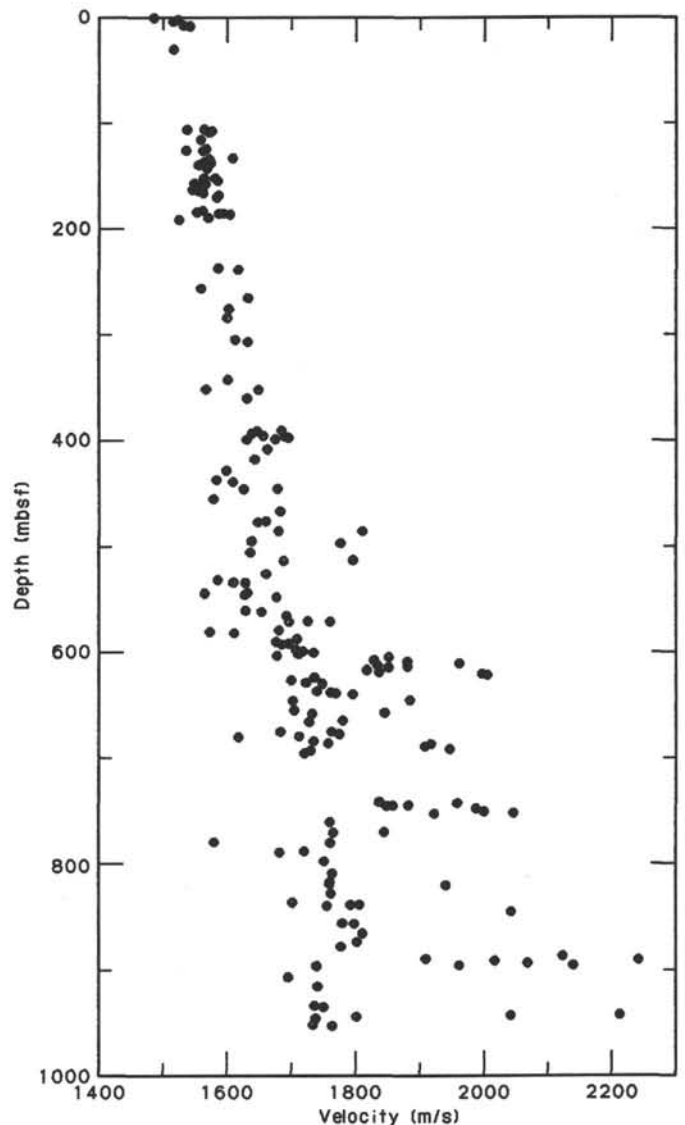


Figure 24. Sonic velocity vs. depth at Site 718, Holes B, C, and E.

logic Units III, IV, and subunit VA (see "Lithostratigraphy" section).

Log quality is good apart from the interval between 100 mbsf and 190 mbsf where sonic transit time is not useful due to the large diameter of the borehole. A large borehole causes the tool to measure the speed of sound in the borehole fluid (KCl drilling mud) because the transit time measurement is based on first arrivals. Hole size can only be estimated, as a hole diameter measurement was not available. This has an important consequence because all logged curves should be corrected for borehole geometry.

#### Hole 718E

The seismic stratigraphic combination tool string provided good-quality data from 173 mbsf to 950 mbsf in this hole. This includes all the bottom of Unit IV and all of Unit V. Log quality is generally better than hole 718C with much better hole conditions apparent from sonic transit time response.

Sonic transit time shows a general decrease downhole from an average value of 160  $\mu$ s/ft to 120  $\mu$ s/ft (1900 to 2530 m/s). Resistivity and gamma-ray response do not show a marked trend.

#### Unit III

Lithologic Unit III can be recognized most clearly on the NGT log from 100 to 157 mbsf. It consists of four distinct intervals characterized by their gamma-ray emissions (Fig. 42). Two of these have an abrupt bottom boundary below an increasing gamma radiation pattern usually referred in conventional log interpretation as a "shaling upwards" sequence. This term is strictly descriptive and should not be understood in the literal lithological sense because shales do not appear in these soft sediments. Figure 43 shows examples of these patterns. Interval 4 best illustrates this pattern. In contrast, interval 1 exhibits a shaling downwards pattern. Interval 2 shows a symmetrical pattern that is a mixture of the two trends. These trends are also present in the resistivity measurements but are much reduced in character.

A careful comparison of the interval 130–150 mbsf to the interbedded fining upward sequences found in Cores 116-718C-14X and -718C-15X is planned.

#### Unit IV

The top of Unit IV (157 to 192 mbsf) is capped by a radioactive marker that appears to correlate with a 1-m interval of silt

Table 9. Sonic velocity from Hole 718B.

Core	Section	Top interval (cm)	Bottom interval (cm)	Sub-bottom depth (m)	Sonic velocity (m/s)
1H	1	113	117	1.13	1491.7
1H	2	95	99	2.45	1529.6
1H	3	85	89	3.85	1527.8
1H	4	60	64	5.10	1521.9
1H	5	113	117	7.13	1536.6
1H	6	63	67	8.13	1546.3

and silt-mud turbidites in Sections 116-718-16X-4, 90 cm to 116-718-16X-5, 40 cm. It is not clear why this particular interval gives such a high gamma response.

Unit IV contains four distinct intervals, all of which show an abrupt bottom boundary and a shaling upward trend on the NGT log (Fig. 44). The absolute magnitude of CGR (total gamma counts minus uranium counts) curve in this unit is considerably less than in the other lithologic units, indicating lower thorium and potassium content especially at 168 and 177 mbsf. Note also that lower uranium content relative to the other units is also indicated. Conventionally, this signature might be interpreted as indicating a more sand-rich interval, but the core recovery shows less than about 10–15% silt layers within a mud-dominated section.

The low NGT readings between 190 and 191.5 mbsf correspond to the grayish green calcareous clay in Core 116-718C-19X-3, 0–140 cm. We believe these lower gamma-ray readings in Unit IV are due to the larger hole size in this interval rather than a true characteristic of the formation. This is supported by a comparison to the bottom 20 m of this unit observed in Hole 718E. The NGT readings in this section of Hole 718E confirm the character observed in the previous log but show elevated gamma-ray emissions in this unit. Measurements in Hole 719B also support the conclusion that a large borehole is shielding the tool from the formation radioactivity. Sonic velocity in this interval in Hole 718E is near 1740 m/s (175  $\mu$ s/ft).

*Subunit VA.* This unit at 192 to 605 mbsf is characterized by a distinctly higher radioactivity signature than Unit IV and an increase in sonic velocity to 1900 m/s, indicating a distinct lithology change at 192 mbsf. Subunit VA is characterized by features similar to Unit III with abrupt bottom boundaries and shaling upward sequences. Shaling downward sequences are also observed (Fig. 45). These trends are also clearly evident on the sonic record and indicate that the base of the shaling upward trends have a greater porosity that decreases upward. The opposite effect is observed through the shaling downward trends.

Shaling upward trends are from 5 to 7 m in thickness and end abruptly either with the bottom of another sequence or more usually from the base of intervals that do not show any distinct pattern. Shaling upward sequences account for 20% of the unit.

More monotonous intervals make up roughly 70% of the logged interval in this unit and are up to 25 m thick. Downward shaling trends account for the remaining 10%.

The interval 389–391 mbsf corresponds to the mud and silt turbidite sequence of Core 116-718C-41X. The interval 531–541 mbsf should be compared to Core 116-718C-56X, which is a silt and clay turbidite sequence that may grade in thickness upward.

Sonic velocity tends to increase with depth from 1900 m/s (160  $\mu$ s/ft) near the top of the unit to close to 2170 m/s (140  $\mu$ s/ft) near the bottom of Subunit VA at 605 mbsf. Sonic character varies from intervals of relatively stable velocity corresponding to the clays to intervals exhibiting greater velocity variation corresponding to the silts. Radioactive markers at 222, 239, and 275 mbsf may provide correlation points to other holes.

Table 10. Sonic velocity from Hole 718B.

Core	Section	Top interval (cm)	Bottom interval (cm)	Sub-bottom depth (m)	Sonic velocity (m/s)
3X	2	67	70	30.47	1521.7
11X	1	113	117	105.43	1569.6
11X	2	60	64	106.40	1542.0
11X	3	110	114	108.40	1580.8
11X	4	60	64	109.40	1576.4
12X	2	60	64	115.90	1563.4
13X	1	110	115	124.40	1571.4
13X	2	110	115	125.90	1568.2
13X	2	77	79	125.57	1540.5
14X	1	130	134	134.10	1613.9
14X	2	60	64	134.90	1575.6
14X	3	115	119	136.95	1568.0
14X	4	72	76	138.02	1578.1
14X	5	114	118	139.94	1560.2
15X	1	113	116	143.43	1572.9
16X	1	133	136	152.93	1567.3
16X	2	37	40	153.67	1585.9
16X	3	110	113	155.90	1589.3
16X	4	124	127	157.54	1553.6
16X	5	56	59	158.36	1570.2
17X	1	144	147	162.74	1560.1
17X	2	103	107	163.83	1550.9
17X	3	140	143	165.70	1560.7
17X	4	100	103	166.80	1566.6
17X	5	108	111	168.38	1589.2
18X	CC	22	25	171.02	1587.2
19X	2	140	143	183.20	1566.0
19X	3	137	140	184.67	1557.9
19X	4	137	140	186.17	1591.2
19X	5	14	17	186.44	1598.6
19X	CC	8	12	186.91	1609.3
20X	1	12	17	189.92	1574.5
20X	2	80	84	192.10	1530.6
25X	1	77	81	238.07	1590.3
25X	2	20	24	239.00	1622.0
27X	1	67	70	256.97	1563.8
28X	CC	0	3	266.22	1637.9
29X	CC	5	8	276.80	1608.5
30X	1	35	38	285.15	1605.2
32X	2	56	59	305.86	1617.8
32X	CC	12	15	307.24	1635.9
36X	CC	5	9	343.25	1605.3
37X	CC	5	8	353.02	1653.3
37X	1	129	133	352.59	1571.4
38X	1	25	30	361.05	1634.8
41X	2	57	60	391.37	1689.0
41X	2	147	150	392.27	1650.6
41X	3	29	32	392.59	1650.5
41X	4	65	68	394.45	1642.7
41X	5	70	73	396.00	1658.5
41X	6	119	122	397.99	1694.6
41X	7	39	42	398.69	1699.2
42X	1	95	98	399.75	1634.0
42X	CC	0	3	400.52	1678.6
43X	1	65	68	408.95	1667.3
44X	1	80	83	418.60	1647.2
45X	2	19	22	428.99	1601.7
46X	1	113	117	437.93	1586.7
46X	2	100	104	439.30	1612.5
47X	1	11	16	446.41	1629.2
47X	2	10	14	447.90	1682.0
48X	1	11	15	455.91	1580.2
49X	2	11	15	466.91	1688.9

*Subunit VB.* The top of this unit is not distinctive on the logs but roughly corresponds to a decrease in sonic velocity at 605 mbsf. This unit displays NGT characteristics virtually identical to Subunit VA. Sonic velocity shows a steady increase through the unit from 2025 m/s (150  $\mu$ s/ft) near the top to 2530 m/s (120  $\mu$ s/ft) near the bottom at 920 mbsf. The highest velocity observed is near 2890 m/s (105  $\mu$ s/ft) in a 1-m interval centered on 878 mbsf. The sonic log shows an alternation of intervals of little character and intervals of greater variation. Homogeneous

Table 10 (continued).

Core	Section	Top interval (cm)	Bottom interval (cm)	Sub-bottom depth (m)	Sonic velocity (m/s)
50X	2	5	9	476.35	1662.9
50X	2	82	85	477.12	1651.5
51X	1	121	125	485.51	1699.0
51X	CC	3	7	486.12	1815.0
51X	CC	3	7	486.12	1684.3
52X	1	129	133	495.09	1641.4
52X	CC	8	12	496.35	1780.8
53X	CC	4	7	504.44	1639.0
54X	1	0	4	512.80	1690.9
54X	1	84	88	513.64	1799.3
55X	CC	16	20	525.46	1665.6
56X	1	22	26	532.02	1589.5
56X	2	118	122	534.48	1613.4
56X	3	15	19	534.95	1631.8
56X	CC	20	24	537.36	1725.2
57X	2	116	120	543.96	1635.0
57X	3	116	120	545.46	1568.6
57X	4	50	54	546.30	1630.6
57X	CC	14	18	548.56	1681.3
59X	1	89	93	561.19	1632.8
59X	2	32	36	562.12	1656.6
59X	4	22	26	565.02	1695.8
60X	1	126	130	571.06	1700.4
60X	2	7	11	571.37	1728.7
60X	CC	6	10	571.66	1764.8
61X	1	85	89	580.15	1684.2
61X	2	31	35	581.11	1576.6
61X	3	7	11	582.37	1613.9
62X	1	102	106	589.82	1711.6
62X	2	138	142	591.68	1680.7
62X	3	102	106	592.82	1698.7
62X	CC	16	20	593.46	1686.5
63X	1	106	110	599.36	1711.2
63X	2	76	80	600.56	1718.9
63X	3	70	74	602.00	1736.7
63X	4	56	60	603.36	1715.2
63X	5	45	49	604.75	1680.1
63X	6	44	48	606.24	1853.5
64X	1	59	64	608.39	1830.7
64X	2	81	85	610.11	1882.2
64X	3	44	48	611.24	1963.9
64X	4	72	76	613.02	1835.9
64X	5	104	108	614.84	1883.8
64X	6	92	96	616.22	1853.0
65X	1	94	97	618.24	1819.8
65X	2	99	102	619.79	1838.4
65X	3	99	102	621.29	2000.0
65X	4	25	28	622.05	2007.6
65X	5	66	69	623.96	1738.1
66X	1	20	23	627.00	1703.8
66X	2	117	120	629.47	1725.7
66X	3	11	14	629.91	1750.6
67X	1	101	104	637.31	1742.5
67X	2	131	133	639.11	1762.9
67X	3	69	71	639.99	1771.7
67X	CC	20	23	640.63	1798.8
68X	1	1	3	645.81	1887.4
68X	1	106	110	646.86	1705.1
69X	1	73	78	656.03	1706.1
69X	2	143	147	658.23	1734.8
69X	CC	17	21	658.47	1847.3
70X	1	112	116	665.92	1729.1

Table 10 (continued).

Core	Section	Top interval (cm)	Bottom interval (cm)	Sub-bottom depth (m)	Sonic velocity (m/s)
70X	1	112	116	665.92	1782.7
71X	1	76	80	675.06	1687.6
71X	2	8	12	675.88	1764.8
71X	3	120	124	678.50	1776.3
71X	4	138	142	680.18	1714.3
71X	5	51	55	680.81	1621.9
72X	1	65	69	684.45	1737.2
72X	2	67	71	685.97	1759.5
72X	3	41	45	687.21	1919.3
72X	4	131	134	689.61	1909.5
72X	6	99	103	692.29	1948.4
73X	1	79	83	694.09	1730.5
73X	2	136	140	696.16	1722.6
73X	CC	33	37	697.80	1776.1
74X	1	122	126	704.02	1758.5
74X	CC	9	13	704.54	1745.2
78X	1	109	113	741.89	1838.9
78X	2	82	86	743.12	1960.6
78X	3	79	83	744.59	1884.1
78X	4	5	10	745.35	1860.1
78X	4	111	115	746.41	1852.2
78X	CC	12	16	748.30	1990.1
79X	1	99	103	751.29	2001.9
79X	2	52	54	752.32	2047.9
79X	3	21	25	753.51	1925.0
80X	1	109	111	760.89	1760.1
80X	2	45	47	761.75	1763.0
81X	1	113	115	770.43	1846.5
81X	2	34	36	771.14	1767.5
82X	1	141	145	780.21	1582.0
82X	2	17	20	780.47	1764.0
83X	1	66	70	788.96	1722.0
83X	CC	35	39	790.15	1684.7
84X	1	27	31	798.07	1753.8
85X	2	19	22	808.99	1766.1
86X	1	50	54	817.30	1762.5
86X	2	55	59	818.85	1762.1
86X	3	42	46	820.22	1943.7
87X	1	102	104	827.32	1763.3
87X	2	8	12	827.88	1764.0
88X	1	57	61	836.37	1703.6
88X	2	127	131	838.57	1805.4
88X	3	55	59	839.35	1795.2
88X	4	4	8	840.34	1758.2
89X	1	29	33	845.59	2043.9
90X	1	132	136	856.12	1780.9
90X	CC	3	7	856.90	1798.7
91X	CC	30	33	865.35	1811.9
92X	CC	9	12	873.89	1803.0
93X	1	18	20	878.18	1779.0
94X	1	31	35	887.81	2124.4
94X	2	103	107	890.03	1910.6
94X	3	72	76	891.22	2243.4
94X	4	19	23	892.19	2018.4
94X	5	75	79	894.25	2069.5
94X	6	148	150	896.48	1965.4
94X	7	10	14	896.60	2141.2
95X	1	25	29	897.25	1741.7
95X	C	1	6	897.85	1806.8
96X	1	52	56	907.02	1698.3
97X	1	30	34	916.30	1741.6

intervals show little variation in resistivity or NGT values. These characteristics will facilitate an electrofacies analysis and a comparison with cores.

**Geochemical Combination**

This tool string provided data of questionable log quality in Hole 718C from 225 mbsf to the obstacle in the hole at 575 mbsf. Useful information on aluminum yield may be extracted from the log by computer manipulation of the data. The LDT

measurements of bulk density and photoelectric cross section are of better quality than the GST yields.

Despite the hole-size problems mentioned above, the maximum values of density appear to be reliable and to show an increase with depth from 1.7 g/cm<sup>3</sup> in Units III and IV to 2.1-2.2 g/cm<sup>3</sup> in the silt-rich intervals of Unit V. The photoelectric factor (PEF) is anomalously low in the enlarged hole interval from 100 to 190 mbsf (Units III and IV), averages approximately 3.5 from 190 mbsf to 450 mbsf, and then decreases to an average of 3.0 down to 550 mbsf.

Table 11. Sonic velocity from Hole 718E.

Core	Section	Top interval (cm)	Bottom interval (cm)	Sub-bottom depth (m)	Sonic velocity (m/s)
1R	1	124	128	934.34	1736.4
1R	2	42	46	935.02	1751.1
2R	1	56	58	943.16	2213.4
2R	1	67	71	943.27	2042.7
2R	2	79	83	944.89	1801.9
2R	3	26	28	945.86	1738.8
3R	1	14	18	952.24	1734.7
3R	2	9	13	953.69	1765.5

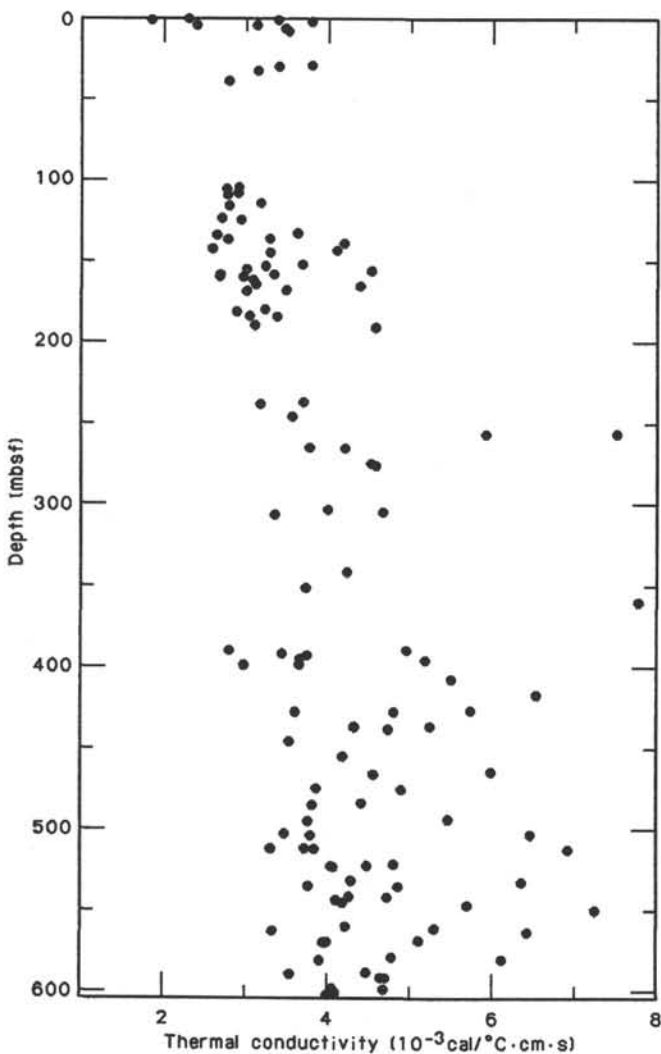


Figure 25. Thermal conductivity vs. depth at Site 718, Holes B and C.

### Summary and Interpretation

Several patterns in the log response may aid in the sedimentary interpretation of these data.

The shaling upward sequences are interpreted as a series of turbidites which were deposited in successively thinner beds upward, giving a characteristic log response. The shaling downward sequences can possibly be interpreted as a series of turbidites deposited in successively thicker beds. This may be a signature of compensation cycles in turbidite sand lobes as first suggested by Mutti and Sonnino (1981). These features can be

Table 12. Thermal conductivity measurements from Hole 718B.

Core	Section	Top interval (cm)	Bottom interval (cm)	Sub-bottom depth (m)	Thermal conductivity ( $10^{-3} \text{ cal} \cdot \text{°C}^{-1} \cdot \text{cm}^{-1} \cdot \text{s}^{-1}$ )
1H	1	113	114	1.13	2.3080
1X	1	148	149	1.48	1.8650
1H	1	149	150	1.49	3.4140
1H	2	60	61	2.10	3.8080
1H	3	113	114	4.13	2.4090
1H	4	60	61	5.10	3.1440
1H	5	113	114	7.13	3.5110
1H	6	60	61	8.10	3.5290

investigated further by a comparison of the log response with the core data.

A preliminary analysis of the NGT data for mineral identification shows some subtle differences between the units (Fig. 46). Almost all the data from all three units fall within the smectite and mixed-layer clay region of the plots. There are a few points in Unit III that indicate illite. Unit 4 shows some chlorite and kaolinite. Subunit VA has points in all three regions and some trending towards micas and feldspar.

As the radioactive markers mentioned above do not lie within sections of recovered core, a comparison with other holes will be necessary to establish the composition of these beds. If these can be identified, an electrofacies analysis may allow a more definitive lithological interpretation of the entire logged section.

### SUMMARY AND CONCLUSIONS

Four holes were drilled at Site 718 on the distal Bengal Fan in a water depth of 4730 m. Hole 718A was a single APC core 9.42 m long that was taken specifically for detailed pore-water geochemical measurements of the uppermost sediments. Hole 718B was then a repeat APC and together with 718C drilled a continuous section from the sea floor to 935 mbsf, setting yet another depth record for XCB penetration. Core recovery, however, was relatively poor—only 30% of the interval cored—mainly because of the abundance of unconsolidated silts and sandy silts that were apparently washed away ahead of the bit. Hole 718D was washed down to 70 mbsf to take additional water samples and temperature measurements where these had failed previously. Two cores were attempted in the zone where recovery in Hole 718C was zero and 0.17 m of loose sandy silt was recovered. After completion of scientific objectives at Site 719, the ship returned to Site 718. Hole 718E was washed to 933 m and then rotary cored in an attempt to extend the record of fan sedimentation further back in time. However, only three additional cores were obtained before drilling had to be suspended because of poor hole conditions. Hole 718C was logged from 140 m to bridge at about 560 mbsf. One logging run was made in Hole 718E from 913 mbsf to 173 mbsf.

Site 718 was drilled on the tilted fault block immediately to the south of the block drilled at Site 717 in an area of locally high heat flow (Figs. 2 and 3). Two main seismic units can be identified, a lower predeformational sequence (1.15 to 1.35 s thick), that shows a constant character throughout the area, and an upper postdeformational sequence (0.25 s thick). This upper sequence overlies reflector A and is markedly thinner than at the reference section of Site 717, with some possible erosion below reflector B (Fig. 2).

The stratigraphic section recovered ranges in age from Holocene to early Miocene (about 17 Ma) and has been divided into five major lithologic units (Fig. 5). Unit 1 (0–2.0 mbsf) is a thin upper layer of muds and pelagic oozes of Holocene and latest

Table 13. Thermal conductivity measurements from Hole 718C.

Core	Section	Top interval (cm)	Bottom interval (cm)	Sub-bottom depth (m)	Thermal conductivity ( $10^{-3} \text{ cal} \cdot \text{ }^{\circ}\text{C}^{-1} \cdot \text{ cm}^{-1} \cdot \text{ s}^{-1}$ )
3X	1	115	116	29.45	3.8200
3X	2	62	63	30.42	3.4130
3X	3	115	116	32.45	3.1670
4X	1	30	31	38.10	2.8150
11X	1	113	114	105.43	2.9280
11X	2	60	61	106.40	2.7810
11X	3	113	114	108.43	2.9230
11X	4	60	61	109.40	2.7930
12X	1	113	114	114.93	3.2110
12X	2	1	2	115.31	3.2040
12X	3	13	14	116.93	2.8140
13X	1	115	116	124.45	2.7270
13X	2	115	116	125.95	2.9510
14X	1	115	116	133.95	3.6490
14X	2	62	63	134.92	2.6660
14X	3	115	116	136.95	3.3200
14X	4	62	63	137.92	2.8070
14X	5	100	101	139.80	4.2270
15X	1	115	116	143.45	2.6150
15X	2	62	63	144.42	4.1340
15X	3	25	26	145.55	3.3250
16X	1	115	116	152.95	3.7050
16X	2	62	63	153.92	3.2710
16X	3	115	116	155.95	3.0320
16X	4	62	63	156.92	4.5540
16X	5	130	131	159.10	3.3750
16X	5	144	145	159.24	2.7010
16X	6	105	106	160.35	2.7010
16X	6	108	113	160.38	2.9970
17X	1	90	91	162.20	3.1050
17X	2	63	64	163.43	3.1030
17X	3	115	116	165.45	3.1470
17X	4	63	64	166.43	4.4260
17X	5	115	116	168.45	3.5210
17X	6	63	64	169.43	3.0360
19X	1	113	114	181.43	3.2650
19X	2	60	61	182.40	2.9230
19X	3	113	114	184.43	3.0740
19X	4	60	61	185.40	3.4100
20X	1	105	106	190.85	3.1400
20X	2	64	65	191.94	4.6170
25X	1	70	71	238.00	3.7250
25X	2	20	21	239.00	3.2140
26X	1	20	21	247.00	3.6020
27X	1	107	108	257.37	5.9490
27X	CC	19	20	257.61	7.5460
28X	1	31	32	266.11	3.7890
28X	CC	19	20	266.41	4.2430
29X	1	60	61	275.90	4.5650
29X	CC	9	10	276.84	4.6180
32X	1	113	114	304.93	4.0290
32X	2	59	60	305.89	4.7060
32X	CC	18	19	307.30	3.3880
36X	1	115	116	342.95	4.2560
37X	1	115	116	352.45	3.7590
38X	1	60	61	361.40	7.8100
41X	1	113	114	390.43	4.9920
41X	2	63	64	391.43	2.8230
41X	3	113	114	393.43	3.4730
41X	4	63	64	394.43	3.7770
41X	5	113	114	396.43	3.6860
41X	6	60	61	397.40	5.2190
42X	1	113	114	399.93	3.6740
42X	1	148	149	400.28	3.0060
43X	1	57	58	408.87	5.5320
44X	1	39	40	418.19	6.5670
45X	1	100	101	428.30	5.7710
45X	2	28	29	429.08	3.6290
45X	2	36	37	429.16	4.8350
46X	1	93	94	437.73	5.2770
46X	2	63	64	438.93	4.3500
46X	CC	5	6	439.41	4.7760
47X	1	115	116	447.45	3.5600
48X	1	30	31	456.10	4.2110
49X	1	60	61	465.90	6.0200
49X	2	60	61	467.40	4.5900

Table 13 (continued).

Core	Section	Top interval (cm)	Bottom interval (cm)	Sub-bottom depth (m)	Thermal conductivity ( $10^{-3} \text{ cal} \cdot \text{ }^{\circ}\text{C}^{-1} \cdot \text{ cm}^{-1} \cdot \text{ s}^{-1}$ )
50X	1	115	116	475.95	3.8980
50X	2	62	63	476.92	4.9440
51X	1	115	116	485.45	4.4380
51X	2	15	16	485.95	3.8500
52X	1	115	116	494.95	5.5090
52X	2	75	76	496.05	3.7820
53X	1	31	32	503.61	3.4990
53X	1	103	104	504.33	6.4950
53X	CC	12	13	504.52	3.8200
54X	1	32	33	513.12	3.7440
54X	1	60	61	513.40	3.3390
54X	1	87	88	513.67	3.8660
54X	CC	17	18	513.98	6.9640
55X	1	103	104	523.33	4.8350
55X	1	123	124	523.53	4.5140
55X	2	64	65	524.44	4.0800
55X	2	91	92	524.71	4.0900
56X	1	113	114	532.93	4.3190
56X	2	60	61	533.90	6.3590
56X	3	113	114	535.93	3.7990
56X	4	60	61	536.90	4.8920
57X	1	115	116	542.45	4.2920
57X	2	62	63	543.42	4.7640
57X	3	115	116	545.45	4.1320
57X	4	62	63	546.42	4.2090
57X	5	100	101	548.30	5.7350
58X	1	40	41	551.20	7.2981
59X	1	115	116	561.45	4.2555
59X	2	62	63	562.42	5.3330
59X	3	100	101	564.30	3.3640
59X	4	62	63	565.42	6.4610
60X	1	31	32	570.11	5.1469
60X	1	110	111	570.90	4.0206
60X	2	10	11	571.40	3.9860
61X	1	115	116	580.45	4.8199
61X	2	62	63	581.42	6.1540
61X	3	25	26	582.55	3.9348
62X	1	98	99	589.78	4.5130
62X	2	65	66	590.95	3.5720
62X	3	113	114	592.93	4.6830
62X	CC	18	19	593.48	4.7330
63X	1	113	114	599.43	4.0868
63X	2	60	61	600.40	4.7161
63X	3	103	104	602.33	4.1248
63X	4	60	61	603.40	4.0351

Table 14. Shear-strength measurements from Hole 718B.

Core	Section	Top interval (cm)	Bottom interval (cm)	Sub-bottom depth (m)	Shear strength (kPa)
1H	1	39	40	0.39	28.4
1H	5	120	121	7.20	21.3

Pleistocene age, overlying the thick poorly recovered section of silt and silt-mud turbidites that makes up Unit II (2-100 mbsf). Units III and IV (100-189.8 mbsf) comprise thin to medium-bedded mud turbidites, some thin silt-mud turbidites, and inter-bedded pelagic clays of Pliocene and late Miocene age. There is a highly condensed early Pleistocene to late Pliocene section toward the top of Units III and IV and another condensed sequence between the Pliocene and Miocene. The average accumulation rate for these units is about 20 m/m.y. whereas that for the overlying silts is at least an order of magnitude greater. The remaining section (Unit V) is characterized by silt and silt-mud turbidites with horizons of pelagic red and green clays, very thin-bedded green silt-mud turbidites and thin carbonate-silt turbidites becoming more common in the early Miocene section below 605 mbsf (Unit Vb). Accumulation rates for Unit V

Table 15. Shear-strength measurements from Hole 718C.

Core	Section	Top interval (cm)	Bottom interval (cm)	Sub-bottom depth (m)	Shear strength (kPa)
3X	2	61	62	30.41	33.1
11X	1	120	121	105.50	139.5
11X	2	65	66	106.45	158.4
11X	4	65	66	109.45	215.2
12X	1	104	105	114.84	158.4
12X	2	42	43	115.72	125.3
13X	1	119	120	124.49	212.8
13X	2	80	81	125.60	141.9
14X	1	135	136	134.15	108.8
14X	2	65	66	134.95	179.7
14X	3	112	113	136.92	92.2
14X	4	69	70	137.99	186.8
14X	5	120	121	140.00	134.8
15X	1	118	119	143.48	130.0
15X	2	17	18	143.97	198.6
16X	1	139	140	153.19	167.9
16X	2	42	43	153.72	120.6
16X	3	118	119	155.98	198.6
16X	4	127	128	157.57	78.0
16X	5	60	61	158.40	257.7
16X	6	84	85	160.14	231.7
17X	1	107	108	162.37	99.3
17X	1	141	142	162.71	177.3
17X	3	100	101	165.30	229.3
17X	4	101	102	166.81	307.4
20X	1	18	19	189.98	125.3
20X	2	85	86	192.15	158.4
25X	1	75	76	238.05	118.2
25X	2	17	18	238.97	264.8
41X	7	32	33	398.62	496.5

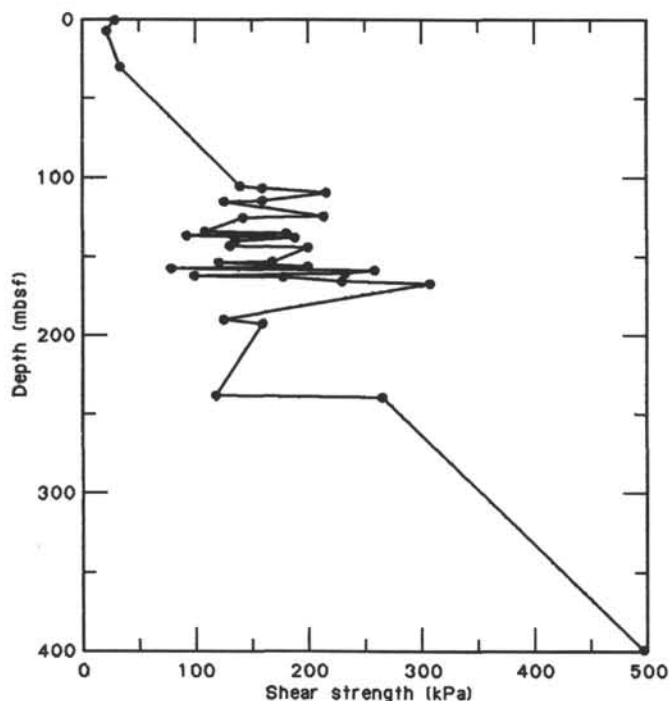


Figure 26. Shear strength vs. depth at Site 718, Holes B and C.

range from 50 to over 200 m/m.y. and average about 75 m/m.y. Seismic reflector B corresponds to the base of Unit II, and reflector A occurs about 60–90 m below the top of Unit V (Fig. 41).

The biostratigraphic control at Site 718 is based on sparse nannofossils and some foraminifers that have been preserved

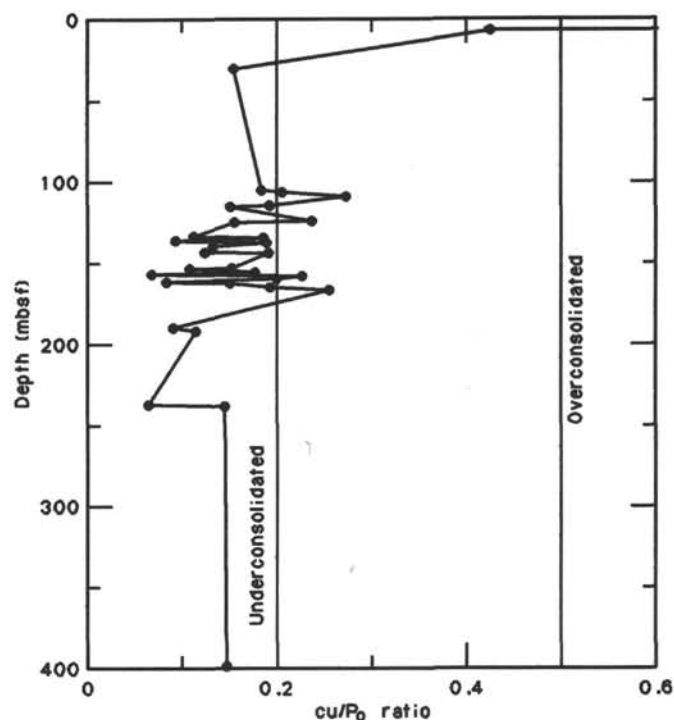
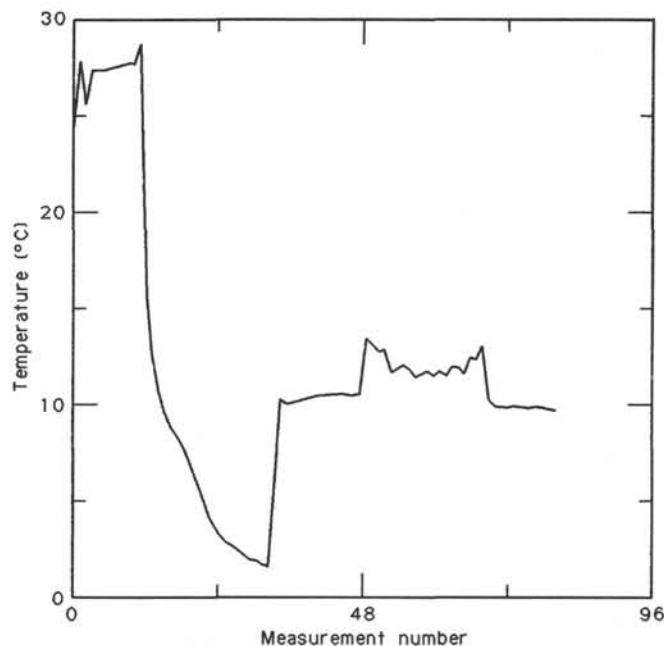
Figure 27. Undrained shear strength ( $c_u$ )/effective overburden pressure ( $P_0$ ) vs. depth at Site 718. Sediments with a ratio of less than 0.2 are underconsolidated.

Figure 28. Temperature vs. time record for temperature run C8X at 75.8 mbsf.

below the carbonate compensation depth by re-sedimentation in turbidites. Abundant calcareous and siliceous microfossils only occur in the uppermost Unit I. The reason for the complete absence of diatoms and radiolarians in the pelagic clays is not clear.

The downhole variation in pore-water geochemistry combined with an unusual temperature inversion observed at about

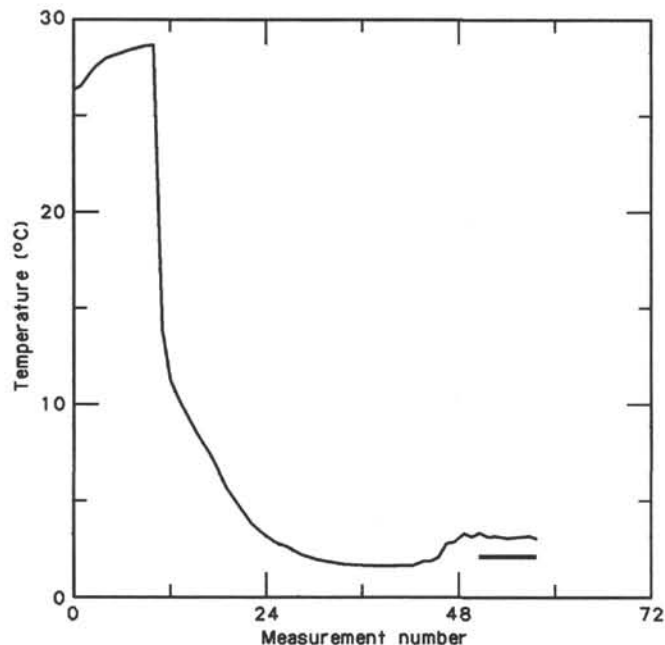


Figure 29. Temperature vs. time record for temperature run C15X at 142.3 mbsf. Bar under temperature record shows portion of readings used to extrapolate to equilibrium temperature.

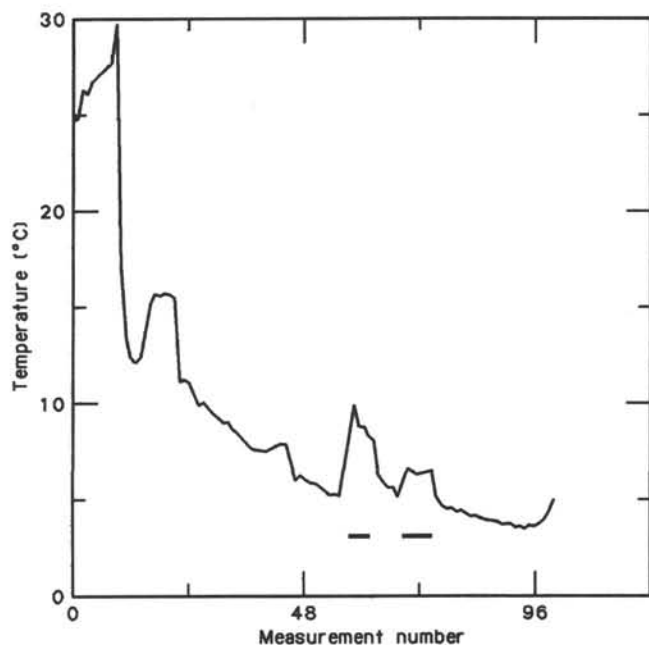


Figure 31. Temperature vs. time record for temperature run C18X at 170.8 mbsf. Bars under temperature record show portions of readings used to extrapolate to equilibrium temperature.

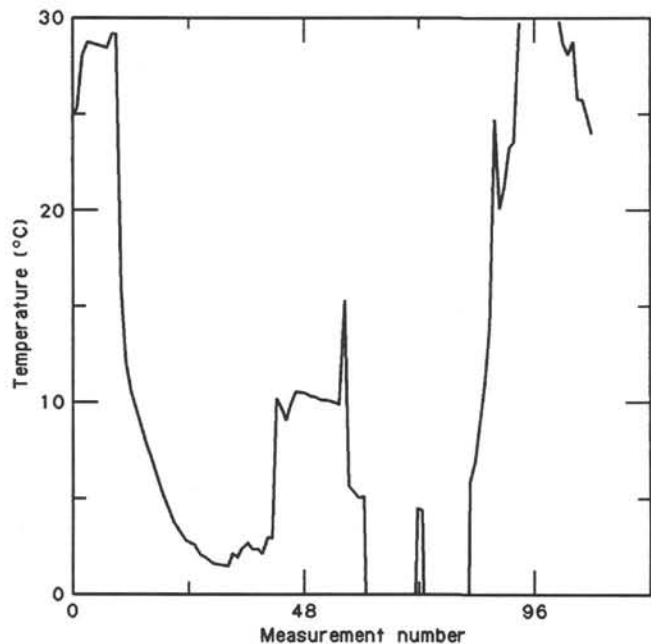


Figure 30. Temperature vs. time record for temperature run C16X at 151.5 mbsf.

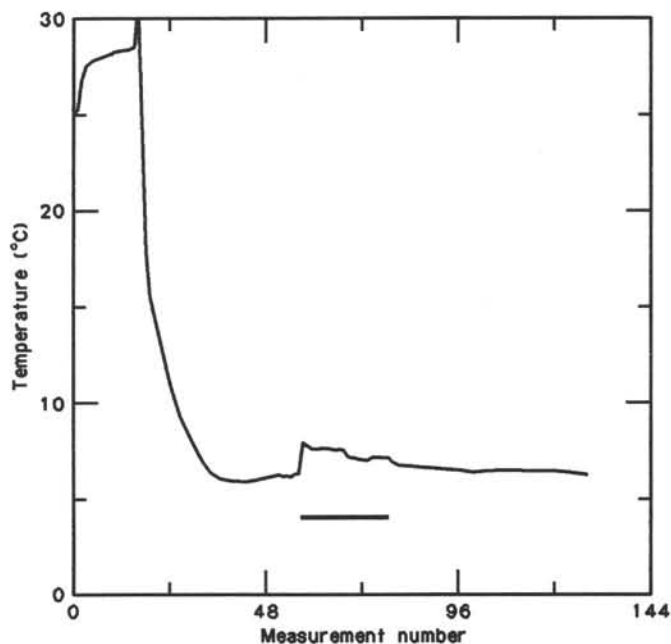


Figure 32. Temperature vs. time record for temperature run C20X at 189.8 mbsf. Bar under temperature record shows portion of readings used to extrapolate to equilibrium temperature.

100 mbsf (Figs. 13 to 22, 36) can be interpreted in terms of an active hydrothermal convection cell or cells. Both Mg and SO<sub>4</sub> show a marked decrease down to about 220 mbsf and then covary through a series of highs and lows through the remaining section.

There are two spikes in alkalinity and silica concentration at depths of about 750 and 820 mbsf that are also best interpreted as reflecting flow of water along permeable horizons. The water is interpreted to have originated from a deeper zone of sedi-

ment-fluid interaction at elevated temperatures, and has very similar characteristics to the water encountered at Site 717 at a depth of about 825 mbsf. A model of possible fluid circulation within the sedimentary section in the area of Site 718 is shown in Figure 22.

Interpretation of other downhole geochemical data together with preliminary observation of sediments and shipboard carbonate, XRD, and XRF data indicates that considerable early

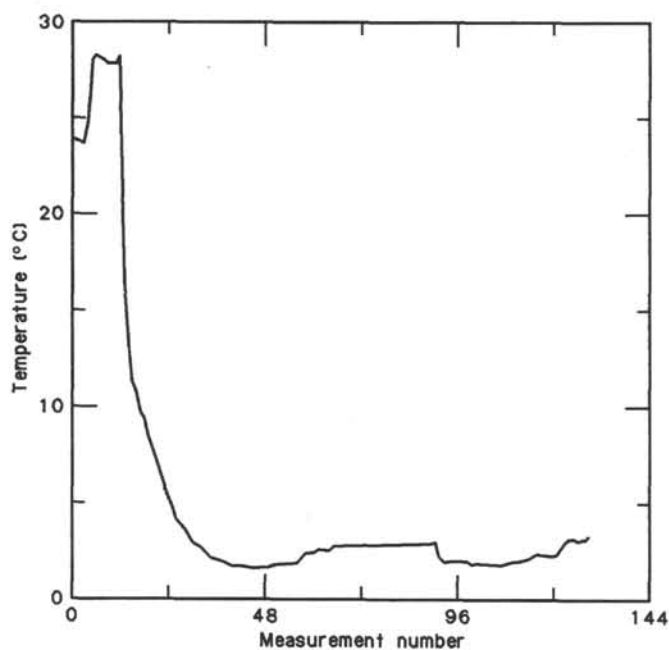


Figure 33. Temperature vs. time record for temperature run D1X at 71.0 mbsf.

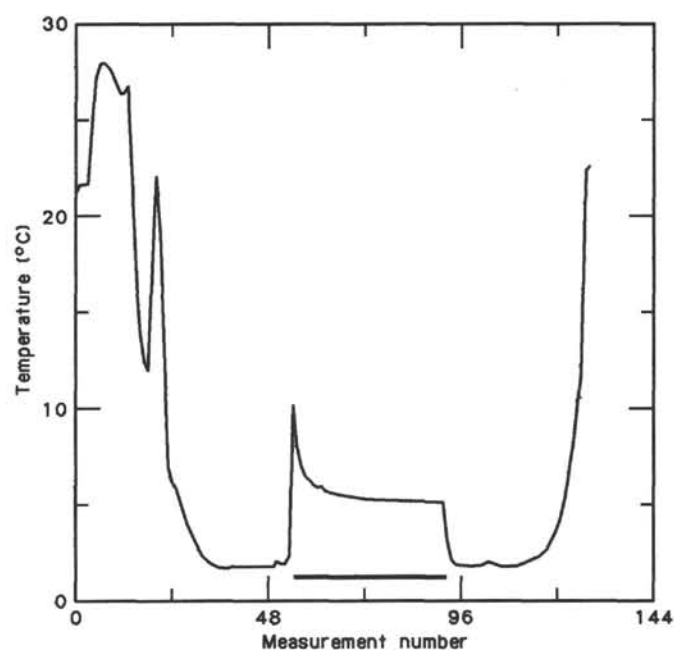


Figure 35. Temperature vs. time record for temperature run D3X at 90.9 mbsf. Bar under temperature record shows portion of readings used to extrapolate to equilibrium temperature.

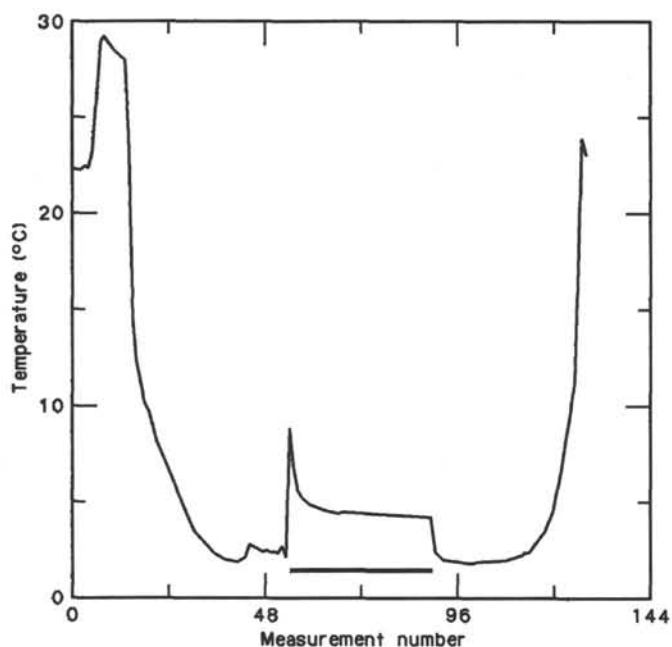


Figure 34. Temperature vs. time record for temperature run D2X at 80.5 mbsf. Bar under temperature record shows portion of readings used to extrapolate to equilibrium temperature.

diagenesis has already taken place. In the lower 200 m of the hole, the red and green pelagic clays are well compacted and semilithified and the carbonate turbidites are weakly cemented, whereas the gray turbidite silts and clays are less compacted. The silts contain up to 24%  $\text{CaCO}_3$  that is probably diagenetic in origin. Further shore-based work will help establish to what extent these diagenetic changes have been affected by the particular heat-flow characteristics at Site 718.

**Table 16. Downhole temperature measurements at Site 718.**

Measurement Hole	Core	Depth (m)	Temperature ( $^{\circ}\text{C}$ )
C	8X	75.8	—
C	12X	104.3	—
C	15X	142.3	3.20
C	16X	151.5	—
C	18X	170.8	6.37
C	20X	189.8	7.54
D	1X	71.0	—
D	2X	80.5	4.18
D	3X	90.0	5.18

The use of paleomagnetic measurements for magnetostratigraphy suffered from the same problems encountered at Site 717 (nonoriented XCB cores, low paleolatitude, and disturbed cores). However, the data on magnetic intensity and susceptibility provide useful information for comparison with the reference section at Site 717, and have been combined with the lithologic and biostratigraphic data to determine what part of the section is missing at Site 718. The main parts of the sequence at Site 717 that are not present at 718 appear to be 50 m of Unit II, at least 80 m of Unit III, and 200 m of Unit IV. Between 50 and 70 m at the top of Unit V is also missing.

Seismic stratigraphic interpretation supports the concept of missing section at Site 718 within the syn-deformational sequence above seismic reflector A (Fig. 38). It appears that erosion may have occurred beneath reflector B, however, it is not clear to what extent nondeposition has accounted for some of the thinning, perhaps due to deflection of turbidity currents by an upstanding fault block to the north. About 750 m of the pre-deformational section was penetrated without signs of nearing the bottom of the fan deposits. The red and green clay intervals of part pelagic origin that characterize Unit Vb were deposited during a time of relatively higher sea level in the middle and late

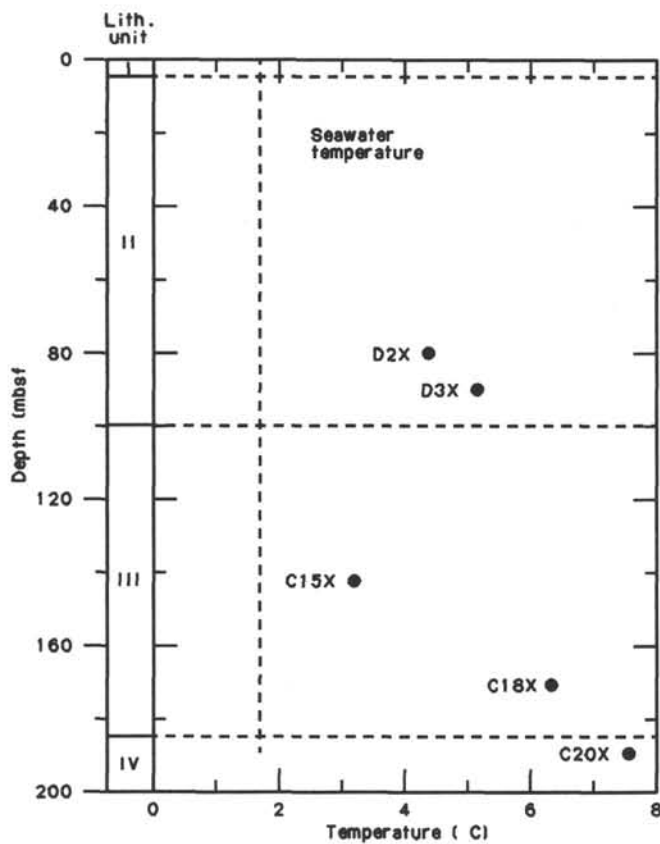


Figure 36. Plot of temperature vs. depth for Hole 718. Horizontal dashed lines show boundaries between lithologic units. Vertical dashed line shows bottom seawater temperature.

Miocene when the turbidite input was probably reduced and the fan building process slower. However, there is no apparent change in the seismic character between the level of the middle of Unit Va and the basement (Fig. 38), so that much of the underlying section may also be fan turbidites.

The physical properties measurements are also compatible with sediment erosion and/or nondeposition at Site 718. The shear-strength values of Units III and IV are similar to those at the base of Unit III and the top of Unit IV at Site 717. The porosity and sonic velocity data both indicate that the red and green clays of Unit VB are slightly overconsolidated for the depth of burial. However, it would appear that they have never been buried more than a few tens of meters deeper than their present depth so that the missing 400 m of section most likely represents both erosion, in conjunction with uplift of the block, and nondeposition. The clays are also weakly cemented, probably with siliceous material. There is limited evidence from the anisotropy of velocity, as at Site 717, for possible horizontal compression within the sedimentary section, but this awaits confirmation by further shore-based studies.

Two logging runs at Hole 718C were completed successfully in the open hole from 560 mbsf up to 100 mbsf. One suite of logs included gamma ray, resistivity, and sonic traces (the NGT-DIT-LSS tool string) while the other suite had gamma ray, spectral gamma, lithodensity and geochemical logs (the ACT-NGT-GST-LDT tool string). The first string was also successfully run into a depth of 933 m in Hole 718E. The interpretation of these conventional logs through unconsolidated muds and loose micaceous silts will require shore-based data reduction. Preliminary results confirm the lithological distinction between Units

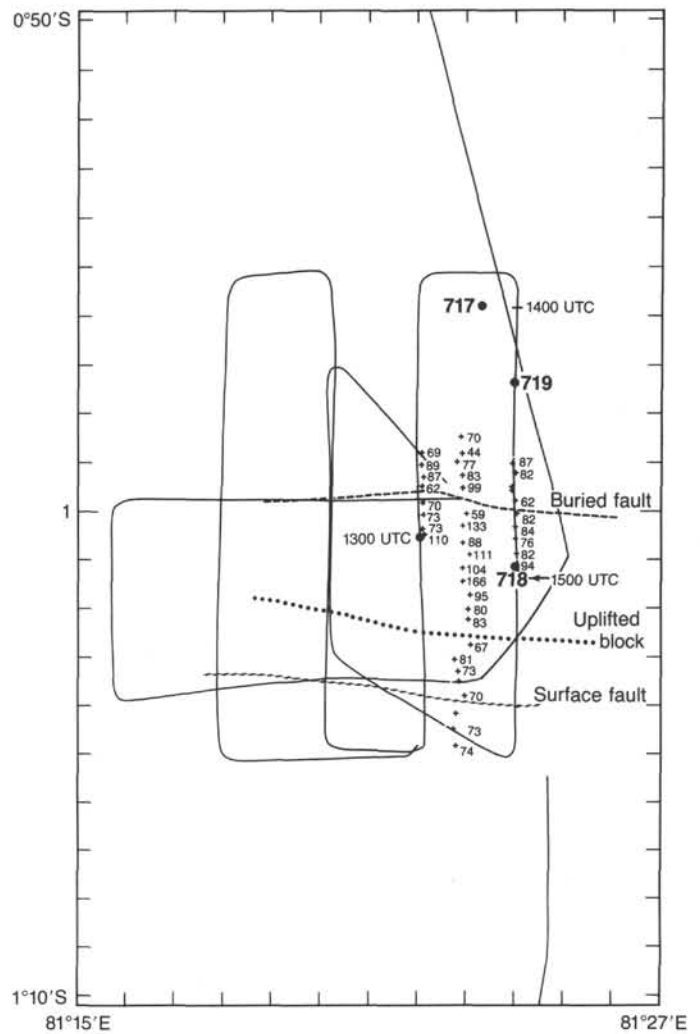


Figure 37. Site survey for Leg 116 sites carried out in 1986 on board *Robert D. Conrad*. Heat-flow stations are shown by small crosses with values in  $mW/m^2$ . Locations of Leg 116 sites are shown by large dots.

II, III, IV, and VA and indicate that zones of poor recovery in Subunit VA consist of the same alternation of silt and silt-mud turbidites as observed in the recovered sections. There are marked coarsening-upward and fining-upward trends within this Subunit on a scale of 3 m to 15 m that might be related to turbidite compensation cycles. In addition, there appears to be a slight overall coarsening-upward trend through the whole of Subunit VA.

In summary, the principal results of drilling at Site 718 are as follows.

1. The entire section recovered back to 17 Ma is dominated by turbidite sedimentation on the distal Bengal Fan. Fan sedimentation probably began at this Site in the earliest Miocene and makes up most of the sedimentary section in this part of the central Indian Ocean.
2. The early part of the predeformation sequence recovered may show evidence of thin silt-mud turbidites derived from a source other than the Ganges Delta source that dominates most of the section. The calcareous biogenic turbidites were probably derived from a local seamount source.
3. Movement on the fault block beneath Site 718 began about 7.5–8 Ma and has led to significant erosion and nondepo-

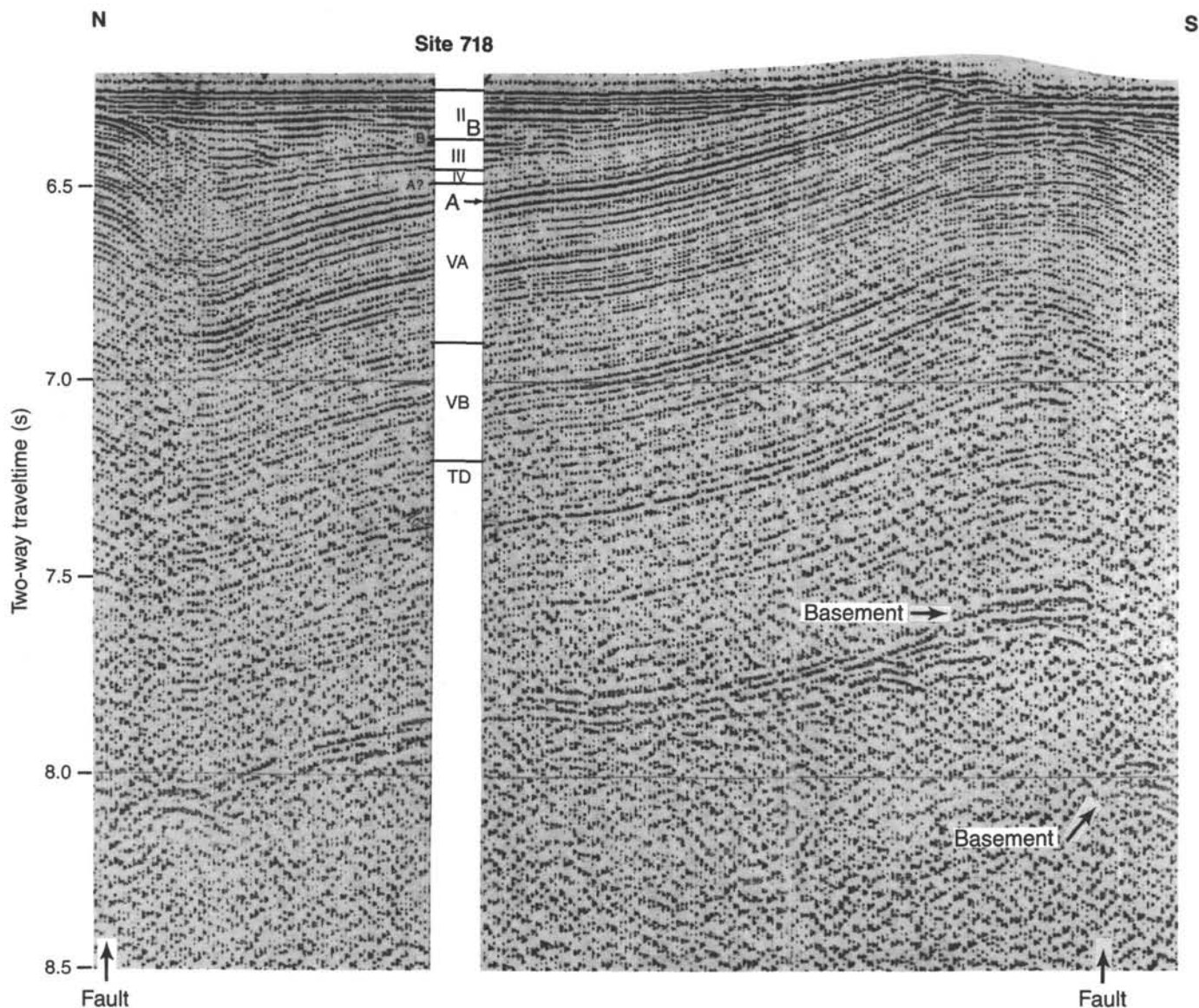


Figure 38. Single-channel seismic reflection line over Site 718 obtained by Robert D. Conrad during site survey for Leg 116. Lithologic units from Hole 718C are shown at location of Site 718 with depths converted to two-way traveltime. Unconformities "A" and "B" discussed in text are noted to left of lithologic column. Total length of profile is about 9.3 km.

sition of the syn-deformation sequence deposited above reflector "A" by comparison with that recovered at Site 717.

4. The pore-water geochemical profiles, combined with down-hole temperature measurements, provide dramatic evidence for vigorous hydrothermal circulation within the sedimentary section on this fault block. This type of circulation, we believe, has developed as a response to the compressive stress system and tectonic activity in the area.

#### REFERENCES

- Anderson, R. N., Langseth, M. G., and Sclater, J. G., 1977. The mechanisms of heat transfer through the floor of the Indian Ocean. *J. Geophys. Res.*, 82:3391-3410.
- Berggren, W. A., Kent, D. V., and van Couvering, J. A., 1985. The Neogene: Part 2, Neogene geochronology and chronostratigraphy. In Snelling, N. J., (Ed.), *The Chronology of the Geological Record*, *Geol. Soc. Mem.* (London) 10:211-260.
- Bjerrum, L. A., and Simons, N. E., 1960. *Proc. specialty conference in shear strength of cohesive soils*, Boulder, CO. American Society of Civil Engineers.
- Bolli, H. M., Saunders, J. B., and Perch-Nielsen, K., 1985. *Plankton Stratigraphy*. Cambridge, U.K. (Cambridge University Press).
- Borehole Research Group, 1986. *Wireline Logging Manual, Ocean Drilling Program: Palisades, N.Y.* (Lamont-Doherty Geological Observatory).
- Boulegue, J., Benedetti, E. L., Dron, D., Mariotti, A., and Letolle, R., 1987. Geochemical and biogeochemical observations on the biological communities associated with fluid venting in Nankai Trough and Japan Trench subduction zones. *Earth Planet. Sci. Lett.*, 83:356-362.
- Caulet, J.-P., 1986. Radiolarians from the Southwest Pacific. In Kennett, J. P., von der Borch, C. C., et al., *Init. Repts. DSDP, 90: Washington* (U.S. Govt. Printing Office), 835-861.
- Claypool, G. E., and Kvenvolden, K. A., 1983. Methane and other hydrocarbon gases in marine sediment, *Ann. Rev. Earth Planet. Sci.*, 11:299-327.
- Curry, J. R., and Moore, D. G., 1971. Growth of the Bengal deep-sea fan and denudation of the Himalayas. *Geol. Soc. Am. Bull.*, 82: 563-572.
- Curry, J. R., Emmel, F. J., Moore, D. G., and Raitt, R. W., 1982. Structure, tectonics and geological history of the northeastern In-

- dian Ocean. In Nairn, A. E. M., and Stehli, F. G. (Eds.), *The Ocean Basins and Margins* (Vol. 6). *The Indian Ocean*: New York (Plenum Press), 399-450.
- Doveton, J. H., 1986. *Log Analysis of Subsurface Geology*: New York (John Wiley and Sons).
- Dron, D., Boulegue, J., Taira, A., and Rangin, C., 1987. Geochemistry of the Tenryu Canyon deep-sea fan community (Kaiko). *Earth Planet. Sci. Lett.*, 83:356-362.
- Epp, D., Sager, W. W., Theyer, F., and Hammond, S. R., 1983. Hot-spot-spin axis motion or magnetic far-sided effect? *Nature*, 303:318-320.
- Geller, C. A., Weissel, J. K., and Anderson, R. N., 1983. Heat transfer and intraplate deformation in the central Indian Ocean. *J. Geophys. Res.*, 88:1018-1032.
- Hag, B. U., Hardenbol, J., and Vail, P. R., 1987. Chronology of fluctuating sea levels since the Triassic. *Science*, 235:1156-1167.
- McMillen, K. J., and Casey, R. E., 1978. Distribution of living polycystine radiolarians in the Gulf of Mexico and Caribbean Sea, and composition with sedimentary record. *Mar. Micropaleontol.*, 3:121-145.
- Moore, D. G., Curray, J. R., Raitt, R. W., and Emmel, F. J., 1974. Stratigraphic-seismic section correlation and implications to Bengal fan history. In Von der Borch, C. C., Sclater, J. G., et al., *Init. Repts. DSDP*, 22: Washington (U.S. Govt. Printing Office), 403-412.
- Mutti, E. and Sonnino, M., 1981. Compensation cycles: a diagnostic feature of turbidite sandstone lobes. In 2nd European Regional Meeting, Bologna, Italy, 1981. *Int. Assoc. Sedimentologists*, 120-123. Abstracts.
- Okada, H., and Bukry, D., 1980. Supplementary modification and introduction of code numbers to the low latitude coccolith biostratigraphic zonation (Bukry, 1973, 1975) *Mar. Micropaleontol.*, 5:321-325.
- Powell, C. M. A., and Conaghan, P. J., 1973. Plate tectonics and the Himalayas. *Earth Planet. Sci. Lett.*, 20:1-12.
- Rashid, M. A., (Ed.) 1985. *Geochemistry of marine humic compounds*: Berlin (Springer-Verlag), 1-34.
- Rice, D. D., and Claypool, G. E., 1981. Generation, accumulation, and resource potential of biogenic gas. *Am. Assoc. Pet. Geol. Bull.*, 5: 5-25.
- Richards, A. F., 1962. Investigations of deep sea sediment cores II: Mass physical properties. U.S. Navy Hydrographic Office, *Tech. Rep.*, 106.
- Schlumberger Well Services (Houston), 1986. *Log Interpretation Charts*. Schlumberger Well Services (Houston), 1987. *Log Interpretation. Principles/Applications*.
- Sclater, J. G., and Fisher, R. L., 1974. The evolution of the east central Indian Ocean with emphasis on the tectonic setting of the Ninety East Ridge. *Geol. Soc. Am. Bull.*, 85:683-702.
- Sclater, J. G., Luyendyk, B. P., and Meinke, L., 1976. Magnetic lineations in the southern part of the central Indian Basin. *Geol. Soc. Am. Bull.*, 87:371-378.
- Serra, O., 1985. *Sedimentary Environments from Wireline Logs*: Houston (Schlumberger Well Services).
- Skempton, A. W., 1970. The consolidation of clay by gravitational compaction. *Quart. J. Geol. Soc. London*, 125:373-411.
- Stein, S., and Okal, E. A., 1978. Seismicity and tectonics of the Ninety east Ridge area: evidence for internal deformation of the Indian plate. *J. Geophys. Res.*, 83:2233-2245.
- Takahashi, K., and Honjo, S., 1981. Vertical flux of Radiolaria: a taxon-quantitative sediment trap study from the western tropical Atlantic. *Micropaleontol.*, 27:140-190.
- Tarling, D. H., 1983. *Palaeomagnetism*: London (Chapman and Hall).
- Thompson, R. W., 1974. Mineralogy of sands from the Bengal and Nicobar fans, sites 218 and 211, eastern Indian Ocean. In von der Borch, C. C., Sclater, J. G., et al., *Init. Repts. DSDP*, 22: Washington (U.S. Govt. Printing Office), 711-714.
- Tissot, B. P., Durand, B., Espitalie, J. and Combaz, A., 1974. Influence of the nature and diagenesis of organic matter in the formation of petroleum. *Am. Assoc. Pet. Geol. Bull.*, 58:499-506.
- Tissot, B. P., and Welte, D. H., 1984. *Petroleum Formation and Occurrence* (2nd ed.): Berlin (Springer-Verlag).
- Weissel, J. K., Anderson, R. N., and Geller, C. A., 1980. Deformation of the Indo-Australian plate. *Nature*, 287:284-291.

Ms 116A-106

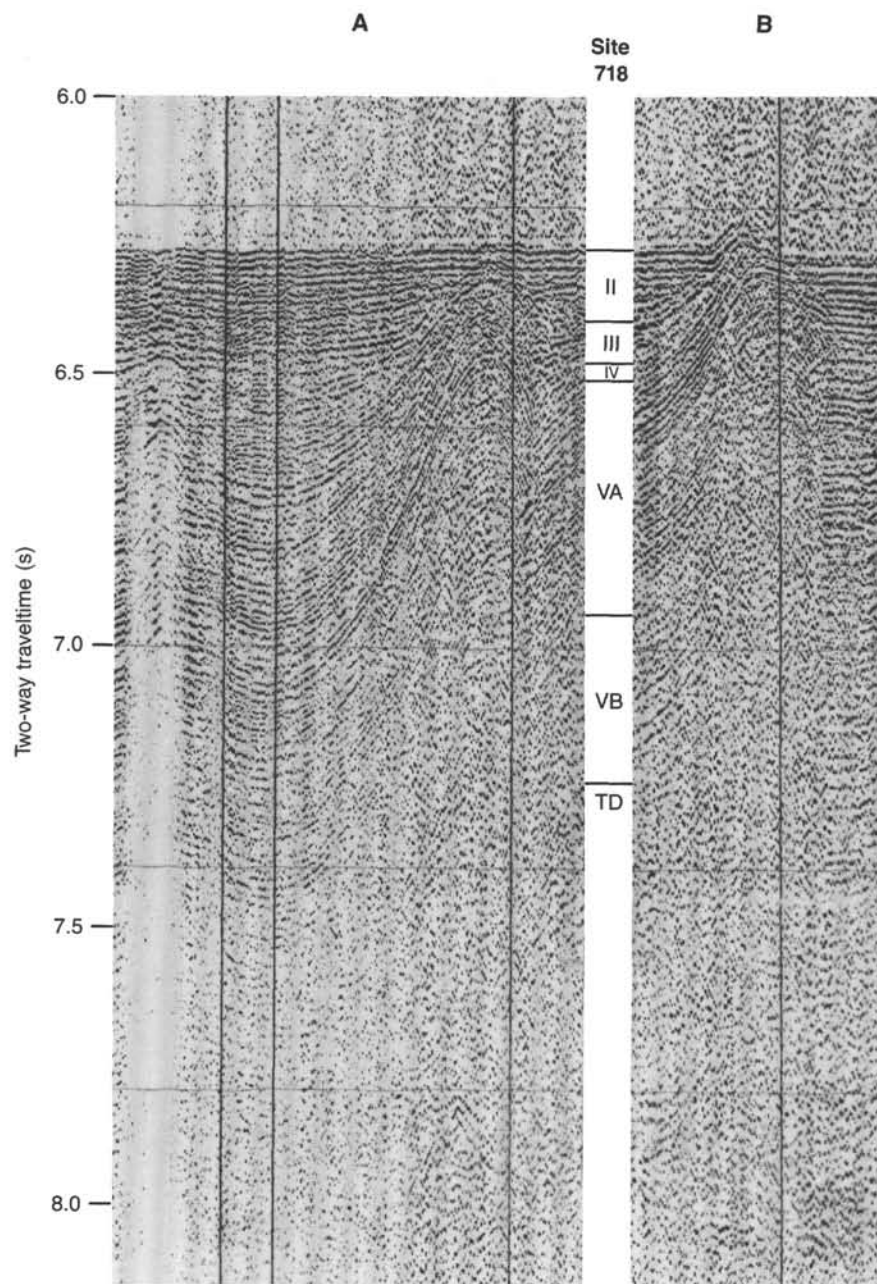


Figure 39. Single-channel seismic reflection line obtained by *JOIDES Resolution* on the final approach to Site 718. Lithologic units from Hole 718C are shown at the location of Site 718 with depths to lithologic boundaries converted to two-way traveltime. Location of line is shown on Figure 38.

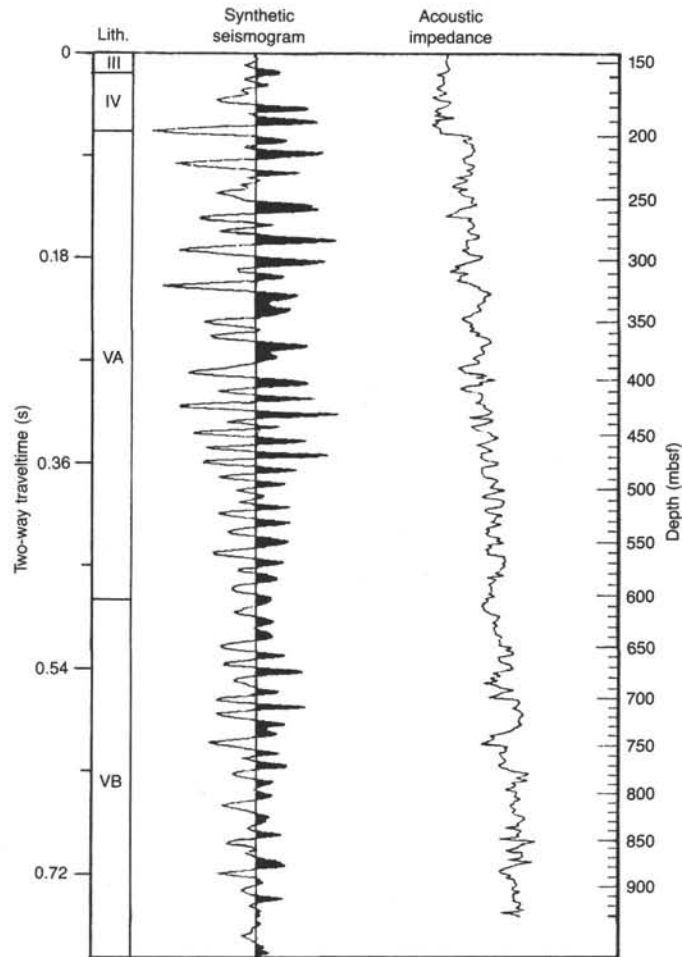


Figure 40. Synthetic seismogram for Site 718 compared with the lithologic column. The acoustic impedance profile was determined from sonic velocity logs combined with a constant bulk density. The two-way travelltime scale is linear and measured from the top of the logged interval (140 mbsf).

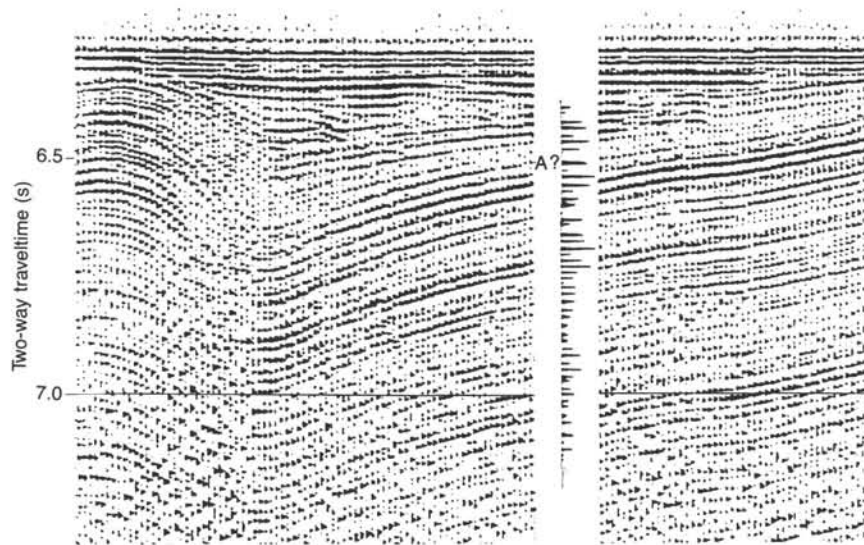


Figure 41. Single-channel seismic reflection record obtained by the *Conrad* at Site 719, along with the synthetic seismogram. Unconformity "A" (discussed in text) is noted in the profile.

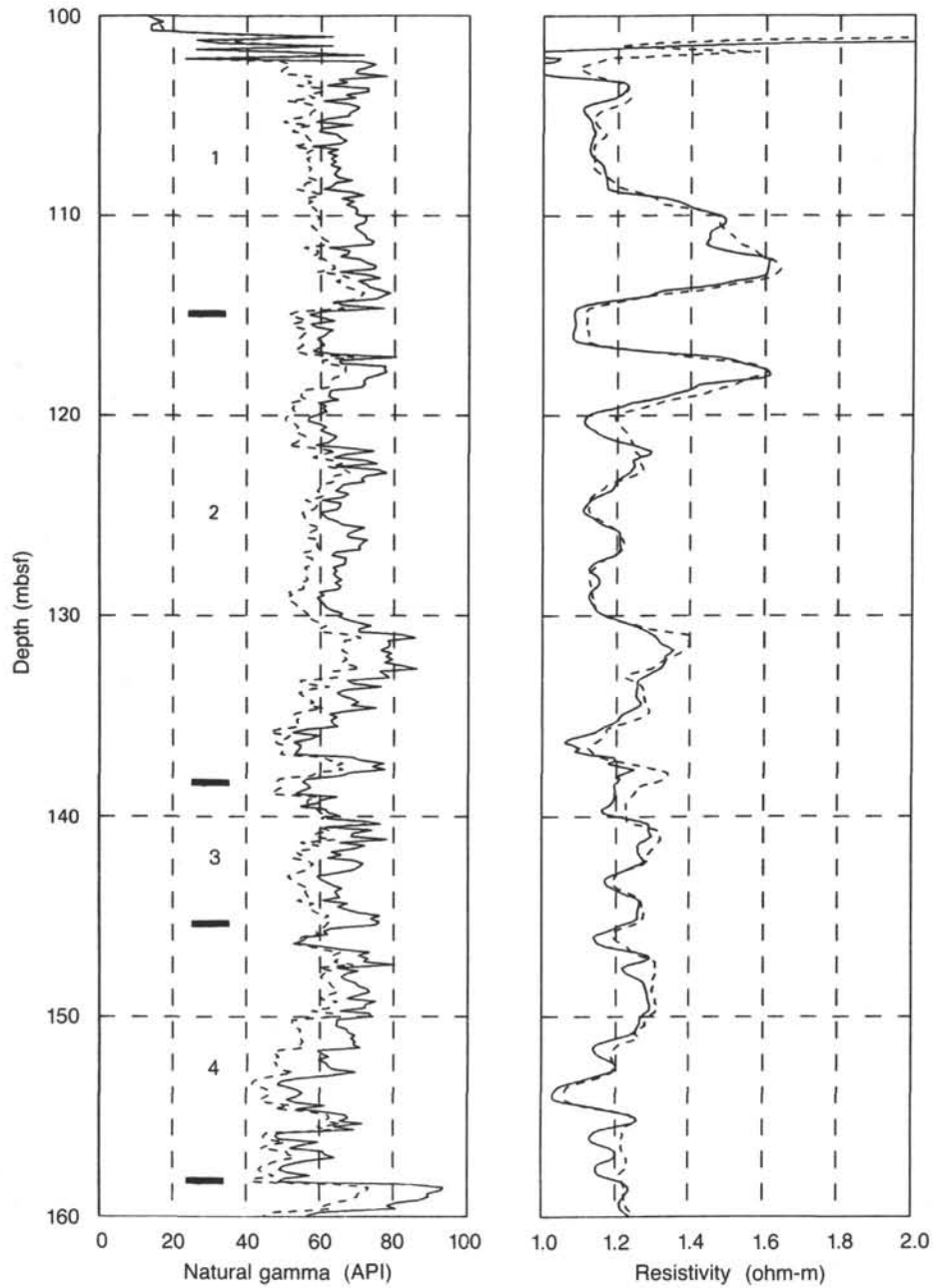


Figure 42. Gamma-ray and resistivity log response in Unit III showing intervals discussed in text and correlation point in cored section, Hole 718C.

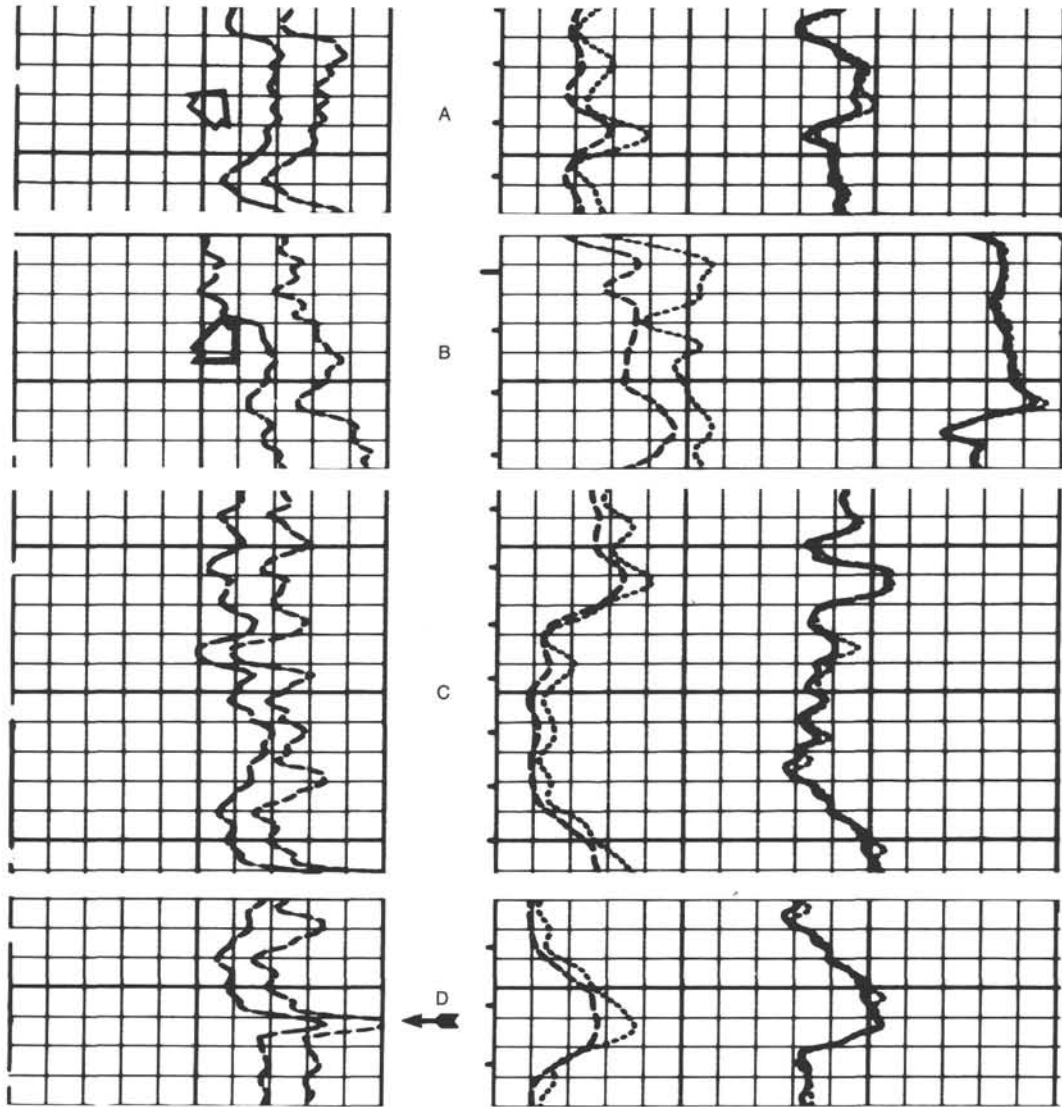


Figure 43. Trends observed on logs: (A) shaling upwards; (B) shaling downwards; (C) sawtooth sequences; (D) radioactive markers. Depth scale: 1 grid interval equals 1 m. Left track is total natural gamma-ray emissions with uranium and without uranium. Resistivity and sonic transit time (DT) are shown in right track.

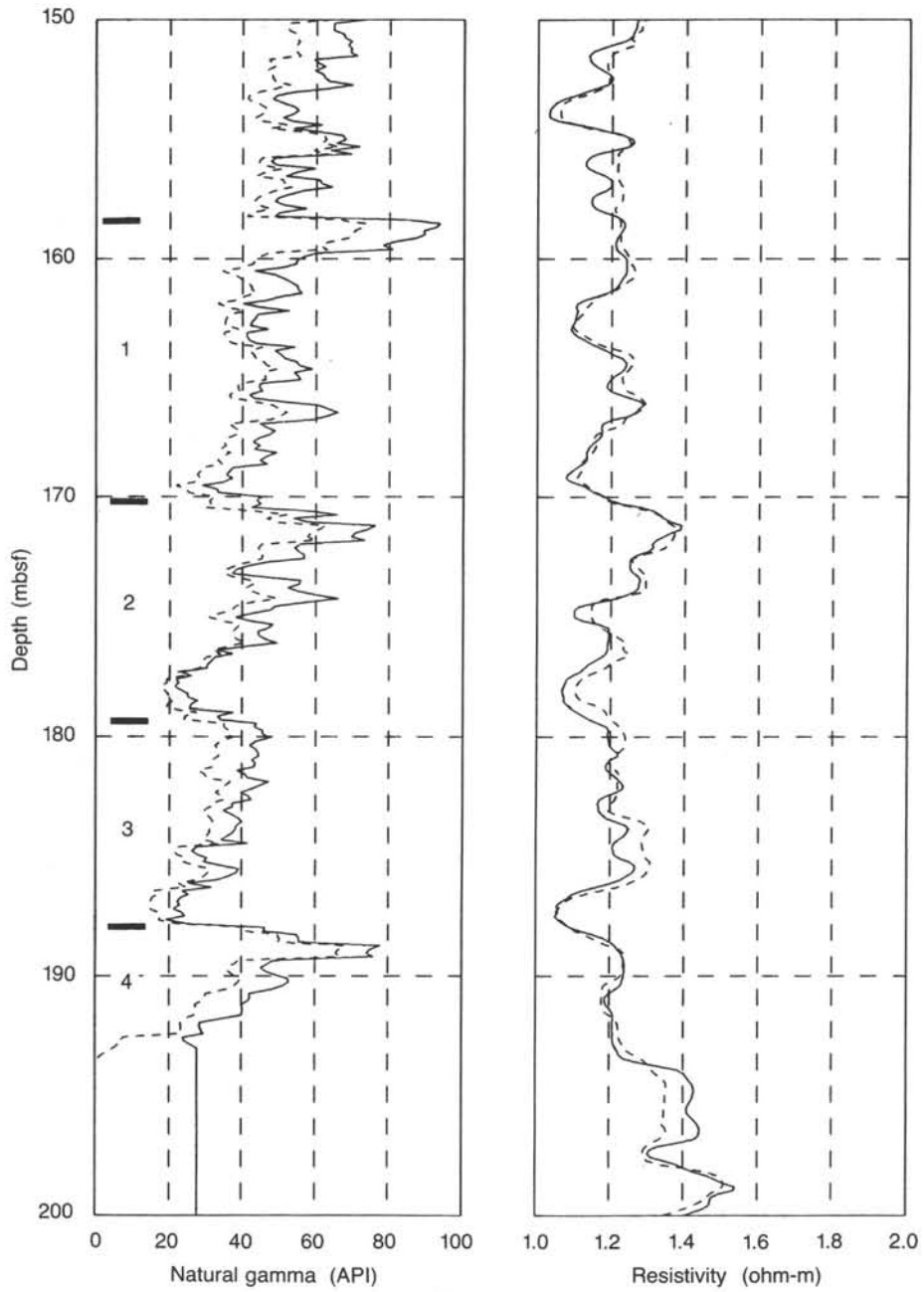


Figure 44. Gamma-ray and resistivity log response in Unit IV showing intervals discussed in text.

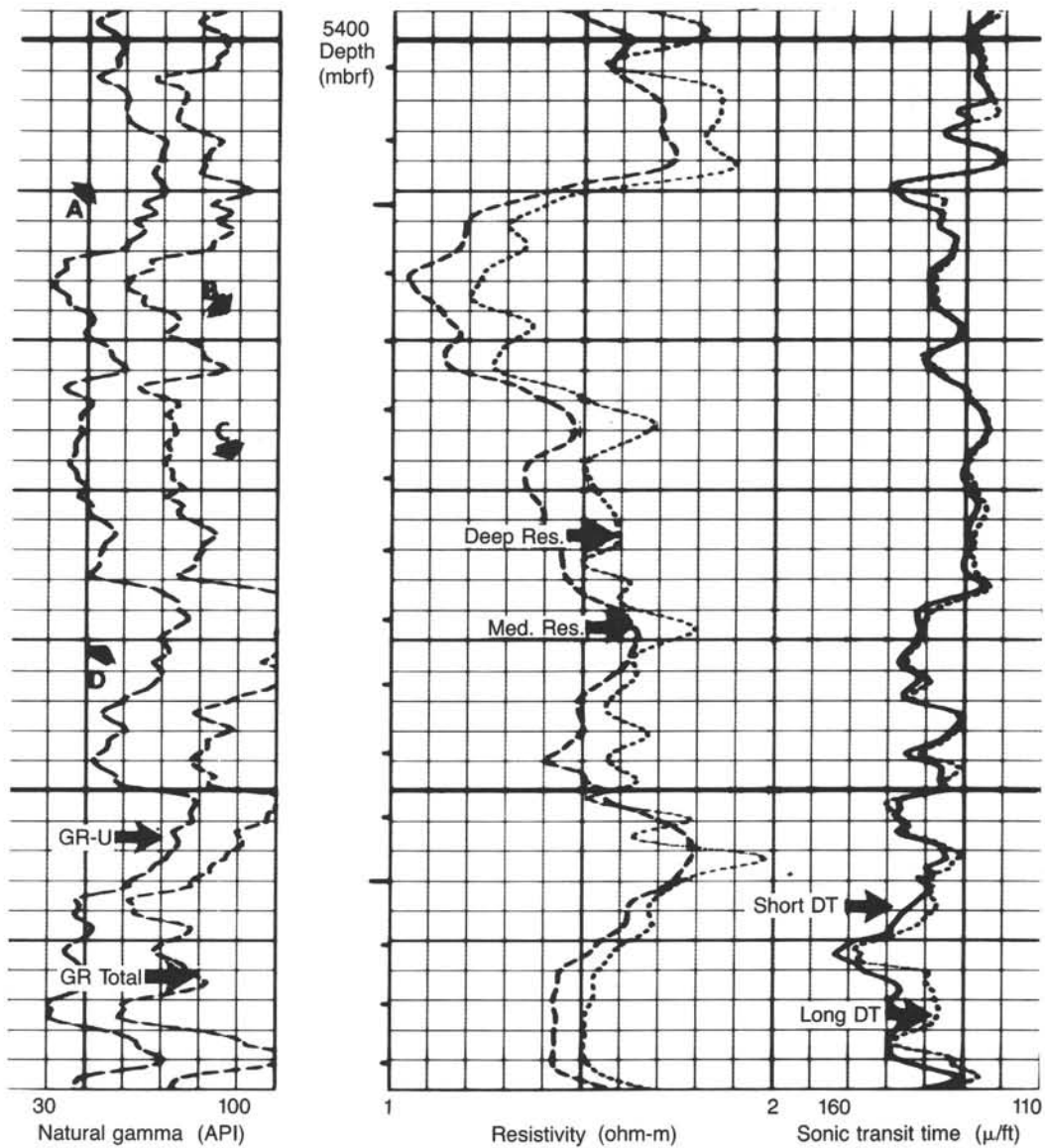


Figure 45. Seismic stratigraphic log response in Unit VB, Hole 718C, showing a distinct pattern interpreted as a possible turbidite compensation cycle. Scales and curve coding are as in Figure 45.

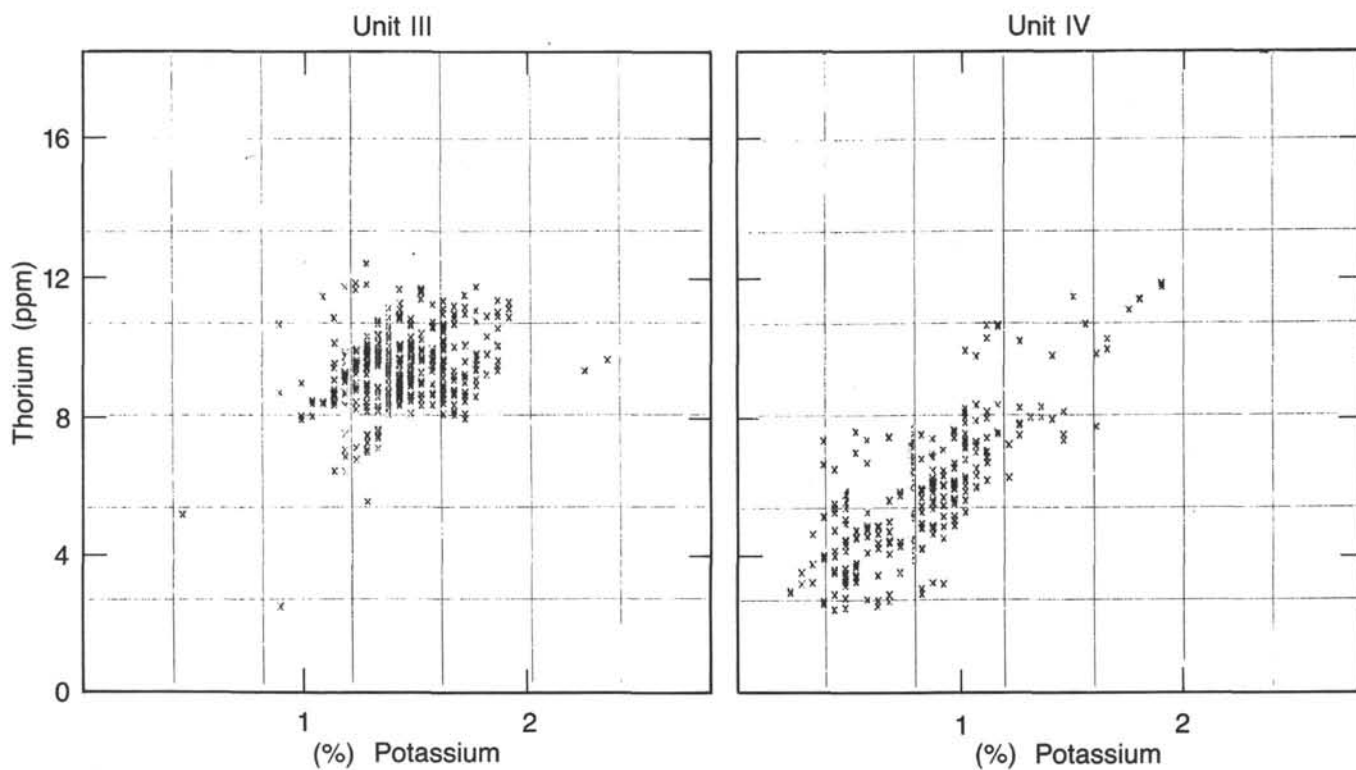


Figure 46. Thorium vs. potassium plot from NGT log data in Units III, IV, and VA.

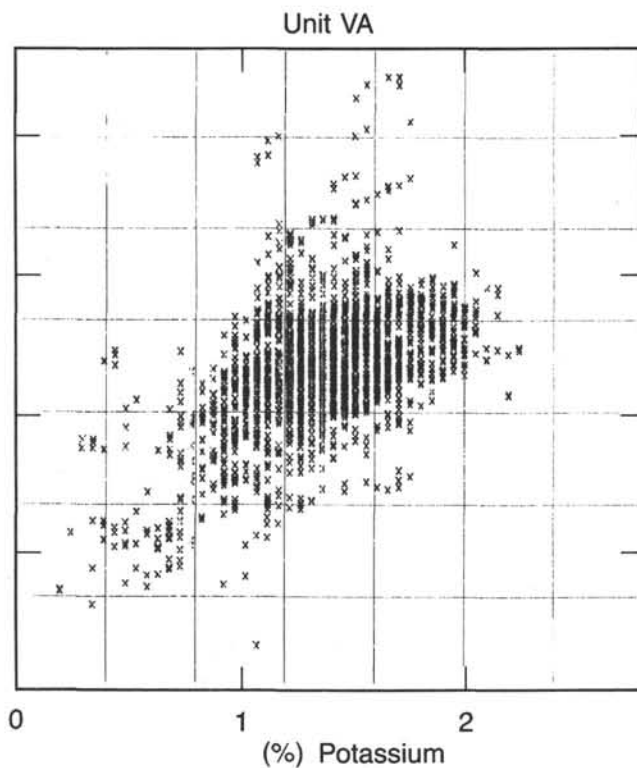
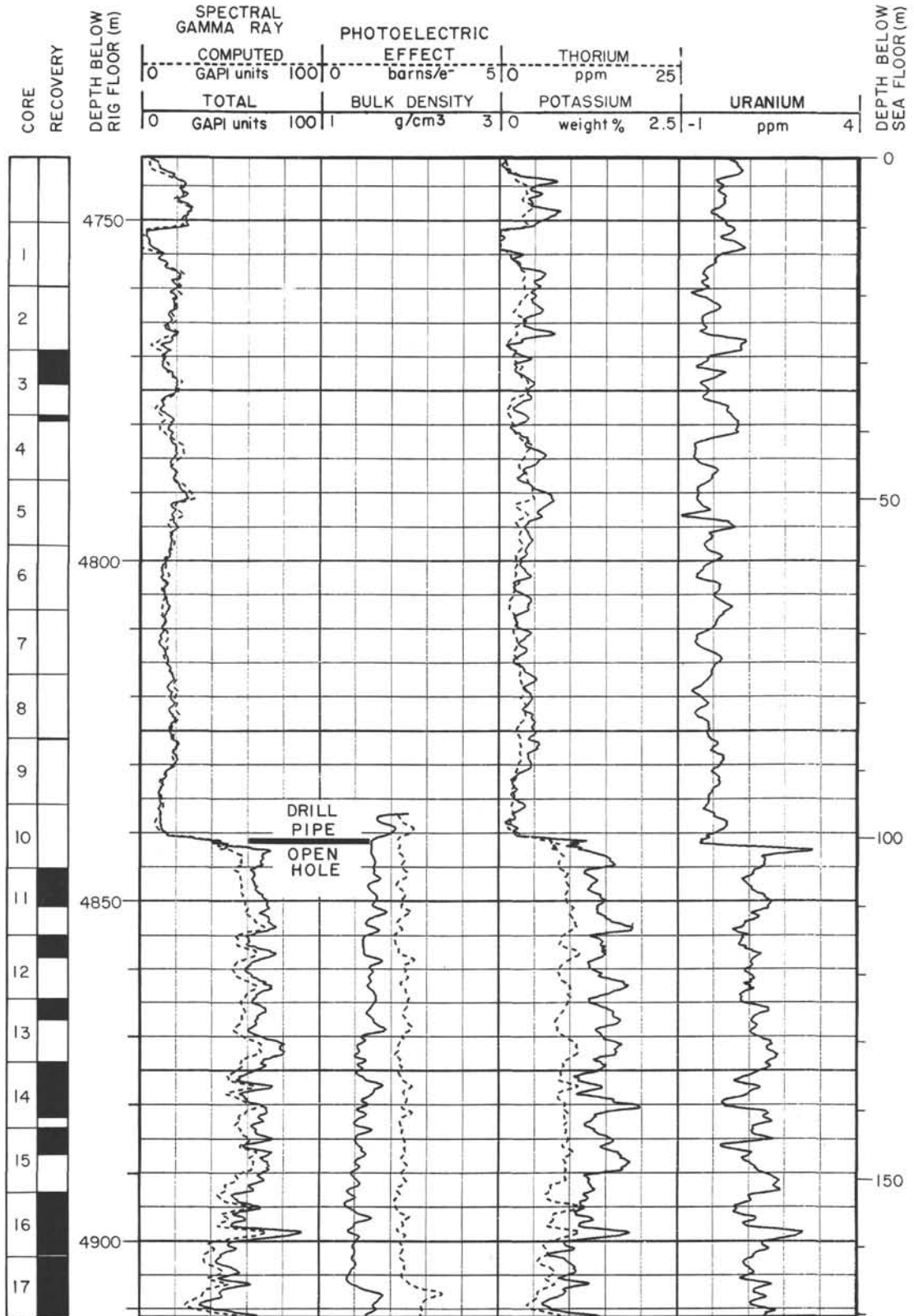
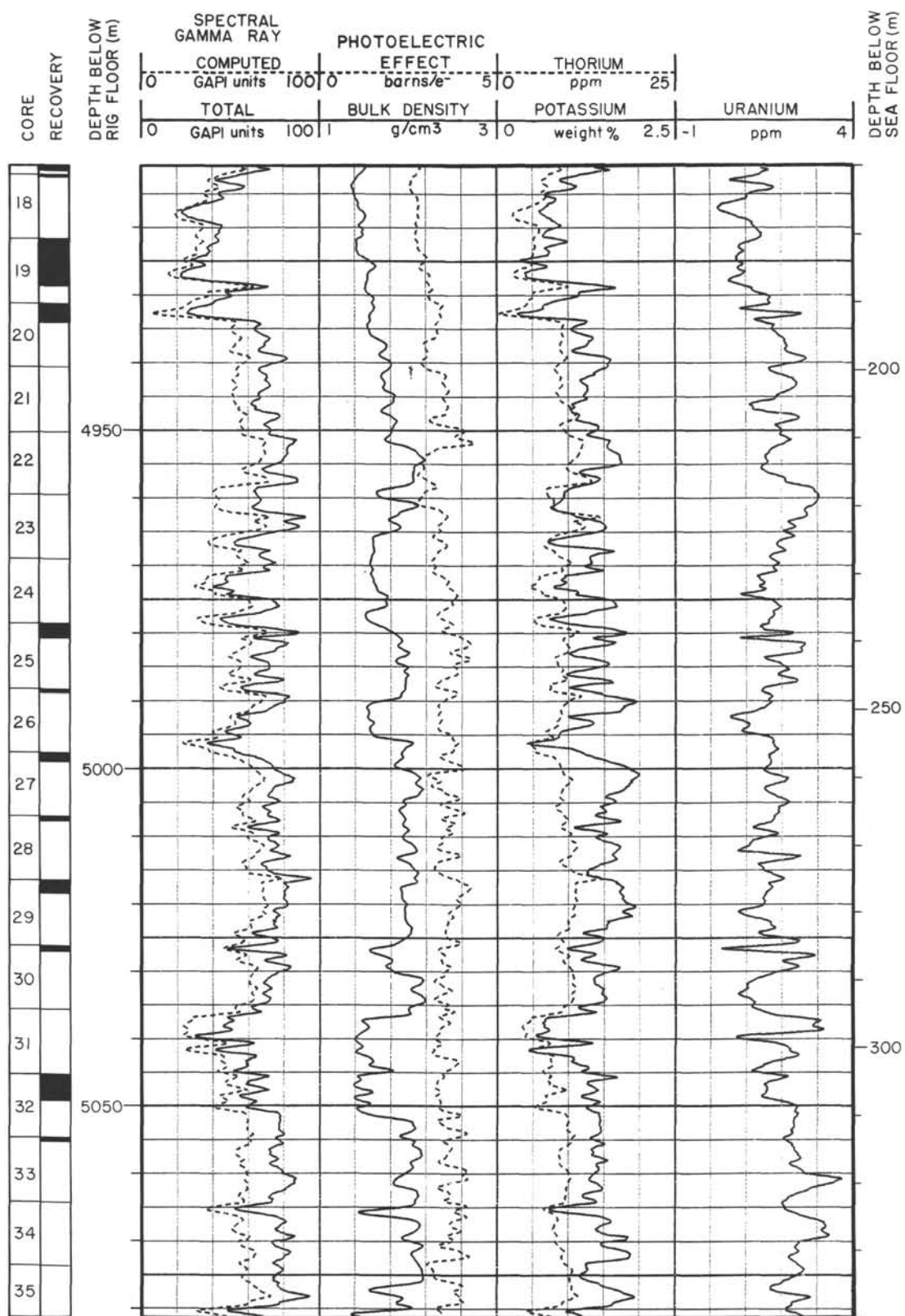


Figure 46 (continued).

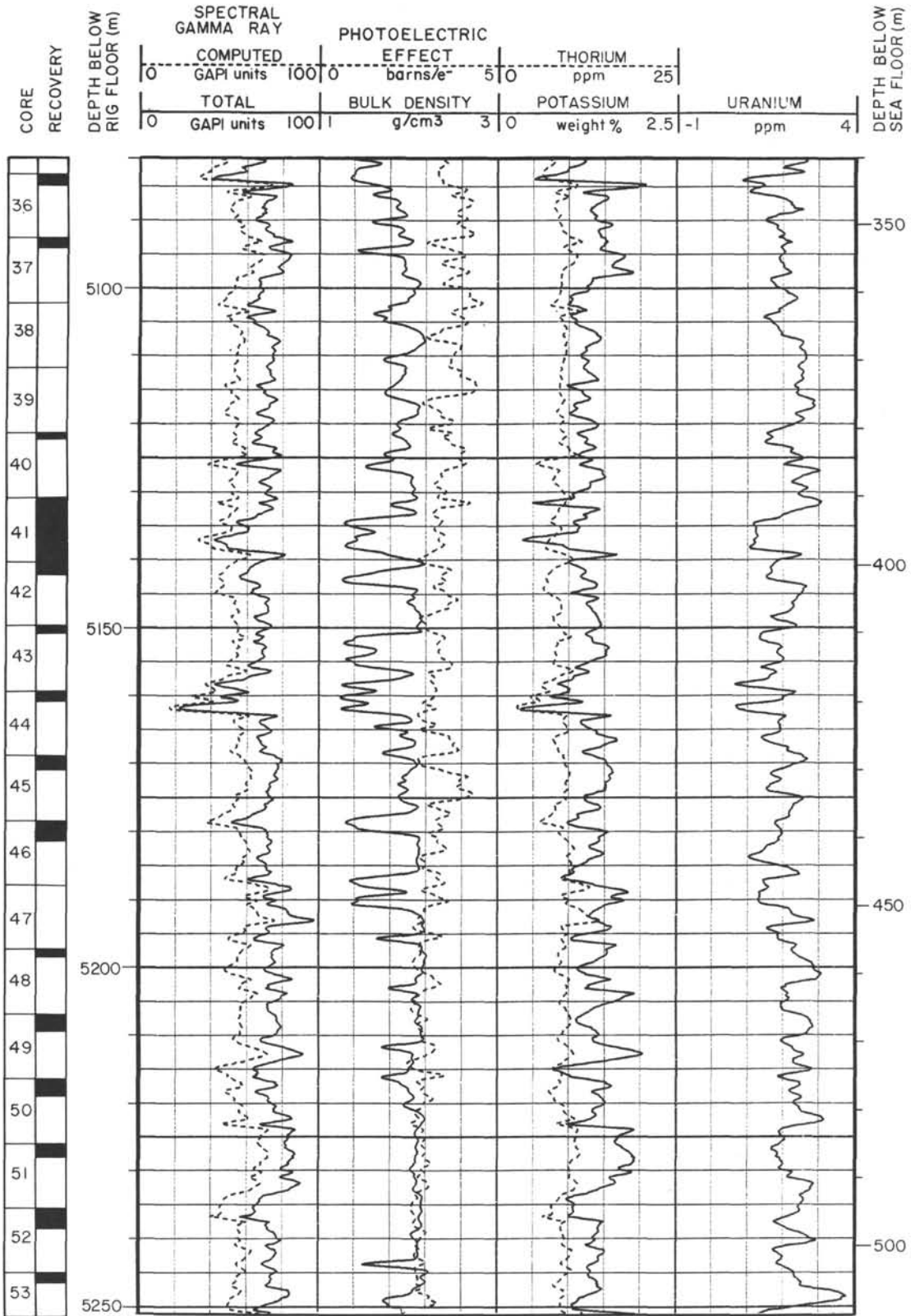
Summary Log for Hole 718C



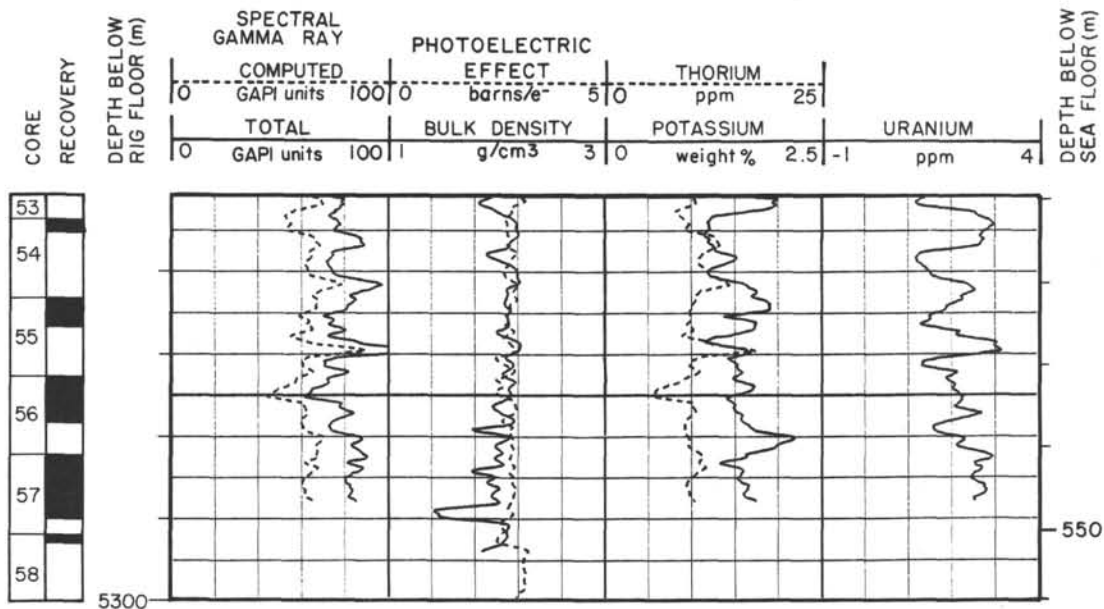
Summary Log for Hole 718C (continued)



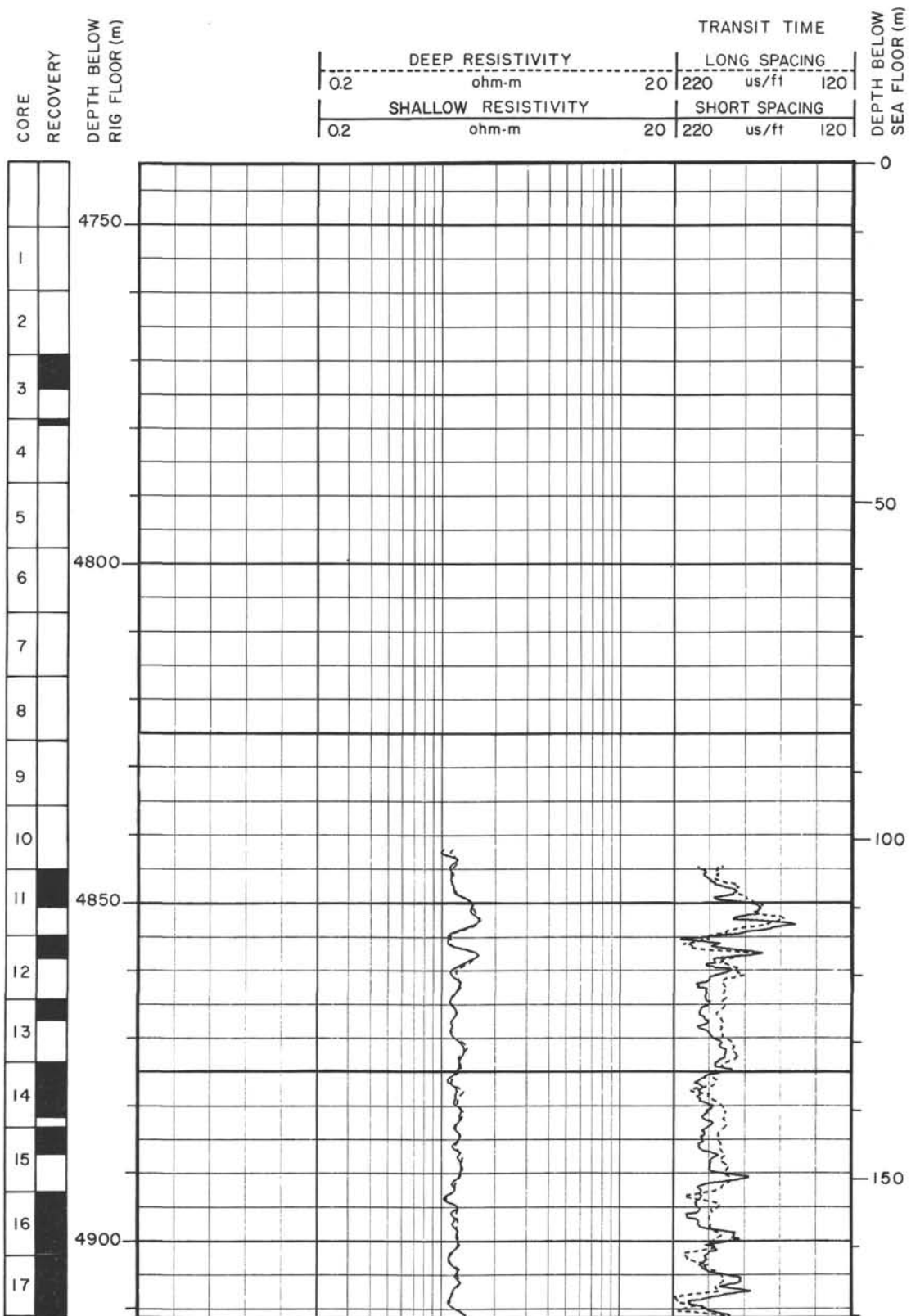
Summary Log for Hole 718C (continued)



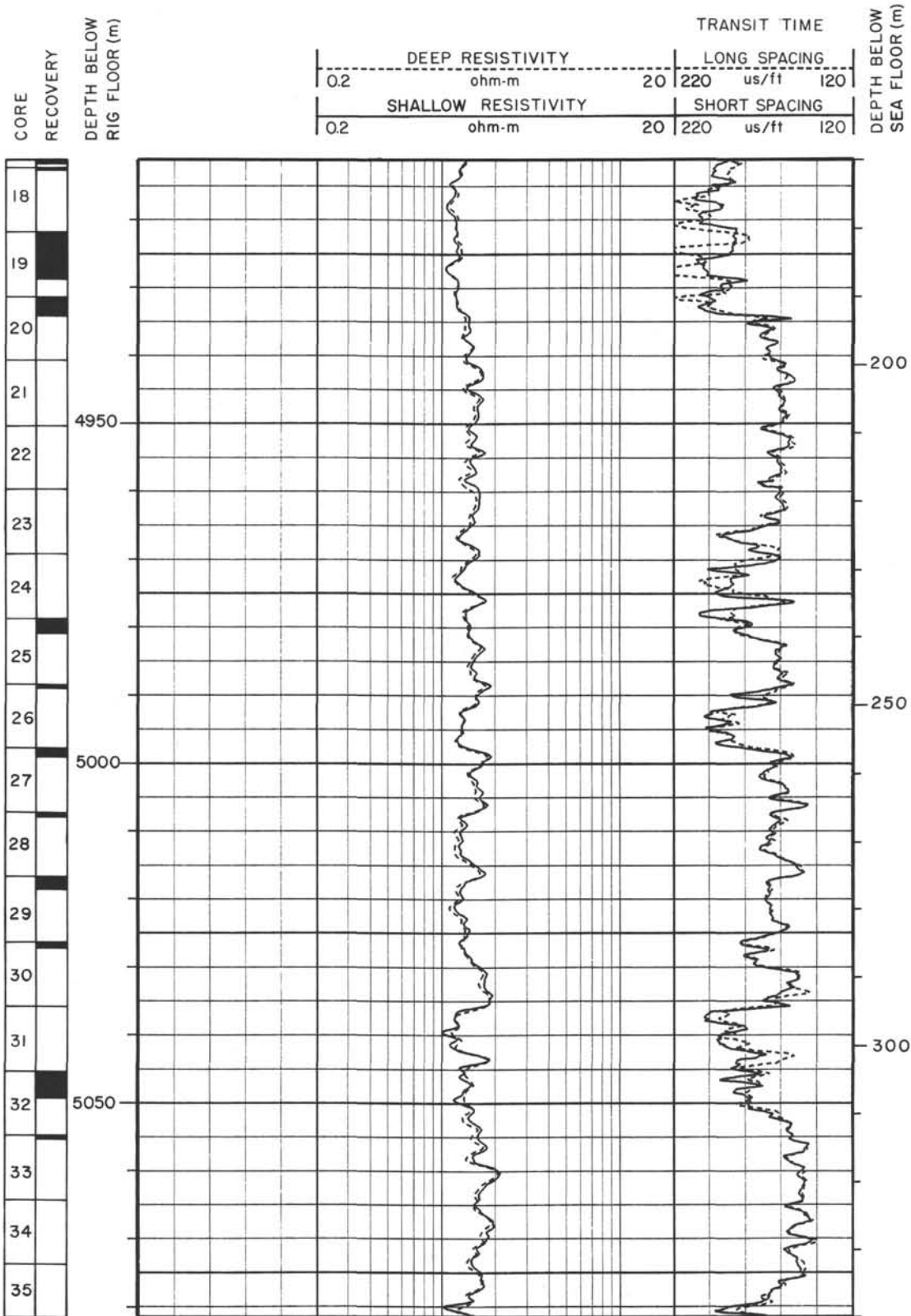
Summary Log for Hole 718C (continued)



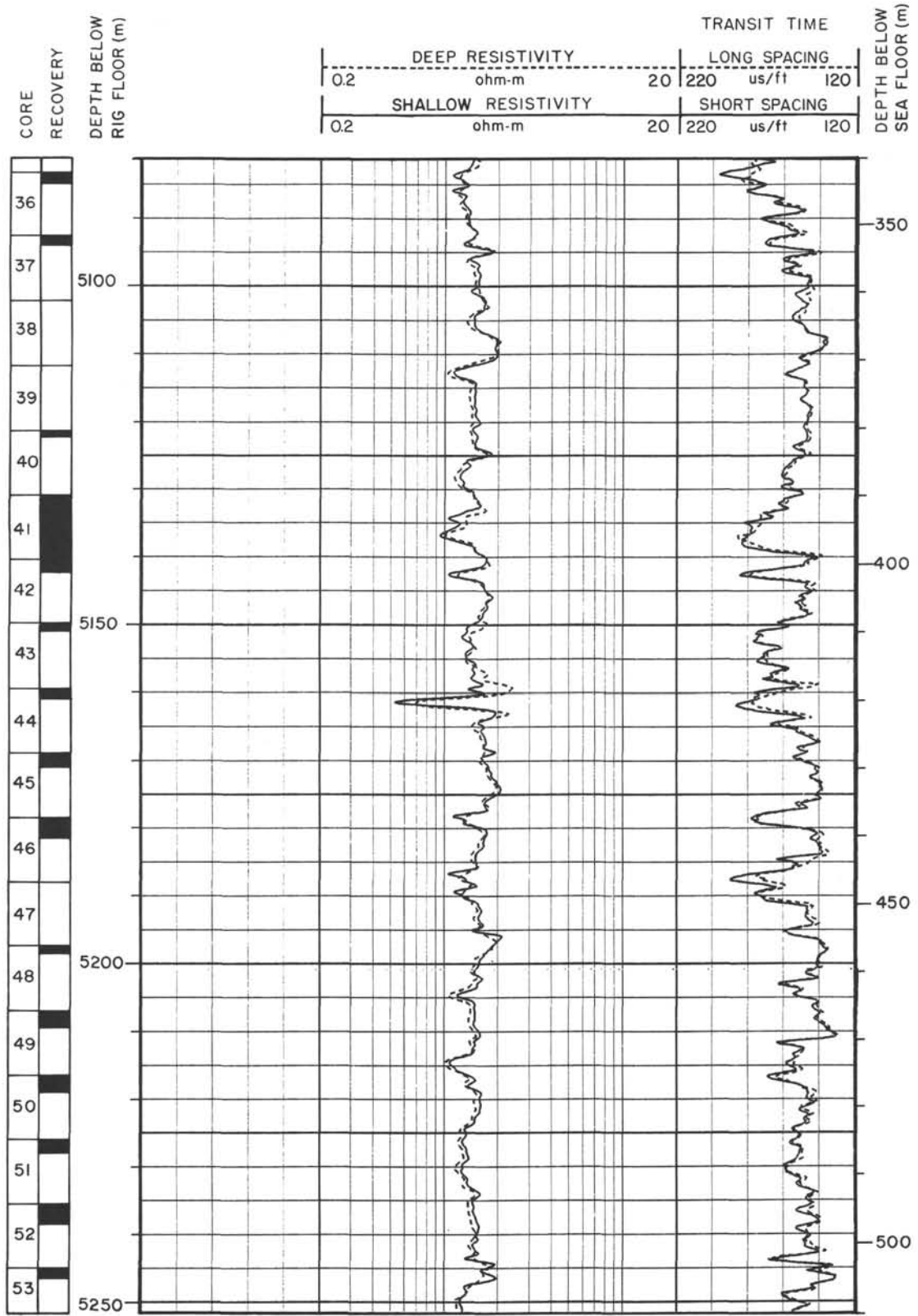
Summary Log for Hole 718C (continued)



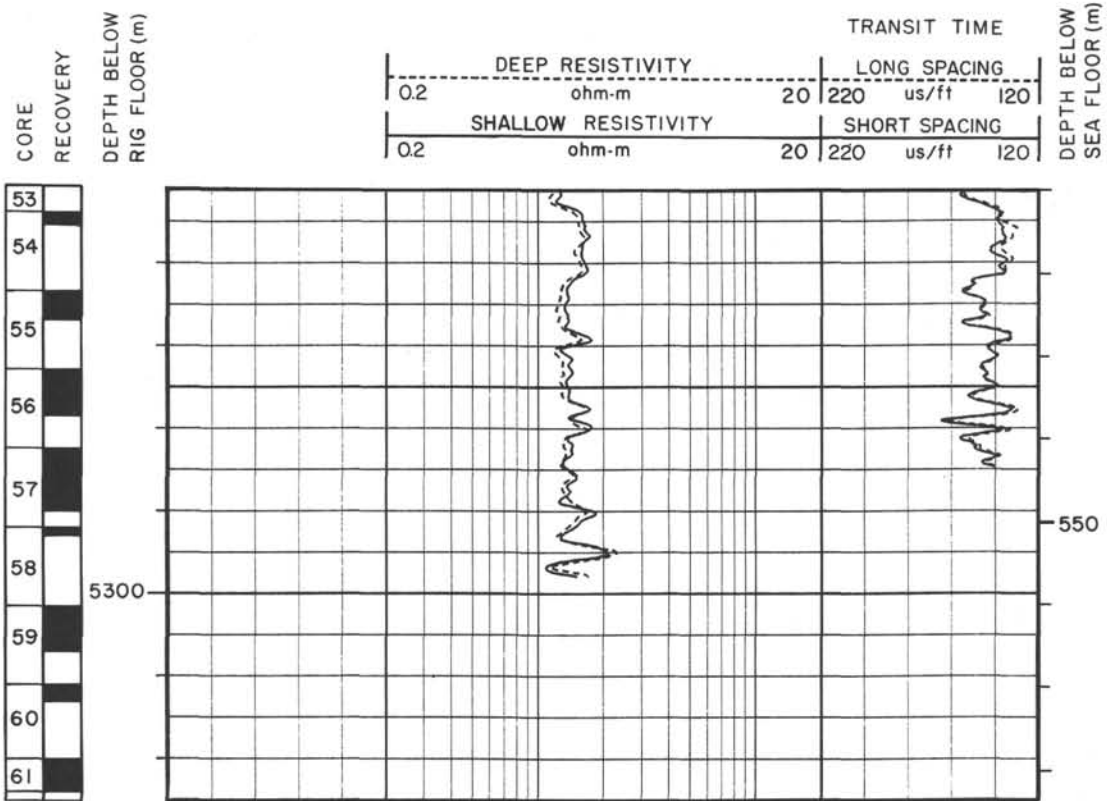
Summary Log for Hole 718C (continued)



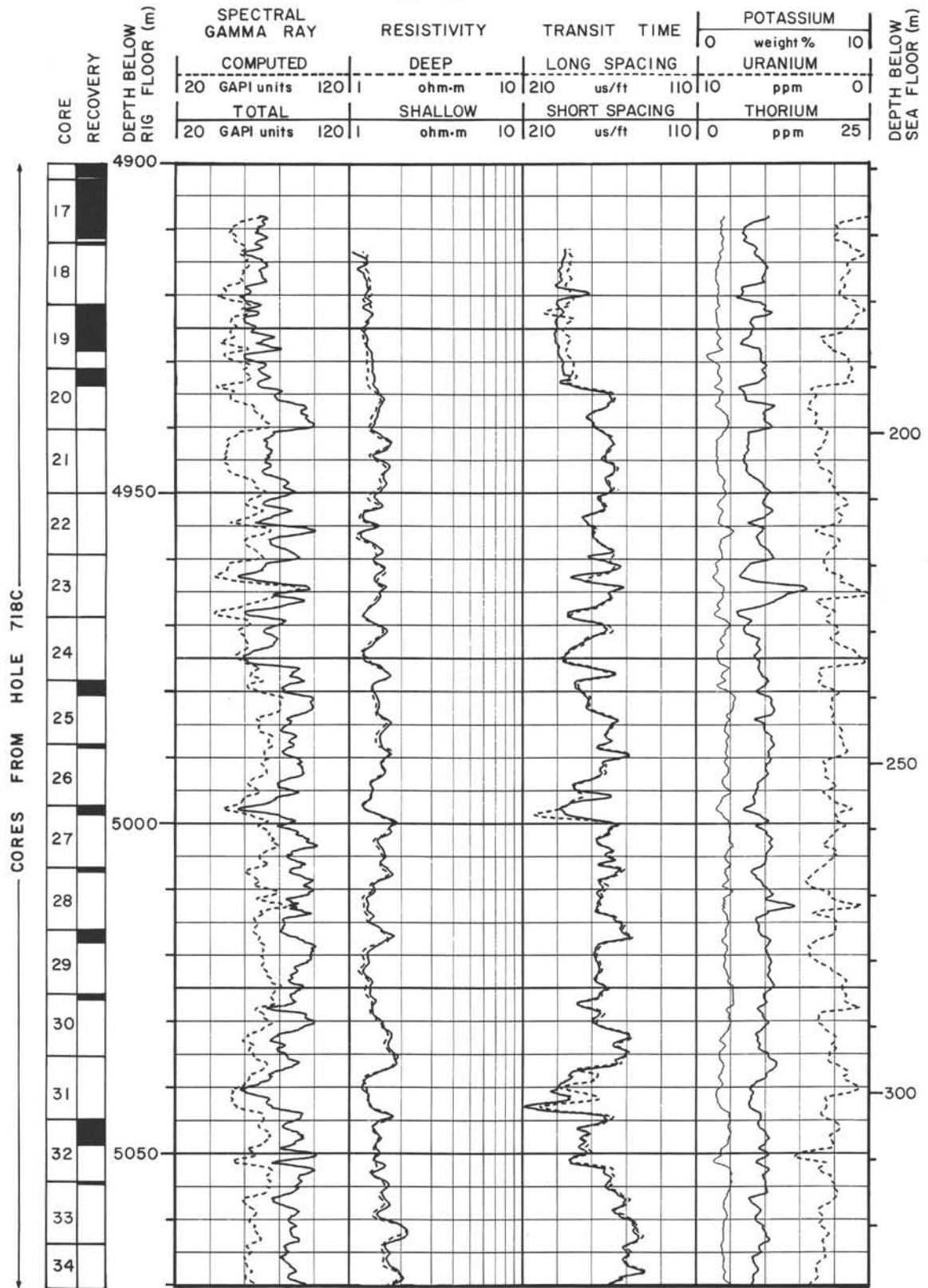
Summary Log for Hole 718C (continued)



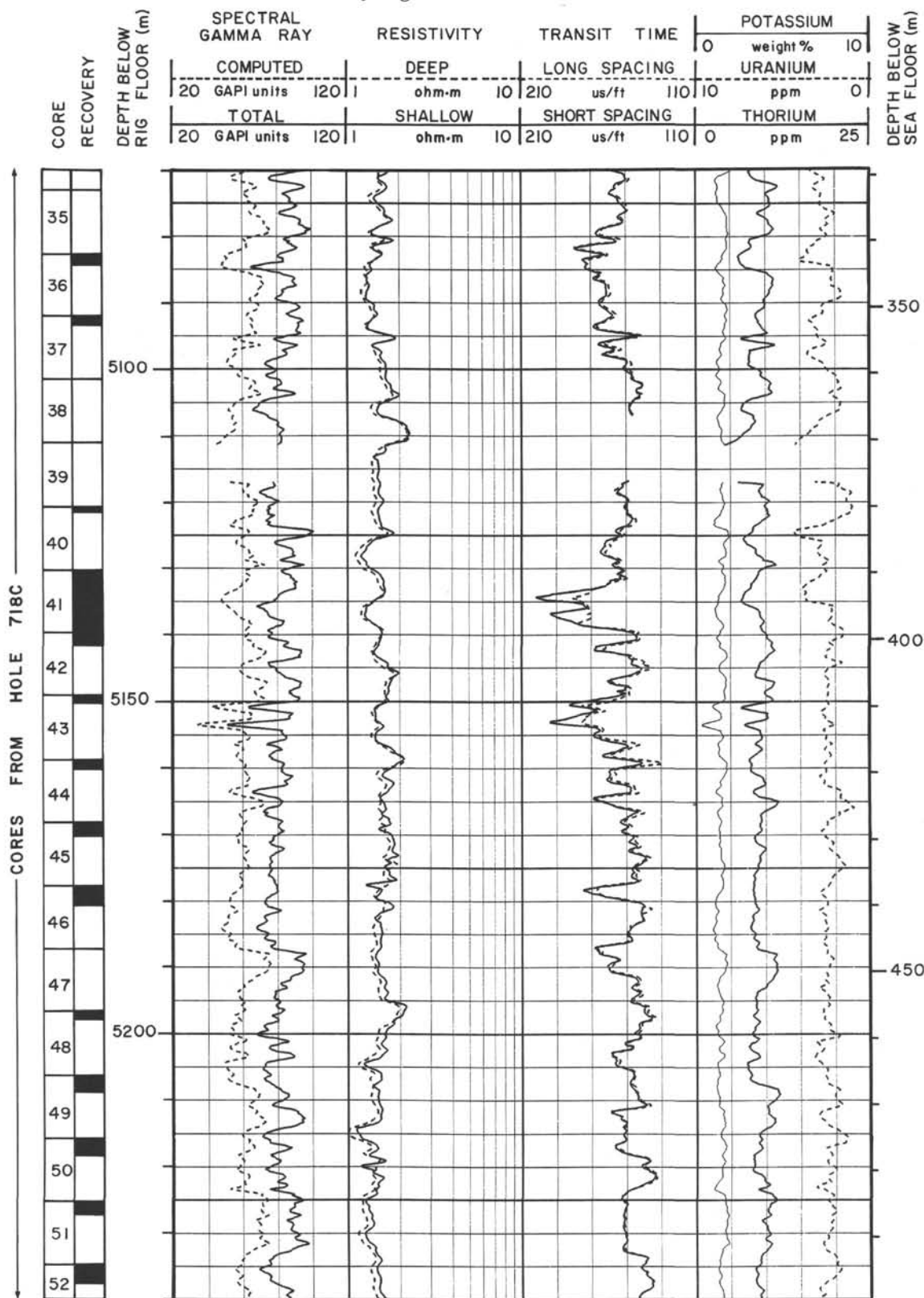
Summary Log for Hole 718C (continued)



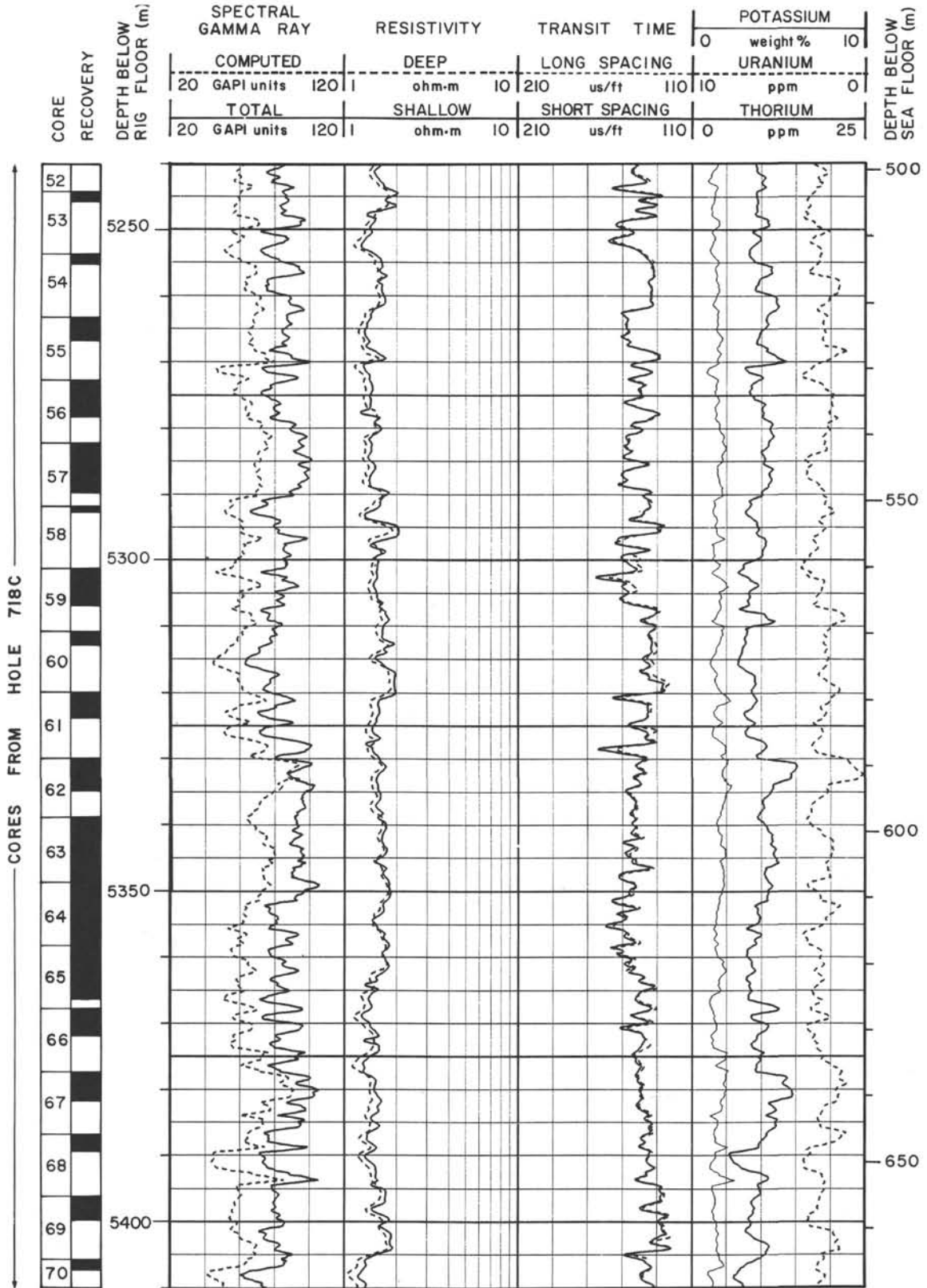
Summary Log for Hole 718E



Summary Log for Hole 718E (continued)

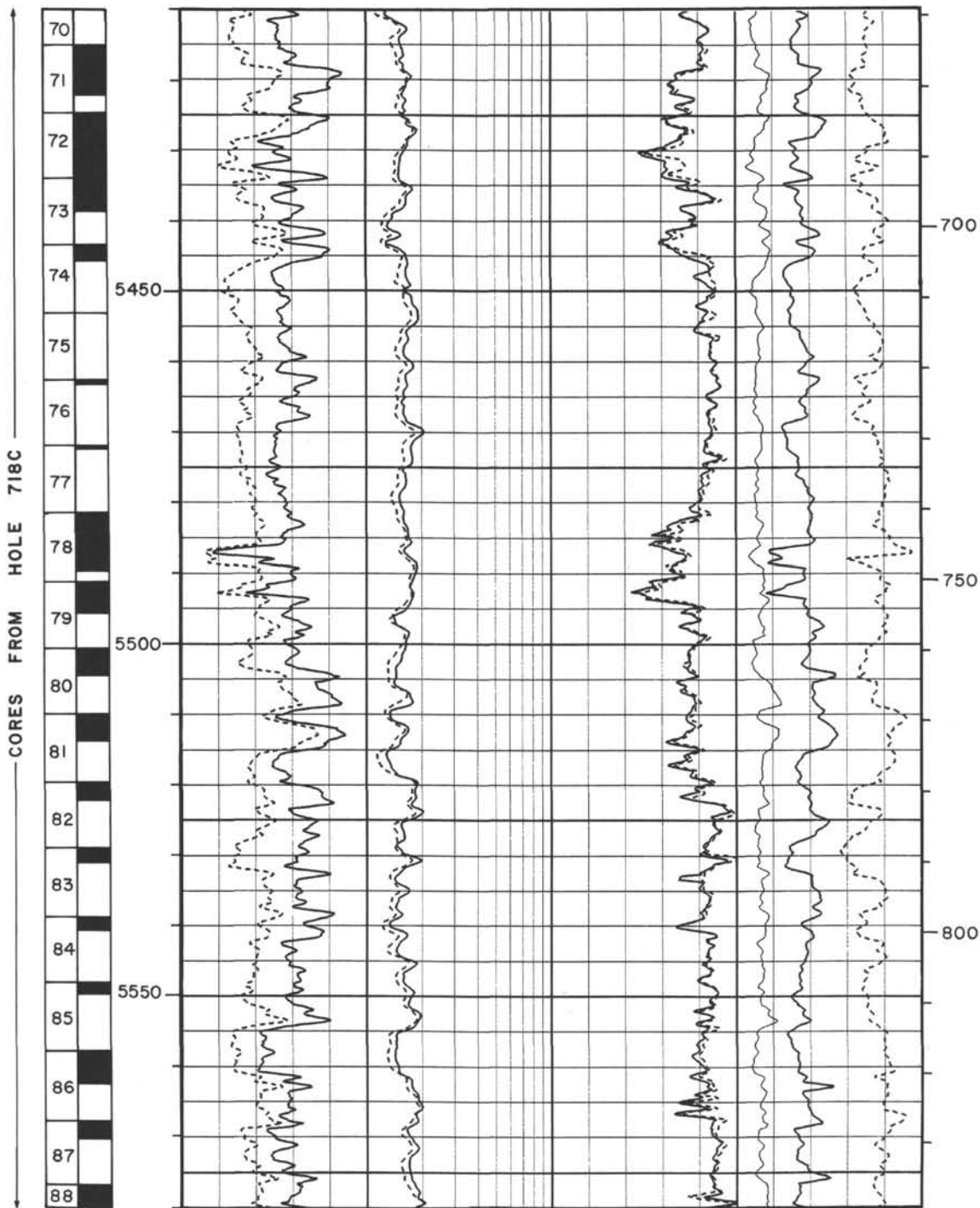


Summary Log for Hole 718E (continued)

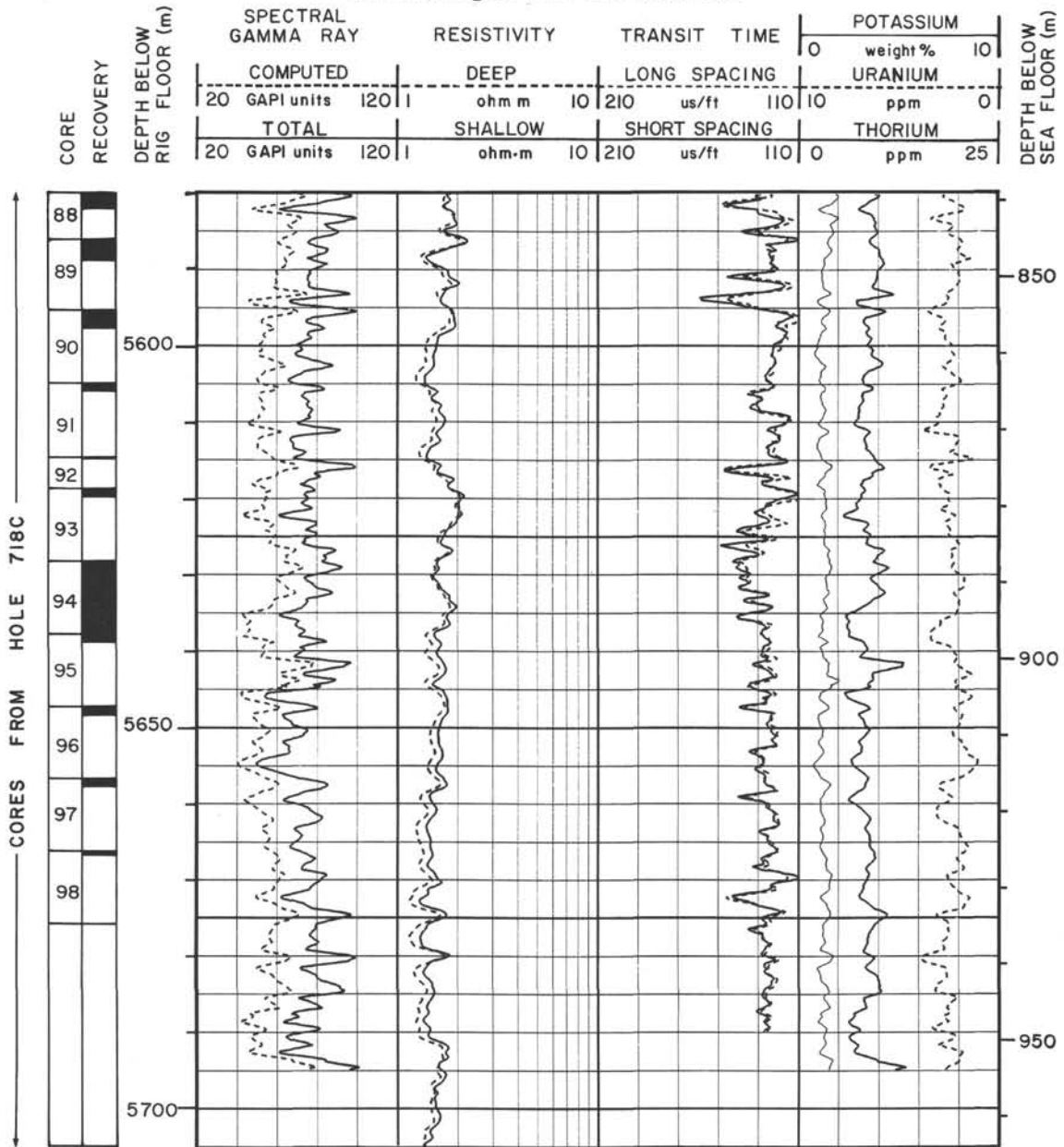


Summary Log for Hole 718E (continued)

CORE RECOVERY	SPECTRAL GAMMA RAY		RESISTIVITY		TRANSIT TIME		POTASSIUM		DEPTH BELOW RIG FLOOR (m)	
	COMPUTED		DEEP		LONG SPACING		0	weight %		10
	TOTAL		SHALLOW		SHORT SPACING		URANIUM			0
	20	GAPI units	120	ohm-m	10	210	us/ft	110		10
20	GAPI units	120	ohm-m	10	210	us/ft	110	0	ppm	25



Summary Log for Hole 718E (continued)



**NOTE: All core description forms ("barrel sheets") and core photographs have been printed on coated paper and bound as Section 3, near the back of the book, starting on page 213.**